Supporting Information for

# Mechanistic Basis for Efficient, Site-Selective, Aerobic Catalytic Turnover in Pd-Catalyzed C–H Imidoylation of Heterocycle-Containing Molecules

*Stephen J. Tereniak and Shannon S. Stahl**

Department of Chemistry, University of Wisconsin-Madison,
1101 University Avenue, Madison, WI, 53706
stahl@chem.wisc.edu

**Table of Contents**

**I. General Considerations.**

All commercially available reagents were purchased from Sigma-Aldrich and used as obtained, except where otherwise noted. Benzoic acid-$d_5$, which was used to synthesize *N*-methoxybenzamide-$d_5$, was purchased from CDN Isotopes. $Pd_2(dba)_3$•$CHCl_3$ was synthesized and recrystallized according to the literature.[1] ($^t$BuNC)$_2$Pd($O_2$) **1**[2] and ($^{4tBu}$py)$_2PdCl_2$[3] **0C** were synthesized according to the literature. ($^t$BuNC)$_2PdCl_2$ was synthesized according to the literature[4] and then recrystallized from $CH_3CN$. *N*-methoxybenzamide,[5] *N*-methoxybenzamide-$d_5$,[5] *N*-methoxy-4-fluorobenzamide,[5] and *N*-methoxy-2,6-difluorobenzamide[6] were synthesized according to the literature and purified by silica gel column chromatography followed by sublimation *in vacuo*. The imidoylation product 3-(*N*-methoxyimino)-*N*'-*t*-butylisoindolinone was synthesized as reported in the literature.[6] $H_2O_2$ (33.5 wt% in water) was titrated against $KMnO_4$ in a dilute aqueous solution of $H_2SO_4$. $^1$H, $^{13}$C{$^1$H}, $^{19}$F{$^1$H}, $^1$H-$^{15}$N HMBC, and $^1$H-$^{19}$F HMBC NMR spectra were recorded on a Bruker Avance-400 or Avance-500 NMR spectrometer. Chemical shift values are given in parts per million relative to $CDCl_3$ (7.26 ppm for $^1$H or 77.23 ppm for $^{13}$C), $CD_2Cl_2$ (5.32 ppm for $^1$H or 54.00 ppm for $^{13}$C). $^{15}$N chemical shifts are referenced to an external nitromethane sample in $CDCl_3$ (defined as 0 ppm; the chemical shift as recorded was 376.00 ppm). NMR spectra were plotted with MestReNova v10.0.2-15465 (MestreLab Research S. L. 2015). High resolution mass spectra were obtained using a Waters LCT HPLC-ESI-Q-MS by the mass spectrometry facility at the University of Wisconsin-Madison Department of Chemistry. In situ IR spectroscopic data were collected using a Mettler Toledo ReactIR ic10 with an AgX probe. Solid state FT-IR spectroscopic data were collected in ATR mode using a Bruker TENSOR 27 spectrometer located in the Chemical Instrumentation Instructional Laboratory at the University of Wisconsin-Madison Department of Chemistry. HPLC analyses were performed on a Shimadzu Prominence analytical HPLC with a Kinetex reverse phase LC column (5 µm particle size, XB-C18 phase, 100 Å pore size, 250 x 4.6 mm dimensions, Phenomenex Inc., part number 00G-4605-E0) and a UV detector. Elemental analyses were provided by Robertson Microlit Laboratories, Ledgewood, NJ, USA.

**II. Synthesis and Characterization of Non-Commercial Compounds.**

*N-methoxy-2,6-difluorobenzamide*. As mentioned in the General Considerations, the synthesis of this compound was accomplished according to the literature.[6] Purification involved silica gel column chromatography (50:50 hexanes:EtOAc), rotary evaporation of the product-containing fractions, and then vacuum sublimation. Two species, proposed to be rotamers, are present in the sublimed material. The ratio of the two rotamers, 1:0.12, was ascertained by integrating the signals by $^{19}$F NMR. The major rotamer is assigned as the species in which the methoxy group is *cis* to the carbonyl, whereas the minor rotamer is assigned as the species in which the methoxy group is *trans* to the carbonyl. $^1$H NMR (400 MHz, $CDCl_3$) δ 8.78 (bs, 1H, *H*N of major rotamer), 8.60 (bs, 1H, *H*N of minor rotamer), 7.40 (m, 1H, *p*-$H_3F_2C_6$-), 6.95 (m, 2H, *m*-$H_3F_2C_6$-), 3.90 (s, 3H, $H_3$CO- of major rotamer), 3.62 (s, 3H, $H_3$CO- of minor rotamer). $^{13}$C{$^1$H} NMR (126 MHz, $CDCl_3$) δ 160.36 (dd, $^1J_{C\text{-}F}$ = 255 Hz, $^3J_{C\text{-}F}$ = 7.6 Hz, 2C, $H_3CONHC(O)[C(CF)_2(CH_2)(CH)]$), 158.54 (s, 1C, $H_3CONHC(O)[C(CF)_2(CH_2)(CH)]$), 132.74 (t, $^3J_{C\text{-}F}$ = 11 Hz, 1C, $H_3CONHC(O)[C(CF)_2(CH_2)(CH)]$), 112.20 (dd, $^2J_{C\text{-}F}$ = 21 Hz, $^4J_{C\text{-}F}$ = 4 Hz, 2C, $H_3CONHC(O)[C(CF)_2(CH_2)(CH)]$), 111.22 (t, $^2J_{C\text{-}F}$ = 19 Hz, 1C, $H_3CONHC(O)[C(CF)_2(CH_2)(CH)]$), 64.98 (s, 1C, $H_3CONHC(O)[C(CF)_2(CH_2)(CH)]$). $^{19}$F{$^1$H} (376 MHz, $CDCl_3$) δ -111.34 (s, major rotamer), -112.47 (s, minor rotamer). HRMS (ESI) Calcd. for $C_8H_7O_2NF_2$ ([M+H]$^+$): 188.0518, found: 188.0516.

**Synthesis and Characterization of Pd Complexes**

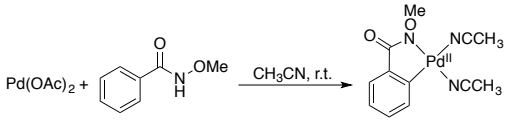


**2A**

*($CH_3CN$)$_2$Pd(C~N)* **2A**. $Pd(OAc)_2$ (238 mg, 1.06 mmol) was dissolved in 8 mL $CH_3CN$, and then a solution of *N*-methoxybenzamide (161 mg, 1.07 mmol) in 4 mL $CH_3CN$ was added dropwise with stirring. The mixture gradually lightened and turned cloudy. After three days, the mixture had turned clear

and pale yellow. It was then filtered through Celite, concentrated *in vacuo* to 6 mL, and then placed in a refrigerator. After 10 days, the mother liquor was decanted. Pale yellow crystals of **2A** that had grown were dried *in vacuo* to give **2A** (148 mg, 0.43 mmol, 41% yield). The mother liquor was concentrated to 2 mL and placed in a refrigerator, and after four more days, a second crop of crystals of **2A** was collected (total yield 239 mg, 0.71 mmol, 67% yield). A single crystal of **2A** from the first crop was selected for X-ray diffraction data collection (see Section VII for details). The sample submitted for elemental analysis was dried *in vacuo* with heating until all the acetonitrile was removed, as judged by $^1$H NMR spectroscopy. $^1$H NMR (500 MHz, DMSO-$d_6$) δ 7.63 (d, $^2J_{H\text{-}H}$ = 7.6 Hz, 1H), 7.18 (dd, $^2J_{H\text{-}H}$ = 7.2 Hz, $^3J_{H\text{-}H}$ = 1.7 Hz, 1H), 7.02 (td, $^2J_{H\text{-}H}$ = 7.2 Hz, $^3J_{H\text{-}H}$ = 0.9 Hz, 1H), 6.94 (td, $^2J_{H\text{-}H}$ = 7.6 Hz, $^3J_{H\text{-}H}$ = 1.7 Hz, 1H), 3.62 (s, 3H, $H_3$CO-), 2.07 (s, 6H, $H_3$CCN displaced by DMSO). Anal. Calcd. for ($C_8H_7PdNO_2$): C, 37.60; H, 2.76; N, 5.48. Found: C, 37.04; H, 2.83; N, 5.77.

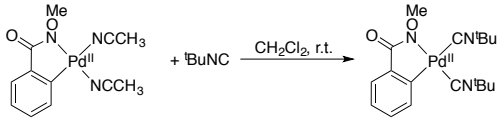


**2A** **2**

*($^t$BuNC)$_2$Pd(C~N)* **2**. **2A** (52.5 mg, 0.155 mmol) was slurried in 10 mL $CH_2Cl_2$, and then 8.0 equiv $^t$BuNC (140 µL, 1.24 mmol) was added dropwise. After stirring overnight, the volatiles were removed *in vacuo* on the Schlenk line. The crude material was redissolved in 2 mL $CH_2Cl_2$, 5 mL pentane was added, and the mixture was put in the fridge. After six days, the mother liquor was decanted, and colorless crystals were dried *in vacuo* (63 mg, 0.149 mmol, 96% yield). A single crystal grown of **2** from slow evaporation of an ethyl acetate/hexanes mixture was selected for X-ray diffraction data collection (see Section VII for details). $^1$H NMR (500 MHz, $CDCl_3$) δ 7.61 (dd, $^2J_{H\text{-}H}$ = 7.4 Hz, $^3J_{H\text{-}H}$ = 1.5 Hz, 1H), 7.13 (m, 2H), 7.03 (td, $^2J_{H\text{-}H}$ = 7.4 Hz, $^3J_{H\text{-}H}$ = 1.5 Hz, 1H), 3.73 (s, 3H, $H_3$CO-), 1.64 (t, $^3J_{H\text{-}N}$ = 2 Hz, 9 H, ($H_3$C)$_3$NC-), 1.57 (s, 9 H, ($H_3$C)$_3$NC-). $^{13}$C{$^1$H} NMR (126 MHz, $CDCl_3$) δ 178.56 (s, 1C, $C_5H_4C$(O)N-), 148.21, 139.36, 136.46 (m, 1C, ($H_3$C)$_3$N*C*-), 135.05, 133.47 (t, $^2J_{C\text{-}N}$ = 19 Hz, 1C, ($H_3$C)$_3$N*C*-), 129.25, 127.98, 125.84, 62.08 (s, 1C, $H_3$*C*O-), 58.48 (t, $^2J_{C\text{-}N}$ = 5 Hz, 1C, ($H_3$C)$_3$*C*NC-), 57.89 (bs, 1C, ($H_3$C)$_3$*C*NC-), 30.35 (s, 3C, ($H_3C$)$_3$CNC-), 30.21 (s, 3C, ($H_3C$)$_3$CNC-). FT-IR ($\nu_{CN}$, cm$^{-1}$, ATR) 2220, 2203. Anal. Calcd. for ($C_{18}H_{25}PdN_3O_2$): C, 51.25; H, 5.97; N, 9.96. Found: C, 51.16; H, 5.97; N, 9.97.

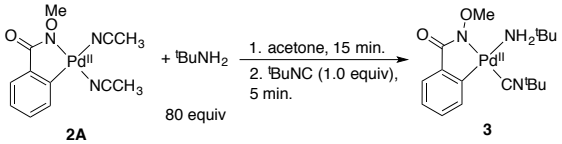


**2A** **3**

*($^t$BuH$_2$N)($^t$BuNC)Pd(C~N)* **3**. To a slurry of **2A** (47 mg, 0.14 mmol) in 5 mL acetone was added 80 equiv $^t$BuNH$_2$ (1.17 mL, 11 mmol). The slurry rapidly turned into a colorless solution. After stirring for 15 minutes, the mixture was filtered through Celite, and then the volatiles were removed from the filtrate *in vacuo*. The filtrate was redissolved in 5 mL acetone, and then a solution of $^t$BuNC (15.5 µL, 0.14 mmol) in 2 mL acetone was added dropwise with stirring. After five minutes, the volatiles were removed *in vacuo* to give a colorless foamy residue. The major species in the $^1$H NMR spectrum of this material, **3**, matches one of the species observed in the crude reaction of ($^t$BuNC)$_2$Pd(O$_2$) **1** with 2.1 equiv *N*-methoxybenzamide and 2.0 equiv $^t$BuNC. Some residual acetone and t-butyl amine is also observed in the crude material from the independent synthesis. $^1$H NMR (400 MHz, $CDCl_3$) δ 7.62 (dd, $^2J_{H\text{-}H}$ = 5.9 Hz, $^3J_{H\text{-}H}$ = 1.1 Hz, 1H), 7.12 (m, 2H), 7.01 (td, $^2J_{H\text{-}H}$ = 5.8 Hz, $^3J_{H\text{-}H}$ = 1.3 Hz, 1H), 3.82 (s, 3H, $H_3$CO-), 2.75 (bs, 2H, $H_2$NC(CH$_3$)$_3$), 1.61 (bt, 9H, ($H_3$C)$_3$CNC-), 1.34 (s, 9H, H$_2$NC(C$H_3$)$_3$).

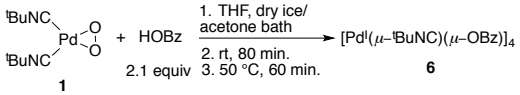


**1** **6**

*[Pd$^I$(µ-$^t$BuNC)(µ-OBz)]$_4$* **6**. ($^t$BuNC)$_2$Pd(O$_2$)$^2$ **1** (108 mg, 0.37 mmol) was added to a 25 mL vial in a glovebox under an $N_2$ atmosphere. This flask, as well as a solution of benzoic acid (96 mg, 0.79 mmol) in 3 mL THF, was cooled with a dry ice-acetone bath in the glovebox cold well. After several minutes of

cooling, the benzoic acid solution was added to the Pd peroxo with stirring. The benzoic acid vial was washed with 2 mL cold THF and pipetted into the reaction vial to ensure all the benzoic acid was transferred. The cold bath was removed, and the reaction was allowed to warm to room temperature with stirring. After 80 minutes, the capped vial was taken out of the glovebox and heated to 50 °C in an oil bath. After one hour, a tan slurry had formed. This slurry was filtered with an aspirator vacuum. The precipitate was washed with 3x1 mL diethyl ether. Volatiles were removed on a Schlenk line with 50 °C heating *in vacuo*. This gave **6** as a mustard yellow precipitate (74 mg, 0.24 mmol, 64% yield). A single crystal of **6** grown by layering a dichloromethane solution with hexanes was selected for X-ray diffraction data collection (see Section VII for details). $^{1}$H NMR (400 MHz, $CD_2Cl_2$) δ 8.00 (m, 8H, *o*-$C_6H_5$), 7.36 (m, 4H, *p*-$C_6H_5$), 7.29 (m, 8H, *m*-$C_6H_5$), 1.37 (s, 36H, ($H_3$C)$_3$CNC-). $^{13}$C{$^{1}$H} NMR (126 MHz, $CD_2Cl_2$) δ 172.85 (s, 4C, -$O_2C$$C_6H_5$), 136.72, 131.09, 130.22, 128.10, 117.70 (s, 4C, ($H_3$C)$_3$CN*C*-), 59.89 (s, 3C, ($H_3$C)$_3$*C*NC-), 31.26 (s, 12C, ($H_3C$)$_3$CNC-). Anal. Calcd. for ($C_{48}H_{56}Pd_4N_4O_8$): C, 46.39; H, 4.54; N, 4.51. Found: C, 45.86; H, 3.95; N, 4.41.

*($^{tBu}$py)$_2$Pd(OAc)$_2$* **0A**. $Pd(OAc)_2$ (206 mg, 0.92 mmol) was dissolved in 8 mL $CH_2Cl_2$. To this red solution was added $^{4tBu}$py (270 µL, 1.84 mmol). The color lightened rapidly. After letting stand for several hours, 5 mL hexanes was added to the solution, the mixture was agitated, and a precipitate formed. The precipitate was filtered off, washed with 3x3 mL hexanes, then 2x2 mL pentane. The precipitate was then pumped down on the Schlenk line *in vacuo* to give the product **0A** (221 mg, 0.45 mmol, 49% yield) as a pale yellow powder.[7] $^{1}$H NMR (400 MHz, $CDCl_3$) δ 8.52 (m, 4H, α-$^{tBu}$py), 7.29 (m, 4H, β-$^{tBu}$py), 1.87 (s, 6H, -$O_2CCH_3$), 1.29 (s, 18H, ($H_3$C)$_3$C-). $^{13}$C{$^{1}$H} NMR (126 MHz, $CDCl_3$) δ 178.38 (s, 2C, -$O_2C$$CH_3$), 163.31 (s, 2C, $^{tBu}$-$C_4H_4N$), 151.01 (s, 4C, α-$^{tBu}$py), 122.13 (s, 4C, β-$^{tBu}$py), 35.21 (s, 2C, ($H_3$C)$_3$*C*-), 30.40 (s, 6C, ($H_3C$)$_3$C-), 23.51 (s, 2C, -$O_2C$$CH_3$).

*($^{tBu}$py)$_2$Pd(OBz)$_2$* **0B**. $Pd(OBz)_2$ (39.0 mg, 0.11 mmol) was dissolved in 3 mL $CH_2Cl_2$. To the orange solution was added $^{4tBu}$py (33 µL, 0.23 mmol). The color rapidly lightened from orange to yellow. After 30 minutes of stirring, 15 mL hexanes were added, and a pale yellow precipitate crashed out. The precipitate was filtered off, washed with 2x1 mL hexanes, then 3x1 mL pentane. The precipitate was redissolved in 1 mL $CH_2Cl_2$, then 10 mL pentane was added to create a suspension, which was placed in a refrigerator. After several hours, the mother liquor was decanted, and the pale yellow precipitate was collected and dried *in vacuo* to give **0B** (21 mg, 0.034 mmol, 31% yield).[7] $^{1}$H NMR (400 MHz, $CDCl_3$) δ 8.56 (m, 4H, α-$^{tBu}$py), 8.03 (m, 4H, *o*-$C_6H_5$-), 7.41 (m, 2H, *p*-$C_6H_5$-), 7.34 (m, 4H, *m*-$C_6H_5$), 7.22 (m, 4H, β-$^{tBu}$py), 1.22 (s, 18 H, ($H_3$C)$_3$C-). $^{13}$C{$^{1}$H} NMR (126 MHz, $CDCl_3$) δ 172.90 (s, 2C, -$O_2C$$C_6H_5$), 163.21 (s, 2C, $^{tBu}$-$C_4H_4N$), 150.50 (s, 4C, α-$^{4tBu}$py), 134.96, 130.86, 129.67, 127.85, 122.22 (s, 4C, β-$^{tBu}$py), 35.15 (s, 2C, ($H_3$C)$_3$*C*-), 30.33 (s, 6C, ($H_3C$)$_3$C-).

*($^{tBu}$py)$_2$Pd(TFA)$_2$* **0T**. To ($^{tBu}$py)$_2$$Pd(OAc)_2$ (111 mg, 0.22 mmol) was added 10 mL MeOH. Then, HTFA (450 µL, 5.88 mmol) was added dropwise. The suspension turned clearer. After stirring overnight, the mixture was concentrated by rotary evaporation to a pale yellow solid. The crude mixture was redissolved in 2 mL $CH_2Cl_2$ and filtered through Celite. 2 mL hexanes and 10 mL pentane was added, and the mixture was cooled in the refrigerator for one hour. Then, the mother liquor was decanted. The recrystallization procedure was repeated, giving pale yellow crystals of **0T** (25 mg, 0.042 mmol, 19% yield).[7] $^{1}$H NMR (400 MHz, $CDCl_3$) δ 8.34 (m, 4H, α-$^{tBu}$py), 7.36 (m, 4H, β-$^{tBu}$py), 1.32 (s, 18 H, ($H_3$C)$_3$C-). $^{13}$C{$^{1}$H} NMR (126 MHz, $CDCl_3$) δ 164.72 (s, 2C, $^{tBu}$-$C_4H_4N$), 162.91 (q, $^{3}J_{C\text{-}F}$ = 38 Hz, 2C, -$O_2C$$CF_3$), 150.17 (s, 4C, α-$^{tBu}$py), 122.74 (s, 4C, β-$^{tBu}$py), 114.08 (q, $^{2}J_{C\text{-}F}$ = 290 Hz, 2C, -$O_2C$$CF_3$), 35.42 (s, 2C, ($H_3$C)$_3$*C*-), 30.37 (s, 6C, ($H_3C$)$_3$C-). $^{19}$F{$^{1}$H} (376 MHz, $CDCl_3$) δ 74.64. Anal. Calcd. for ($C_{22}H_{26}PdN_2O_4F_6$): C, 43.83; H, 4.35; N, 4.65. Found: C, 43.39; H, 4.23; N, 4.54.

*($^{t}$BuNC)$_2$Pd(TFA)$_2$*. To a slurry of $Pd(TFA)_2$ (100 mg, 0.31 mmol) in 5 mL $CH_2Cl_2$ was added 2.0 equiv $^{t}$BuNC (70 µL, 0.62 mmol). After three hours, the reaction was filtered through Celite, and the filtrate was pumped down to give a yellow-orange powder. This material was redissolved in 3 mL $CH_2Cl_2$, layered with pentane, then placed in a refrigerator. The next day, the mother liquor was decanted, then the volatiles were removed *in vacuo* from the crystals. A mixture of red and white crystals was observed.

These crystals were redissolved in 2 mL $CH_2Cl_2$, then quickly filtered through Celite, which left some of the red crystals behind as they were not very soluble. The filtrate was pumped down, then redissolved in 1 mL $CH_2Cl_2$ and layered with pentane. The next day, the mother liquor was decanted from the recrystallization, and the colorless crystals were transferred to a separate vial and dried *in vacuo*, giving the product (39 mg, 0.078 mmol, 25% crystalline yield) as $(^tBuNC)_2Pd(TFA)_2$. $^1H$ NMR (400 MHz, $CDCl_3$) δ 1.57 (s, 18 H, $(H_3C)_3C$-). $^{13}C\{^1H\}$ NMR (126 MHz, $CDCl_3$) δ 162.06 (q, 2C, $^3J_{C\text{-}F}$ = 37 Hz, -$O_2CCF_3$), 115.18 (q, 2C, $^2J_{C\text{-}F}$ = 290 Hz, -$O_2CCF_3$), 108.21 (m, 2C, $(CH_3)_3CNC$-), 61.29 (s, 2C, $(H_3C)_3CNC$-), 29.85 (s, 6C, $(H_3C)_3CNC$-). $^{19}F\{^1H\}$ (376 MHz, $CDCl_3$) δ 73.59. FT-IR ($\nu_{CN}$, $cm^{-1}$, ATR) 2272, 2255. Anal. Calcd. for ($C_{14}H_{18}PdN_2O_4F_6$): C, 33.72; H, 3.64; N, 5.62. Found: C, 33.80; H, 3.35; N, 5.60.

## III. Reactivity Studies

### A. General Procedure for Collection of $Pd_2(dba)_3$-Catalyzed Aerobic C–H Imidoylation Initial Rate Kinetic Data

A 0.50 mL aliquot of a stock solution of *N*-methoxybenzamide, $^t$BuNC, and anisole internal standard in dioxane was injected into a thick-walled test tube contained within a 48-well orbital shaker under air. After heating the substrate solution from room temperature to 60 °C and agitating at 60 °C for at least 10 minutes, a 0.50 mL aliquot of a stock solution of $Pd_2(dba)_3$•$CHCl_3$ in dioxane was added. Aliquots were withdrawn and added to room temperature $CH_3CN$, then the product was quantified by HPLC (UV detection). For initial rate data collected under $O_2$, the 48-well orbital shaker was purged with $O_2$ for five minutes at room temperature after the substrate stock solution was added to the thick-walled test tube.

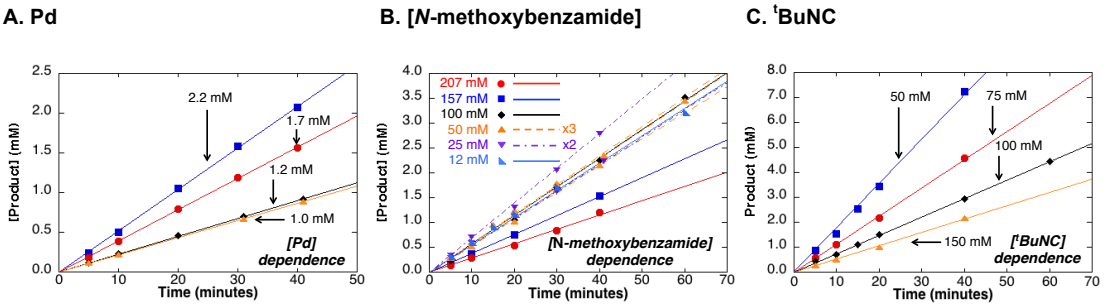


**Figure S1**. Time courses for product formation at varying concentrations of (A) [Pd] (B) [*N*-methoxybenzamide] (C) [$^t$BuNC]. Standard conditions were employed, except for the concentration of the component being varied. These are the raw data for Figure 1 in the manuscript.

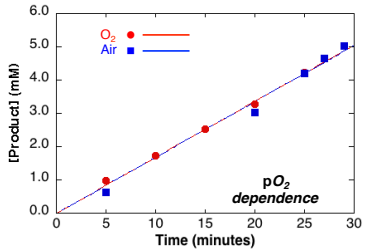


**Figure S2**. Time courses for product formation at varying $pO_2$. Standard conditions were employed (as in Figure 1), except for the $O_2$ pressure.

*KIE $k_H/k_D$ Determination*

To separate thick-walled test tubes contained within a 48-well shaker under air was added 0.50 mL of a solution of *N*-methoxybenzamide (0.100 M)/anisole (0.099 M) in dioxane or 0.50 mL of a solution of *N*-methoxybenzamide-$d_5$ (0.100 M)/anisole (0.099 M) in dioxane. After heating from room temperature to 60 °C and agitating at 60 °C for 10 minutes, a 0.50 mL aliquot of a freshly prepared stock solution of $Pd_2(dba)_3$•$CHCl_3$ (0.0022 M) and $^t$BuNC (0.30 M) in dioxane was added to each test tube. Aliquots were

withdrawn from each reaction and added to room temperature $CH_3CN$, then analyzed by HPLC (UV detection). The data are plotted in Figure 3 of the manuscript.

**B. Procedure for Collection of Pd-Catalyzed Aerobic C–H Imidoylation NMR Time Courses**

Solid *N*-methoxy-4-fluorobenzamide (136.8 mg, 0.81 mmol) and a magnetic stir bar were added to a 25 mL three-neck round bottom flask. Then, a glass stopper was added to one of the side necks, and a 19/22-14/20 adapter and reflux condenser were added to the middle neck. A solution of $^t$BuNC (137.5 μL, 1.22 mmol) and 3-fluorotoluene (90.0 μL, 0.81 mmol) in 4.0 mL dioxane was added to the round bottom flask, the top of the condenser and the other side neck were sealed with septa and copper wire, and a ~500 mL air or $O_2$ balloon was added to the top of the reflux condenser. The flask was immersed in an oil bath preheated to 65 °C and stirred for one hour with water circulation in the reflux condenser, then 4.0 mL of a freshly prepared catalyst stock solution (26.2 mg $Pd_2(dba)_3 \bullet CHCl_3$, 0.025 mmol, 5.0 mM [Pd] in 5.0 mL dioxane) was injected. Aliquots were withdrawn, injected into an NMR tube, and then stored, frozen, in a refrigerator. Later, the aliquots were thawed for $^1$H NMR spectral analysis. Reactions catalyzed by $Pd(OAc)_2$ and $Pd(OBz)_2$ were collected using the same procedure. Time courses of these reactions are plotted in Figure 8 of the manuscript, except for the $Pd_2(dba)_3$ reaction using $O_2$. The $Pd_2(dba)_3$ reactions time courses are plotted in Figure 2 of the manuscript and Figure S5. The raw data appear in Figures S3-S4 and S7-S8.

Reactions catalyzed by the Pd sources (($^t$BuNC)$_2$PdCl$_2$ or ($^t$BuNC)$_2$Pd(TFA)$_2$) were performed differently as follows. A solution of $^t$BuNC (133 μL, 1.18 mmol) and 3-fluorotoluene (90.0 μL, 0.81 mmol) in 8.0 mL dioxane was added to the reaction vessel containing *N*-methoxy-4-fluorobenzamide. The flask was immersed in an oil bath preheated to 65 °C and stirred for one hour open to the ambient atmosphere with water circulation in the reflux condenser, then the solid Pd source (0.040 mmol) was added through the top of the reflux condenser. The top of the condenser was sealed with a septum, and a ~500 mL air balloon was added. The NMR spectroscopic sample preparation and spectral acquisition were performed the same way. These reactions are plotted in Figure 8 of the manuscript. The raw data appear in Figures S9-S10.

The reaction with ($^t$BuNC)$_2$Pd($O_2$) **1** was performed differently as follows. A solution of $^t$BuNC (137.5 μL, 1.22 mmol), dibenzylideneacetone (14.0 mg, 0.060 mmol), and 4-methylanisole (102 μL, 0.81 mmol) in 8.0 mL dioxane was added to the reaction vessel containing *N*-methoxy-4-fluorobenzamide. The mixture was immersed in an oil bath preheated to 65 °C and stirred for five minutes. After five minutes, solid **2** (11.5 mg, 0.040 mmol) was added into the side neck, and the side neck was sealed with a septum and a copper wire. The NMR spectroscopic sample preparation and spectral acquisition were performed the same way. This reaction is plotted in Figure 8 of the manuscript. The raw data appear in Figure S6.

The reaction with **2** was performed in the same manner as the reaction with **1** except that no dba was used. The time course of product concentration is plotted in Figure S12. The raw data appear in Figure S11.

## C. Time Course Data for Oxidative Imidoylation Catalyzed by $Pd_2(dba)_3$

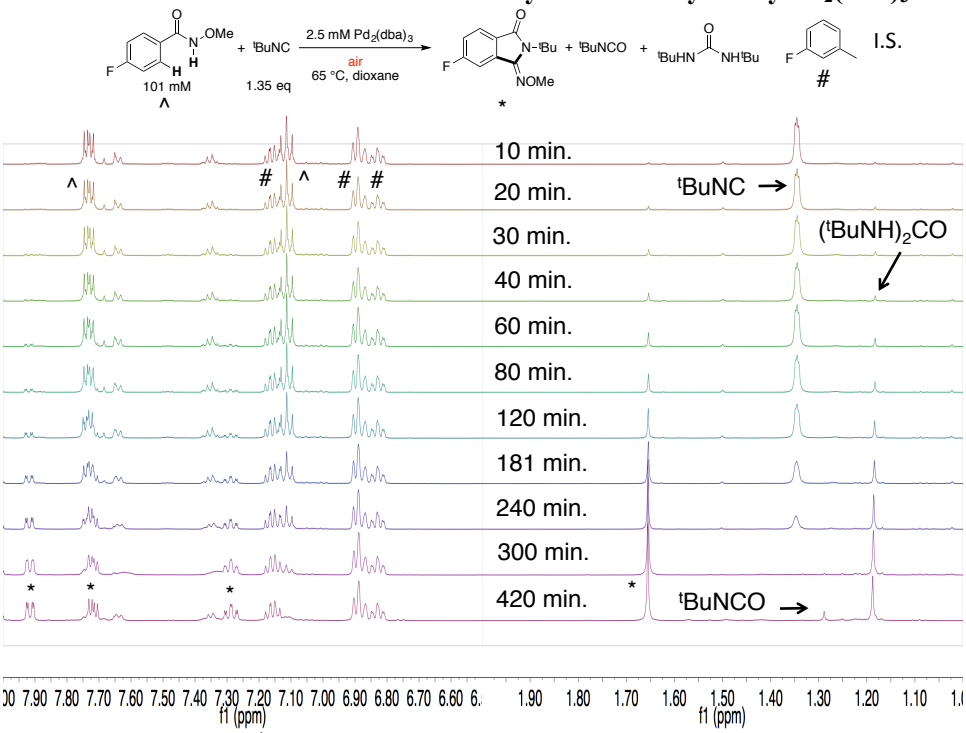


**Figure S3**. Stacked $^1$H NMR time-course spectra obtained from oxidative imidoylation catalyzed by $Pd_2(dba)_3$ under air. Reagents and products are indicated with symbols shown in the equation above the spectra. Conditions are the same as in Figures 2, 8, and S5.

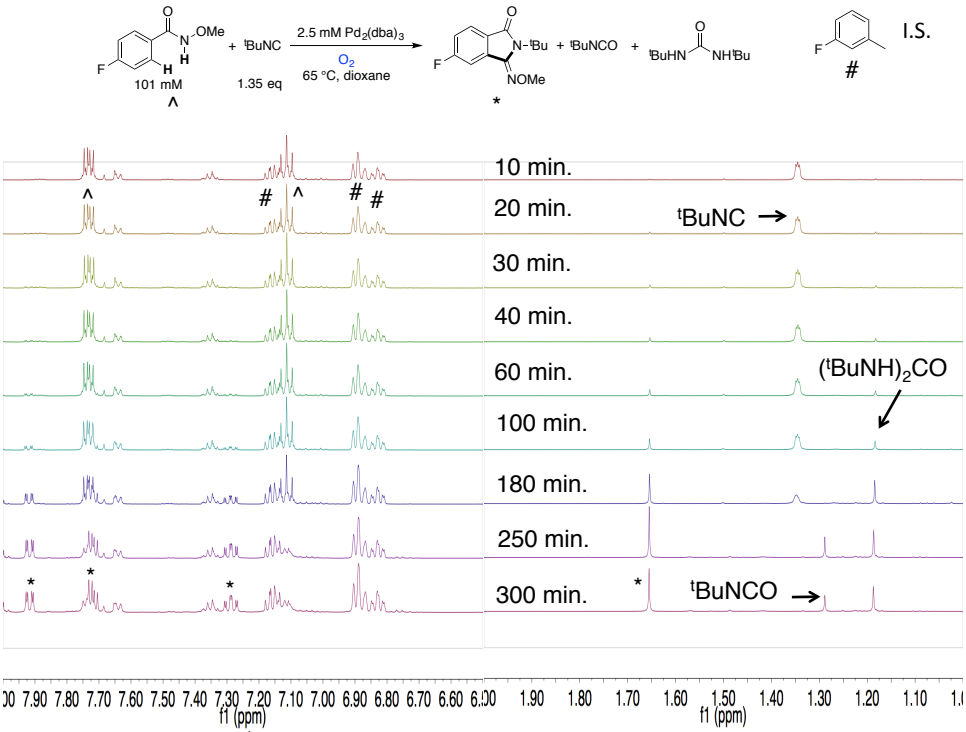


**Figure S4**. Stacked $^1$H NMR spectral time course of the reaction catalyzed by $Pd_2(dba)_3$ under 1 atm $O_2$ with starting materials and products labeled. Conditions are the same as in Figures 2 and S5.

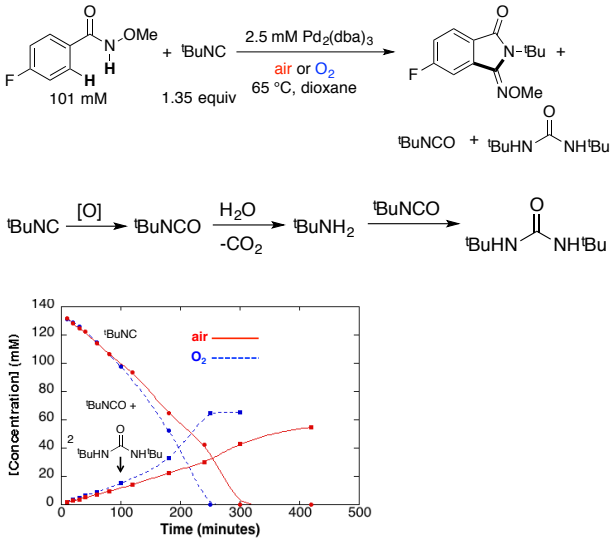


**Figure S5**. Time courses of $^t$BuNC consumption and total oxidized $^t$BuNC products, weighted by the number of $^t$BuNC molecules needed to form the product as shown by the hypothesized mechanism in Eq 1. Reaction conditions are the same as in Figure 2: [*N*-methoxy-4-fluorobenzamide] = 101 mM (0.81 mmol), [$^t$BuNC] = 153 mM (1.22 mmol), [Pd] = 5.0 mM (0.020 mmol $Pd_2(dba)_3$•$CHCl_3$), air or $O_2$ balloon, $V_{total}$ = 8.0 mL, dioxane, 65 °C, Int. St. = 3-fluorotoluene. The dashed grey line represents the concentration of starting material.

## D. Time Course Data for Oxidative Imidoylation Catalyzed by $PdX_2$ Sources

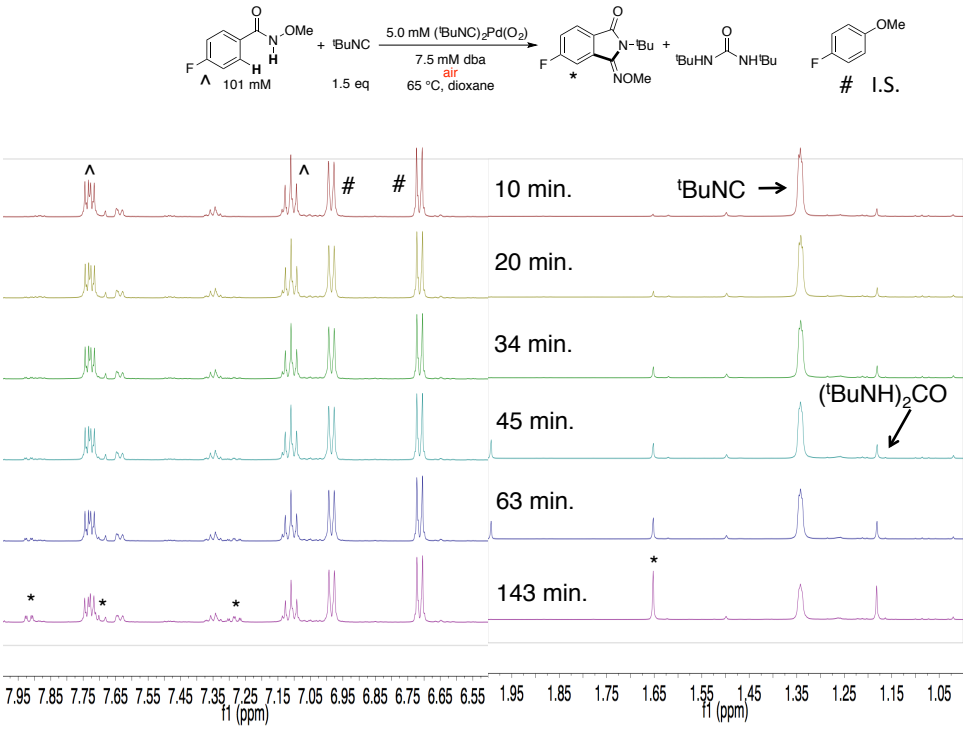


**Figure S6**. Stacked $^1$H NMR time-course spectra obtained from oxidative imidoylation catalyzed by ($^t$BuNC)$_2$Pd($O_2$) **1** under air. Reagents and products are indicated with symbols shown in the equation above the spectra. Conditions are the same as in Figure 8.

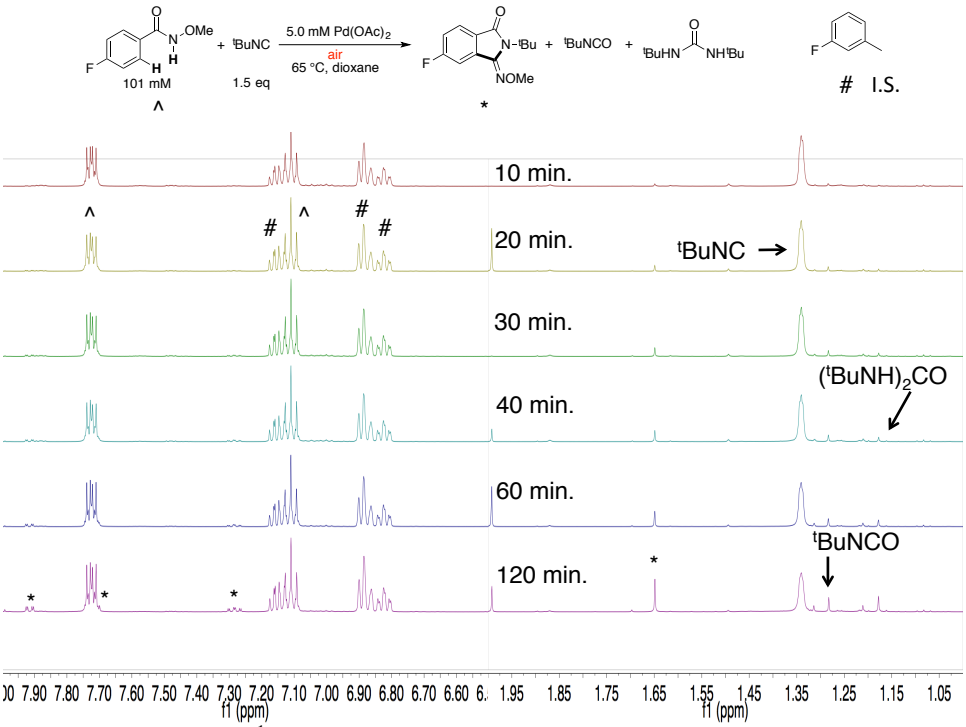


**Figure S7**. Stacked $^1$H NMR time-course spectra obtained from oxidative imidoylation catalyzed by $Pd(OAc)_2$ under air. Reagents and products are indicated with symbols shown in the equation above the spectra. Conditions are the same as in Figure 8.

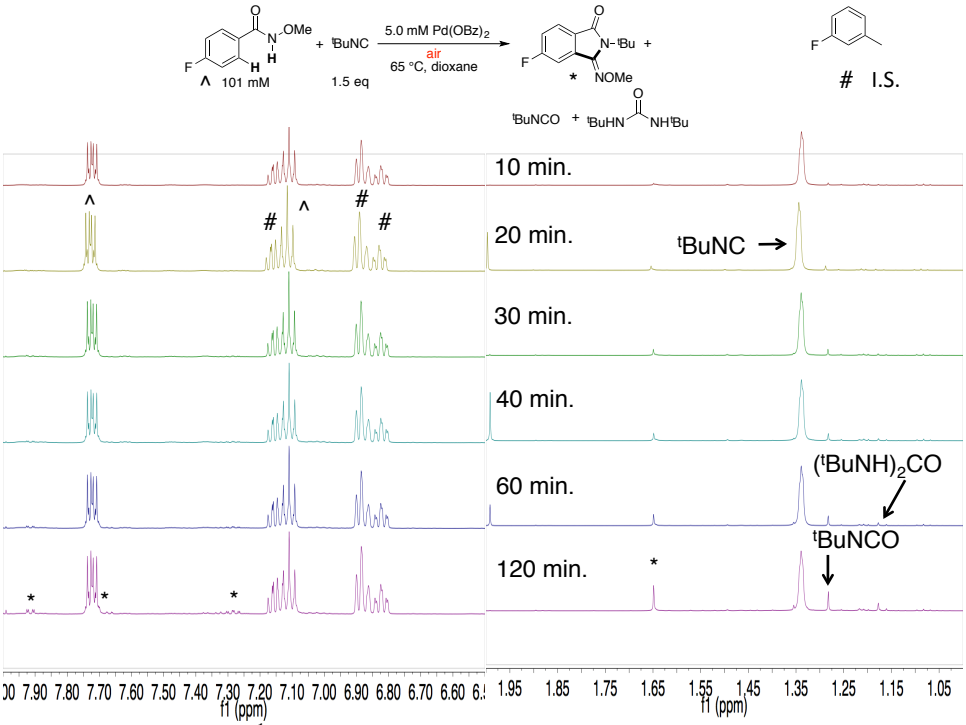


**Figure S8**. Stacked $^1$H NMR time-course spectra obtained from oxidative imidoylation catalyzed by $Pd(OBz)_2$ under air. Reagents and products are indicated with symbols shown in the equation above the spectra. Conditions are the same as in Figure 8.

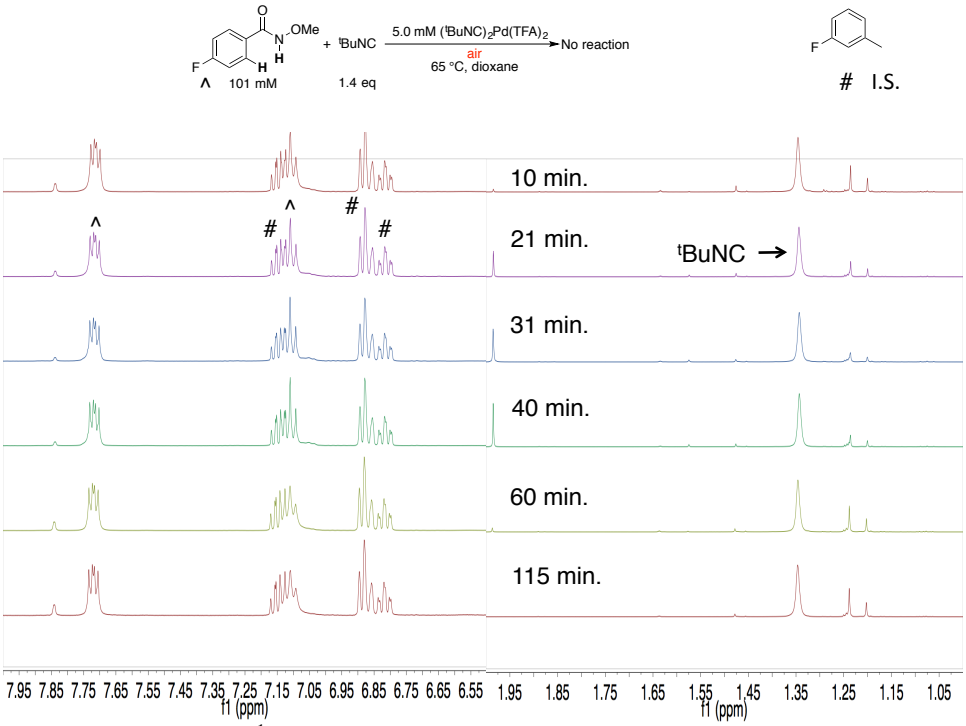


**Figure S9**. Stacked $^1$H NMR time-course spectra obtained from oxidative imidoylation catalyzed by $(^t\text{BuNC})_2\text{Pd(TFA)}_2$ under air. Reagents and products are indicated with symbols shown in the equation above the spectra. Conditions are the same as in Figure 8.

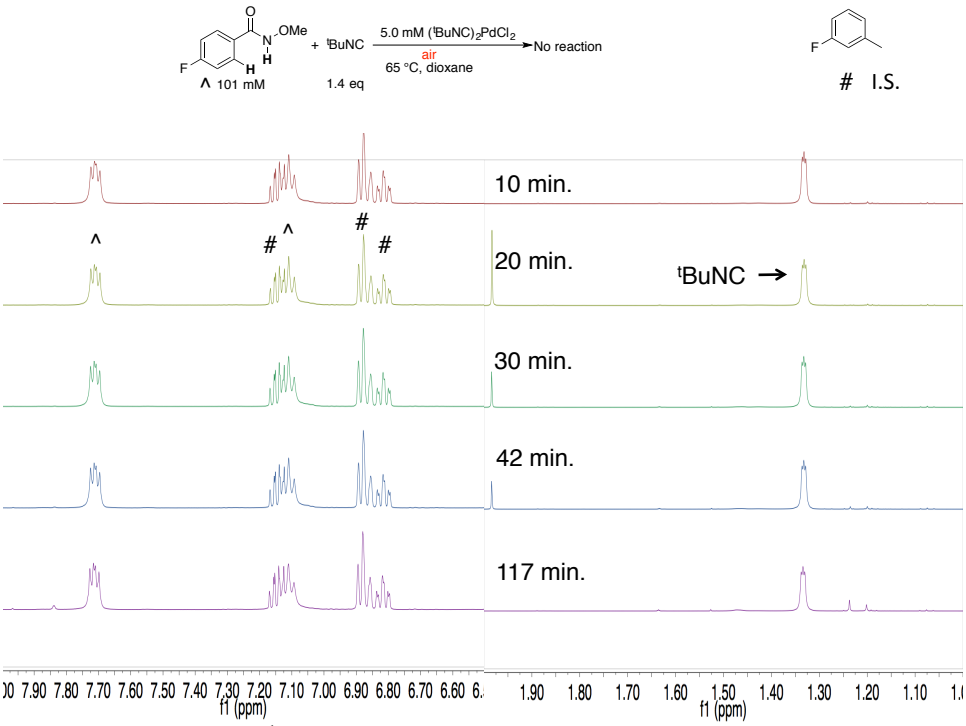


**Figure S10**. Stacked $^1$H NMR time-course spectra obtained from oxidative imidoylation catalyzed by $(^t\text{BuNC})_2\text{PdCl}_2$ under air. Reagents and products are indicated with symbols shown in the equation above the spectra. Conditions are the same as in Figure 8.

## E. Time Course Data for Oxidative Imidoylation Mediated by ($^t$BuNC)$_2$Pd(C~N) 2

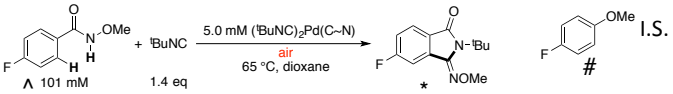


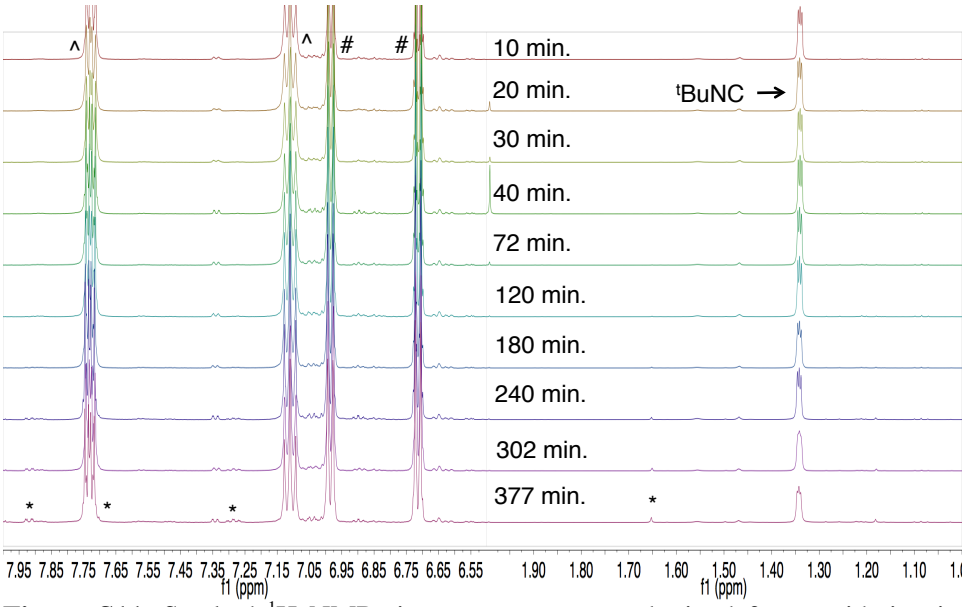


**Figure S11**. Stacked $^1$H NMR time-course spectra obtained from oxidative imidoylation catalyzed by ($^t$BuNC)$_2$Pd(C~N) **2** under air. Reagents and products are indicated with symbols shown in the equation above the spectra. Conditions are the same as in Figure S12.

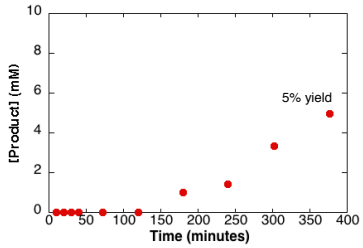


**Figure S12**. Time course of oxidative imidoylation catalyzed by ($^t$BuNC)$_2$Pd(C~N) **2** under air. [*N*-methoxy-4-fluorobenzamide] = 101 mM (0.81 mmol), [$^t$BuNC] = 153 mM (1.22 mmol), [**2**] = 5.0 mM (0.040 mmol), open to air, $V_{total}$ = 8.0 mL, dioxane, 65 °C, Int. Sd. = 4-methylanisole. The low yield and induction period together suggest that **2** is not an on-cycle intermediate.

## F. Investigations of the $O_2$:Product Stoichiometry and the Fate of $H_2O_2$

*(1) Determination of $O_2$:Product Stochiometry via Gas Uptake/NMR Analysis*

A stock solution of $Pd_2(dba)_3$•$CHCl_3$ (52.4 mg, 0.0506 mmol, 5.06 mM) in 10.0 mL dioxane was prepared. A substrate stock solution was prepared using *N*-methoxy-4-fluorobenzamide (340 mg, 2.01 mmol, 201 mM), $^t$BuNC (340 µL, 3.01 mmol, 301 mM, and 5-fluoro-*m*-xylene (100 µL, 0.792 mmol, 79.2 mM) in 10.0 mL dioxane. A 25 mL round bottom flask containing a magnetic stir bar was connected to a volume-calibrated gas uptake apparatus and immersed in an oil bath at a controlled temperature of 65 °C. The flask was evacuated and backfilled with $O_2$ 10 times and then filled to the desired $O_2$ pressure. 1.0 mL of the substrate stock solution was then added. The flask was allowed to equilibrate at 65 °C. Then, 1.0 mL of the catalyst stock solution was injected into the flask containing the substrate. Gas-uptake data were acquired using custom software written within LabVIEW. After the reactions were complete, the product yields were assessed by $^1$H and $^{19}$F{$^1$H} NMR spectroscopies. The quantities of oxidized products were compared to measured $O_2$ uptake and theoretical $O_2$ uptake (Table S1).

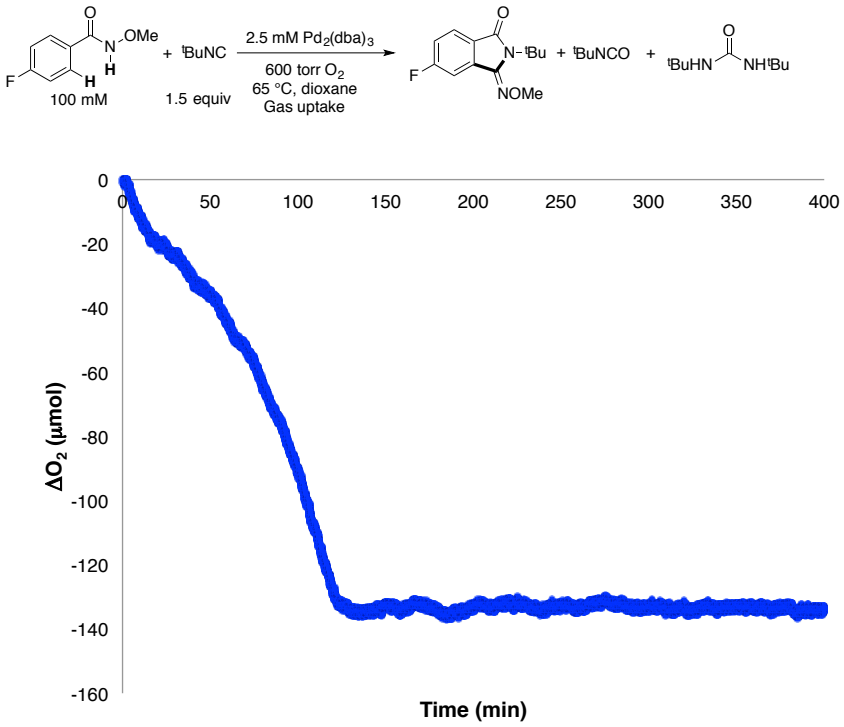


**Figure S13**. Plot of $O_2$ uptake of the Pd-catalyzed C–H imidoylation of 4-fluoro-*N*-methoxybenzamide at 600 torr $pO_2$.

**Table S1**. Comparison of $O_2$ uptake to theoretical $O_2$ uptake[a] and quantities of oxidized products[b].

| Measured $O_2$ Uptake (μmol) | Theoretical $O_2$ Uptake (μmol)[a] | Iminoisoindolinone (μmol) | $^t$BuNCO (μmol) | 2x($^t$BuNH)$_2$CO (μmol)[c] | Total Oxidized Products (μmol) |
|---|---|---|---|---|---|
| 134 | 139 | 84 | 126 | 68 | 278 |

(a) This value was computed assuming all four oxidizing equivalents of $O_2$ were consumed in substrate oxidation.. (b) These were determined using NMR spectroscopy via integration against the 5-fluoro-*m*-xylene internal standard. (c) The amount of di-*t*-butyl urea is doubled because two equivalents of oxidized $^t$BuNC are needed to make one equivalent of the urea.

*(2) Attempted Detection of $H_2O_2$ Following a C–H Imidoylation Reaction*

A reaction was run in the same way as the procedure used to acquire the data in Figure S3, except that aliquots were not taken before the reaction was stopped. After 7 hours, the reaction was removed from the oil bath, and an aliquot was taken. The yield was 35% as determined using NMR spectroscopy. Then, the concentration of $H_2O_2$ was determined using a method modified from that of Karlin and Solomon.[8] 10 mL $H_2O$ and 40 mL ethyl acetate were added to the reaction solution, and the resulting aqueous layer was recovered. 2.0 mL of the aqueous layer was diluted with 18 mL $H_2O$. Then, to 4.0 mL of the diluted aqueous solution was added 0.2 mL of a 15 wt% Ti(O)($SO_4$) solution in $H_2SO_4$ (Aldrich). The absorbance at 405 nm of this solution was compared to that of 4.0 mL of the diluted aqueous solution in which 0.2 mL of $H_2O$ had been added. The difference in absorbance between the two solutions at 405 nm was only 0.0086 (0.024 mM $H_2O_2$), which corresponds to less than 1% of the theoretical value if none of the $H_2O_2$ had reacted (as ascertained using a calibration curve developed via serial dilutions of a solution of $H_2O_2$-urea in DMF).

*(3) Analysis of $H_2O_2$ Disproportionation under C–H Imidoylation Conditions*

A stock solution of *N*-methoxy-4-fluorobenzamide (171 mg, 1.01 mmol, 202 mM), $^t$BuNC (170 µL, 1.51 mmol, 151 mM), and methyl 4-trifluoromethylbenzoate (50 µL, 0.311 mmol, 62.1 mM) in 5.0 mL dioxane was prepared along with a stock solution of $Pd_2(dba)_3$•$CHCl_3$ (26.2 mg, 0.0253 mmol, 2.53 mM) in 5.0 mL dioxane. Four 25 mL round bottom flasks each containing a magnetic stir bar were connected to a multiwell volume-calibrated gas uptake apparatus and immersed in an oil bath at a controlled temperature of 55 °C. The flasks were evacuated and backfilled with $O_2$ 10 times and then filled to 453 torr $pO_2$. 1.0 mL of the substrate stock solution was then added to three of the flasks, and 2.0 mL dioxane was added to the fourth flask (control well). The flasks were allowed to equilibrate at 55 °C. Then, 1.0 mL of the catalyst stock solution was injected into each of the flasks containing the substrate. Data were acquired using custom software written within LabVIEW. Essentially no uptake was observed at 55 °C, so the reactions were heated to 65 °C. After 75 min at 65 °C, 35 µL of water or aqueous $H_2O_2$ was injected into two of the reaction wells [water (35 µL, 1.94 mmol); 33.5 wt% aqueous $H_2O_2$ (35 µL, 0.383 mmol in $H_2O_2$)]. A pressure spike was observed upon the injection into these two flasks. The pressure spike for the $H_2O_2$ injection was significantly greater than that observed from the water injection control (see Figure S14) and is attributed to $H_2O_2$ disproportionation. The quantity of gas evolved (approx. 0.140 mmol) corresponds to a 73% yield of $O_2$ (based on theoretical conversion of $H_2O_2$ into ½ $O_2$ + $H_2O$). The $H_2O_2$-containing reaction stopped consuming $O_2$, whereas the water reaction continued with a slow consumption of $O_2$. After the reactions were complete, the product yields were assessed by $^1$H and $^{19}$F{$^1$H} NMR spectroscopy (Table S2). The reaction into which $H_2O_2$ was injected has increased amounts of isonitrile oxidation, which is predominantly attributed to the $H_2O_2$ that did not undergo disproportionation (see Section III.G. below for further experiments focused on isonitrile oxidation). This analysis, in combination with the $O_2$ uptake data from Table S1, suggests that any $H_2O_2$ generated during the C–H imidoylation reaction will undergo competitive disproportionation (major) and isonitrile oxidation (minor).

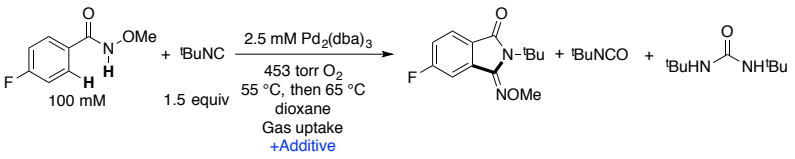


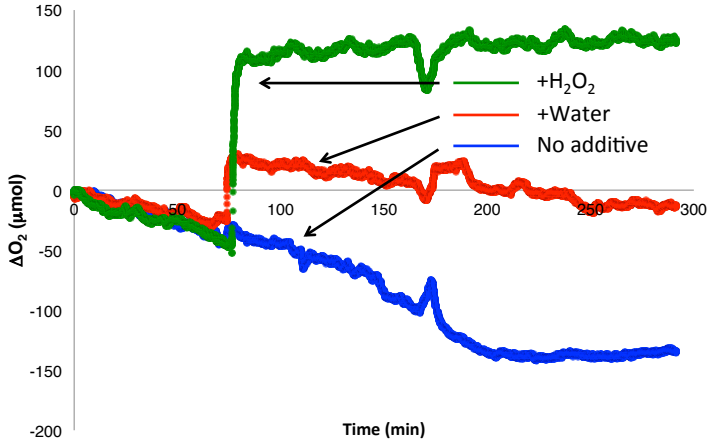


**Figure S14**. Plots of $O_2$ uptake of the Pd-catalyzed C–H imidoylation of *N*-methoxybenzamides with no additive (blue trace), water added during the run (red), or $H_2O_2$ added during the run (green). The reaction with added $H_2O_2$ shows a pressure spike which, after correcting for the pressure increase due to the solvent vapors, corresponds to 0.140 mmol $O_2$ evolved from disproportionation, or a 73% yield.

**Table S2**. Quantities of oxidized products and recovered $^t$BuNC with different additives as assessed by NMR spectroscopy.

| Additive | Iminoisoindolinone (μmol) | $^t$BuNCO (μmol) | 2x($^t$BuNH)$_2$CO (μmol) | Total Oxidized Products (μmol) | Recovered $^t$BuNC (μmol) |
|---|---|---|---|---|---|
| None | 92 | 64 | 80 | 236 | 0 |
| Water | 41 | 45 | 74 | 160 | 98 |
| $H_2O_2$ | 38 | 0 | 183 | 221 | 0 |

**G. Investigations of $^t$BuNC Oxidation**

*Control Experiment 1: Attempted Oxidation of $^t$BuNC without Pd under Aerobic Conditions*

A substrate stock solution was prepared using $^t$BuNC (340 μL, 3.01 mmol, 301 mM) and 5-fluoro-*m*-xylene (100 μL, 0.792 mmol, 79.2 mM) in 10.0 mL dioxane. A 25 mL round bottom flask containing a magnetic stir bar were connected to a multiwell volume-calibrated gas uptake apparatus and immersed in an oil bath at a controlled temperature of 65 °C. The flask was evacuated and backfilled with $O_2$ 10 times and then filled with 599 torr $O_2$. 1.0 mL dioxane was added to the flask, and the flask was allowed to equilibrate at 65 °C. Then, 1.0 mL of the substrate stock solution was injected into the flask containing 1.0 mL dioxane. Gas uptake data were acquired using custom software written within LabVIEW. Only trace isonitrile oxidation (based on $^1$H NMR spectroscopic analysis) and negligible $O_2$ uptake was detected during the 16 h reaction.

*Control Experiment 2: Attempted Oxidation of $^t$BuNC Using $H_2O_2$ without Pd*

A substrate stock solution was prepared using $^t$BuNC (340 μL, 3.01 mmol, 301 mM) and 3-fluorotoluene (225 μL, 2.02 mmol, 202 mM) in 10.0 mL dioxane. A stock solution of $H_2O_2$-urea (141.3 mg, 1.50 mmol, 300 mM) in 5.0 mL $D_2O$ was prepared. 4.0 mL of the substrate stock solution was added to a 25 mL 3-neck round bottom flask with a glass stopper on one of the side arms, a septum secured with copper wire on the other side arm, and an adapter and condenser on the middle arm of the flask with a septum secured with copper wire on the top of the condenser. A 500 mL air balloon attached to a piece of rubber tubing with a Leur lock and needle was placed on this septum. The flask was heated in an oil bath preheated to 65 °C for 15 minutes. Then, 4.0 mL of the $H_2O_2$ stock solution was injected through the side arm septum. Aliquots were taken at 15 minutes and one hour after $H_2O_2$ had been injected. The aliquots were interrogated using $^1$H NMR spectroscopy. No isonitrile oxidation was observed, based on $^1$H NMR spectroscopic analysis of the reaction mixture.

*Control Experiment 3:Pd-Catalyzed $^t$BuNC Oxidation under Aerobic Conditions*

A stock solution of $Pd_2(dba)_3$•$CHCl_3$ (52.4 mg, 0.0506 mmol, 5.06 mM) in 10.0 mL dioxane was prepared. A substrate stock solution was prepared using $^t$BuNC (340 μL, 3.01 mmol, 301 mM) and 5-fluoro-*m*-xylene (100 μL, 0.792 mmol, 79.2 mM) in 10.0 mL dioxane. A 25 mL round bottom flask containing a magnetic stir bar was connected to a volume-calibrated gas uptake apparatus and immersed in an oil bath at a controlled temperature of 65 °C. The flask was evacuated and backfilled with $O_2$ 10 times and then filled with 586 torr $O_2$. 1.0 mL of the substrate stock solution (300 μmol of substrate) was then added to the flask. The flask was allowed to equilibrate at 65 °C. Then, 1.0 mL of the catalyst stock solution was injected into the flask containing the substrate to initiate the reaction. Gas uptake data were acquired using custom software written within LabVIEW. Rapid gas uptake was observed, and the reaction was complete within approx. 10 min (i.e., much faster than the catalytic imidoylation reaction under similar reaction conditions in the presence of the benzamide substrate, which takes approximately 2 h to reach completion). Analysis of the reaction mixture by $^1$H NMR spectroscopy showed 100% conversion of the isonitrile, 88% of which led to the isocyanate or di-$^t$Bu-urea product.

*Control Experiment 4: Pd-Catalyzed $^t$BuNC Oxidation by $H_2O_2$*

A two-neck V-shaped flask was brought into the glovebox. 4.0 mL degassed dioxane was added to the flask along with a stir bar. The flask was sealed with two septa. A stock solution of $Pd_2(dba)_3$•$CHCl_3$ (52.4 mg, 0.0506 mmol, 5.06 mM) in 10.0 mL dioxane was prepared in a vial in the glovebox, and the vial was sealed with a rubber septum. These flask and vial were taken out of the glovebox. One of the two septa on the V-shaped vial was quickly replaced under $N_2$ flow by a ReactIR probe which had been inserted into a septum. Then, $^t$BuNC (135 µL, 1.19 mmol), $H_2O_2$ (110 µL, 33.5 wt% in water, 1.20 mmol), and methyl 4-trifluoromethylbenzoate (200 µL, 1.19 mmol) were added sequentially to the flask. After several minutes of stirring at 65 °C, the ReactIR data acquisition was started with scans every 15 seconds, and then 4.0 mL of the anaerobic $Pd_2(dba)_3$•$CHCl_3$ solution was injected. The reaction and data collection were stopped after one hour, at which point the reaction mixture was still homogeneous and orange. An aliquot was transferred under $N_2$ via syringe to an NMR tube capped with a septum. A $^1$H NMR spectrum was recorded to quantify the products of the reaction (Table S3). The total oxidized product yield was 77%. In order to facilitate analysis of the ReactIR reaction kinetics, a background spectrum of a mixture of dioxane and water (8 mL:110 µL) was subtracted from the reaction spectra. The IR data show that isonitile was consumed rapidly during the first 60 sec of the reaction (indicated by the decrease in intensity of the NC stretch of $^t$BuNC at 2133 $cm^{-1}$). Growth of a peak at 2252 $cm^{-1}$ assigned to the asymmetric NCO stretch of $^t$BuNCO was observed over the first minute after injection, and then a slow decline occurred over the next four minutes. The decrease in the concentration of $^t$BuNCO is attributed to hydrolysis of $^t$BuNCO, which releases $CO_2$ and $^t$BuNH$_2$, The $^t$BuNH$_2$ then reacts with another equivalent of $^t$BuNCO to form di-*t*-butyl urea, which was observed in the product $^1$H NMR spectrum. These results suggest that Pd-catalyzed oxidation of $^t$BuNC by $H_2O_2$ is rapid.

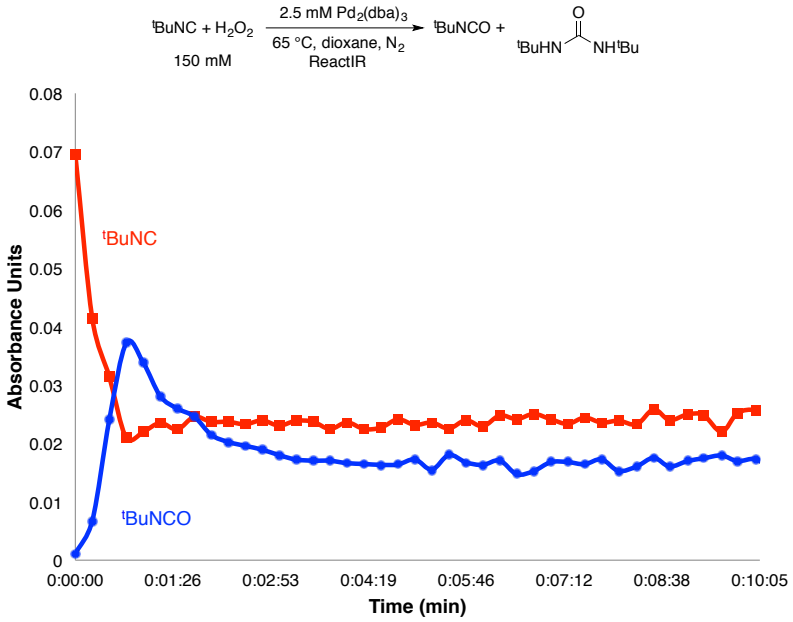


**Figure S15**. Plot of ReactIR peak intensities of the $^t$BuNC NC stretch and the $^t$BuNCO asymmetric NCO stretch following solvent background subtraction. The peak intensities were arbitrarily adjusted so that the $^t$BuNCO peak intensity was 0 at the start, and so that the $^t$BuNC peak intensity was slightly greater than the $^t$BuNCO peak intensity after the reaction had stopped.

**Table S3**. Quantities of oxidized products and $^t$BuNC from anaerobic Pd/$H_2O_2$ oxidation of $^t$BuNC as assessed by NMR spectroscopy.

| $^t$BuNCO (μmol) | 2x($^t$BuNH)$_2$CO (μmol) | Total Oxidized Products (μmol) | Recovered $^t$BuNC (μmol) |
|---|---|---|---|
| 225 | 792 | 1017 | 298 |

**H. Stoichiometric Reaction of ($^t$BuNC)$_2$Pd(O$_2$) (1) and *N*-methoxybenzamide.**

To a 50 mL round bottom flask were added a magnetic stir bar and **1** (53 mg, 0.18 mmol). A 10.0 mL solution containing 2.0 equiv *N*-methoxybenzamide (56 mg, 0.37 mmol), 2 equiv $^t$BuNC (41 μL, 0.36 mmol), and 0.68 equiv hexamethylbenzene internal standard (20 mg, 0.12 mmol) in dioxane was added to the round bottom flask with stirring at room temperature. After 10 minutes, the mixture was heated to 50 °C. After three hours of heating, the mixture was filtered through Celite, the volatiles were removed from the filtrate *in vacuo*, and an aliquot of the solid sample from the filtrate was redissolved in $CDCl_3$ for $^1$H NMR spectroscopic analysis. The NMR spectra are shown in Figures S17-S19.

This analysis revealed a 47% yield of 3-(*N*-methoxyimino)-*t*-butylisoindolinone (relative to *N*-methoxybenzamide) and 49% recovery of *N*-methoxybenzamide. Pd species were identified as follows: **3** (14% yield relative to **2**), **4** (30% yield relative to **2**), and **5** (3% yield relative to **2**). These results are summarized in Scheme 5 and Figure S16.

For the independent synthesis and $^1$H NMR spectroscopic characterization of **3**, see Section II. The proposed species **4** has been observed in $^1$H NMR spectra of crude reaction mixtures during the independent synthesis of **2** in $CDCl_3$ (Figures S17-S19). A key feature of this compound is that the integration of the *t*-butyl resonance relative to the methoxy resonance in $^1$H NMR spectra is consistent with only one $^t$BuNC ligand per Pd center. We propose **4** to be a dimer because only three ligands per Pd (two from the cyclopalladated substrate and one from $^t$BuNC, which we assume bridges two Pd) can be definitely identified.

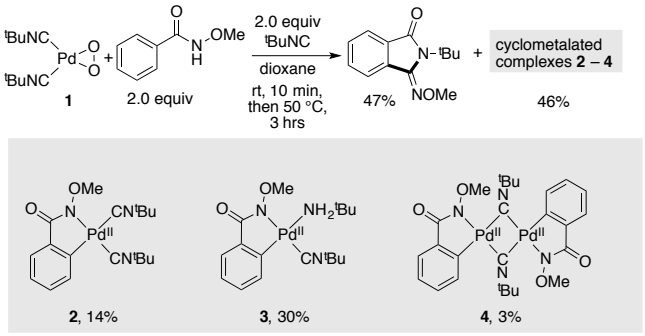


**Figure S16**. Reaction of ($^t$BuNC)$_2$Pd(O$_2$) **1** with *N*-methoxybenzamide to provide the iminoisoindolinone product and several cyclopalladated Pd$^{II}$ species.

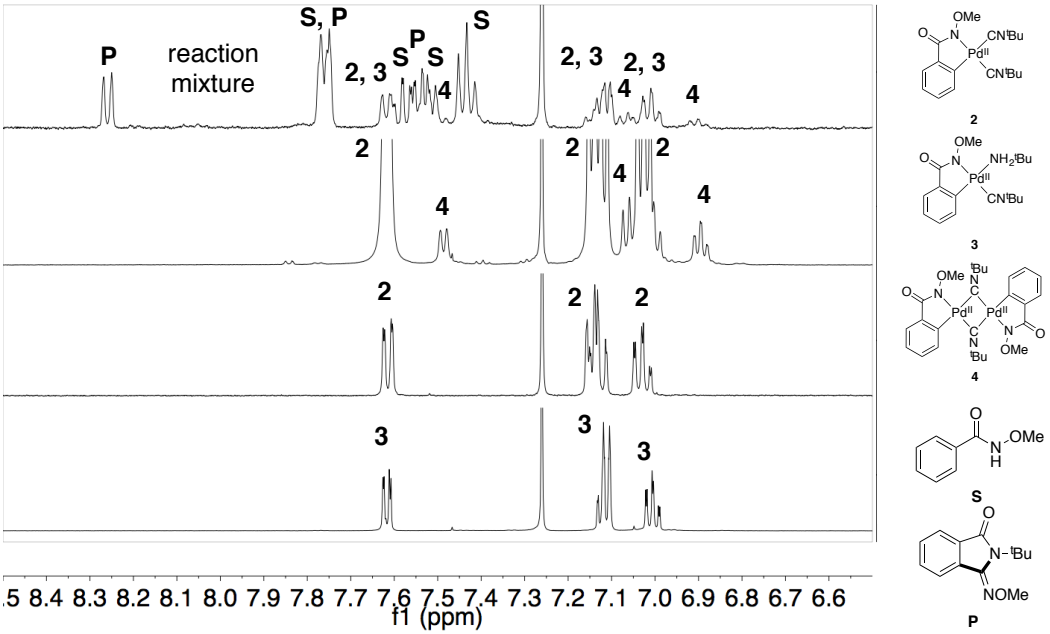


**Figure S17**. Aromatic region of the $CDCl_3$ $^1H$ NMR spectra of (top) the reaction mixture; (second from top) a mixture of **4** and **2**; (second from bottom) recrystallized **2**; and (bottom) crude **3**.

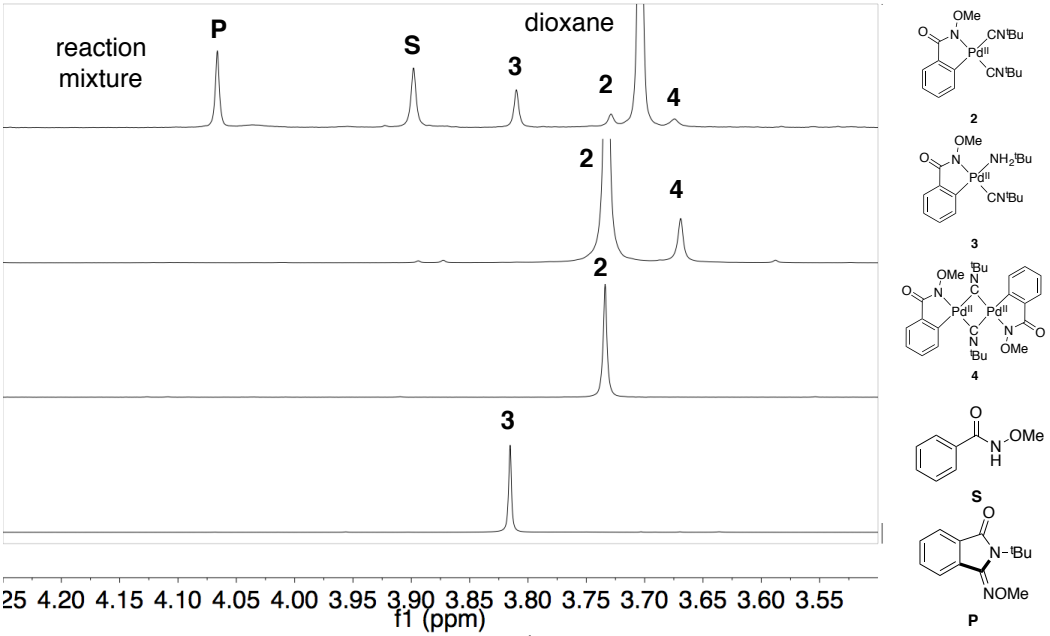


**Figure S18**. Methoxy region of the $CDCl_3$ $^1H$ NMR spectra of (top) the reaction mixture; (second from top) a mixture of **4** and **2**; (second from bottom) recrystallized **2**; and (bottom) crude **3**.

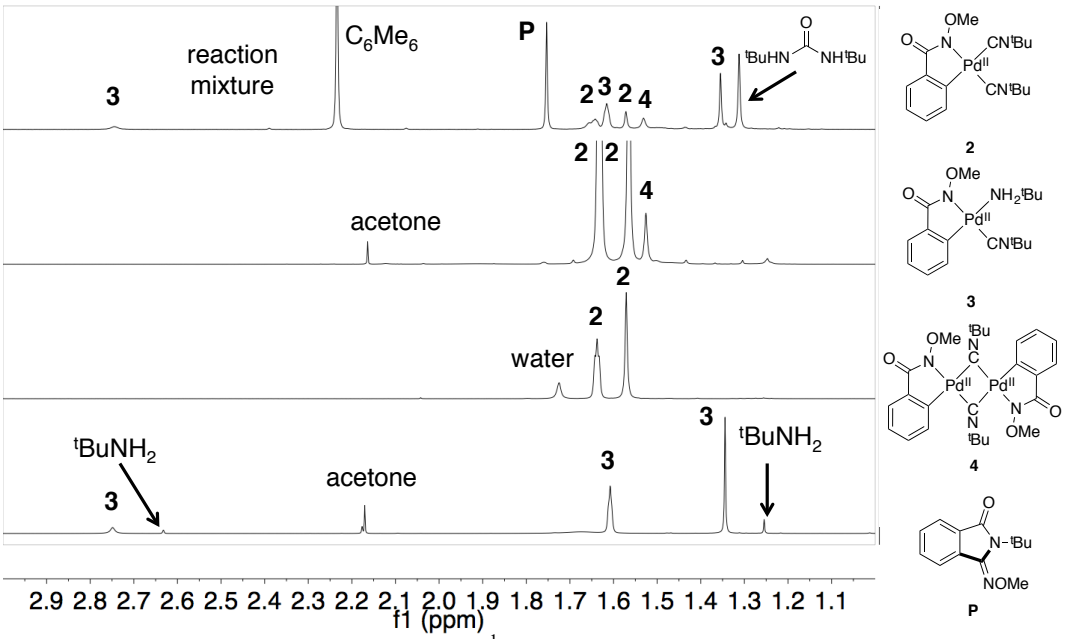


**Figure S19**. Methyl region of the $CDCl_3$ $^1H$ NMR spectra of (top) the reaction mixture; (second from top) a mixture of **4** and **2**; (second from bottom) recrystallized **2**; and (bottom) crude **3**.

## I. NMR Spectroscopic Analysis of the Catalytic Reaction Mixture and Comparison with the Reaction of ($^t$BuNC)$_2$Pd(O$_2$) (1) with HSub$^{4F}$ in the presence of $^t$BuNC

*Analysis of the Catalytic Reaction Mixture.* A catalyst stock solution was prepared by dissolving $Pd_2(dba)_3$•$CHCl_3$ in 0.50 mL dioxane (2.6 mg, 0.0025 mmol). The substrate stock solution was prepared, consisting *N*-methoxy-4-fluorobenzamide (68.0 mg, 0.402 mmol), $^t$BuNC (70.0 µL, 0.036 mmol), and 5-fluoro-*m*-xylene (20.0 µL, 0.158 mmol). 0.40 mL of each solution was mixed in a scintillation vial. From this mixure, 0.20 mL was dispensed via syringe into a thick-walled J. Young tube, which was subsequently pressurized with $O_2$ to a total pressure of 3.1 atm $O_2$. The reaction was monitored by $^1$H (Figure S20, top spectrum) and $^{19}$F{$^1$H} (Figure S21, top spectrum) NMR spectroscopies at 65 °C. The yield of product at the last time point is 29%, and the kinetic trace suggests smooth catalytic turnover throughout the period monitored (Figure S22).

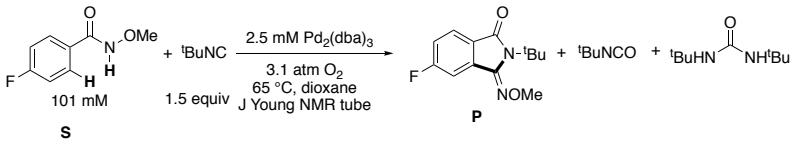

(S1)

*Reaction of ($^t$BuNC)$_2$Pd(O$_2$) (**1**) with HSub$^{4F}$ in the presence of $^t$BuNC.* To a round-bottom flask with a stir bar was added 5.0 mL of a stock solution of HSub$^{4F}$ (36.9 mg, 0.218 mmol), $^t$BuNC (115 uL, 1.02 mmol), and 3-fluorotoluene (40.0 uL, 0.360 mmol) (10.0 mL dioxane) as an internal standard. Then, a solid sample of the Pd-peroxo compound **1** (15.2 mg, 0.0499 mmol) was added. Most of **1** dissolved over the course of an hour. $^1$H and $^{19}$F NMR spectra of the reaction mixture are shown in Figures S20 and S21 (bottom spectrum in each figure). At least two new species are evident, each of which has chemically inequivalent aryl and $^t$Bu groups. These are tentatively assigned to ($^t$BuNC)$_2$Pd(amidinyl)(amidate) species, with two different rotameric forms of the amidate ligand. On the basis of this assignment, the yield of these species is 87%, with respect to **1**.

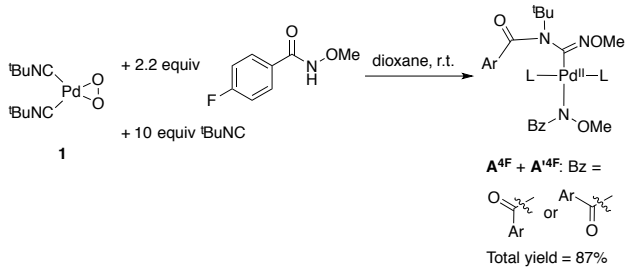

(S2)

The NMR spectra obtained from the catalytic reaction mixture show peaks that closely resemble those obtained from the stoichiometric reaction of the amide substrate and the Pd-peroxo compound **1**. Together with the *operando* XAS data, which supports a Pd$^{II}$ catalyst resting state, we propose that much of the Pd catalyst is pooled as the ($^t$BuNC)$_2$Pd(amidinyl)(amidate) species.

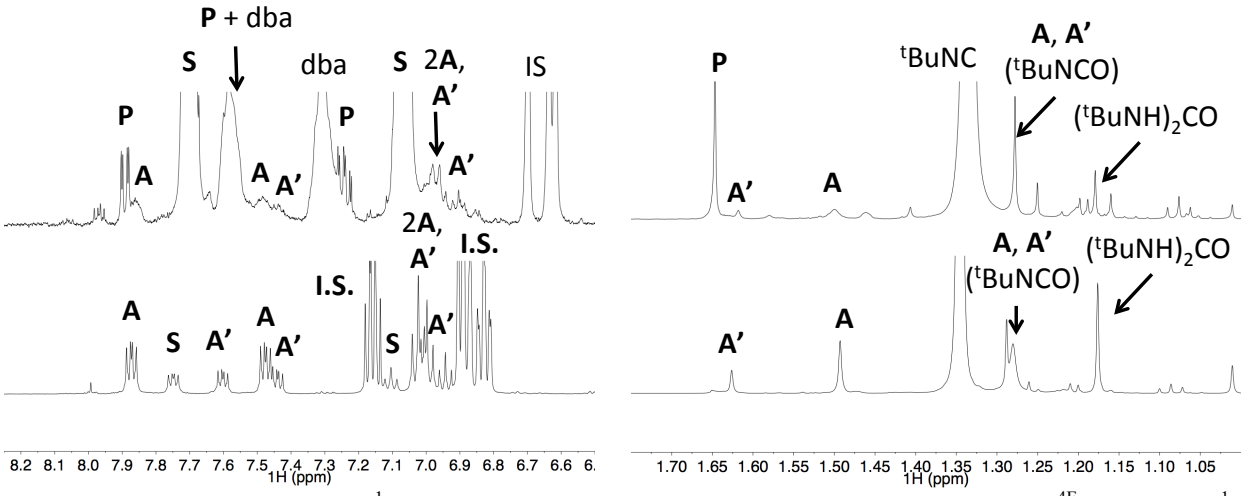


**Figure S20**. (Top) The in situ $^{1}$H NMR spectrum of the catalytic imidoylation of HSub$^{4F}$. (Bottom) $^{1}$H NMR spectrum of the reaction of **1**, HSub$^{4F}$, and $^{t}$BuNC after one hour. Species which are proposed to be the products **A** and **A'** depicted in eq S2 are labeled.

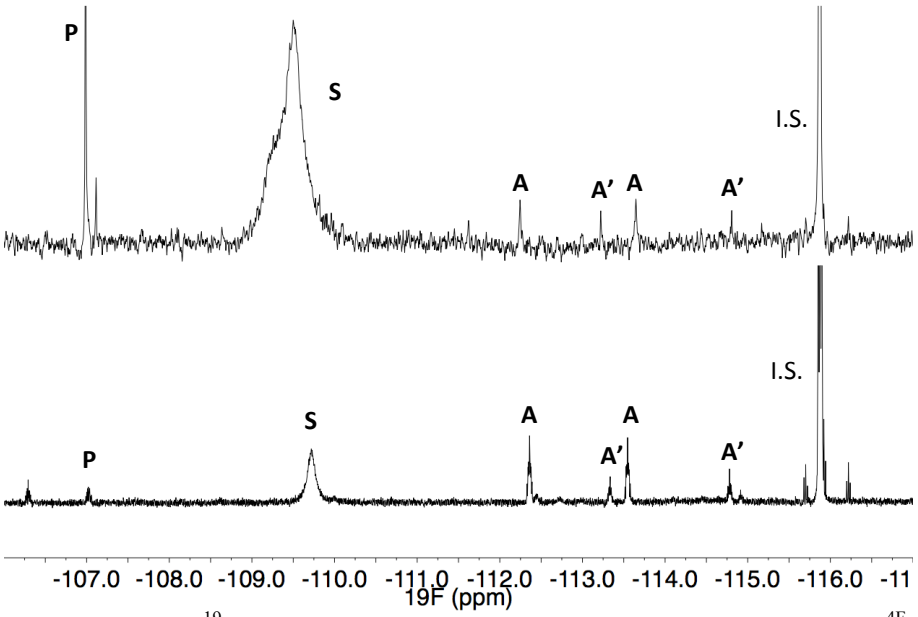


**Figure S21**. **(**Top) The in situ $^{19}$F NMR spectrum of the catalytic imidoylation of HSub$^{4F}$. (Bottom) $^{19}$F NMR spectrum of the reaction of **1**, HSub$^{4F}$, and $^{t}$BuNC after one hour. Species which are proposed to be the products **A** and **A'** depicted in eq S2 are labeled. Note that the spectrum shown on the bottom corresponds to a different sample than that shown in Figure S20 in order to facilitate comparison to the in situ spectrum against the same reference (in this case, 5-fluoro-*m*-xylene, at -115.88 ppm).

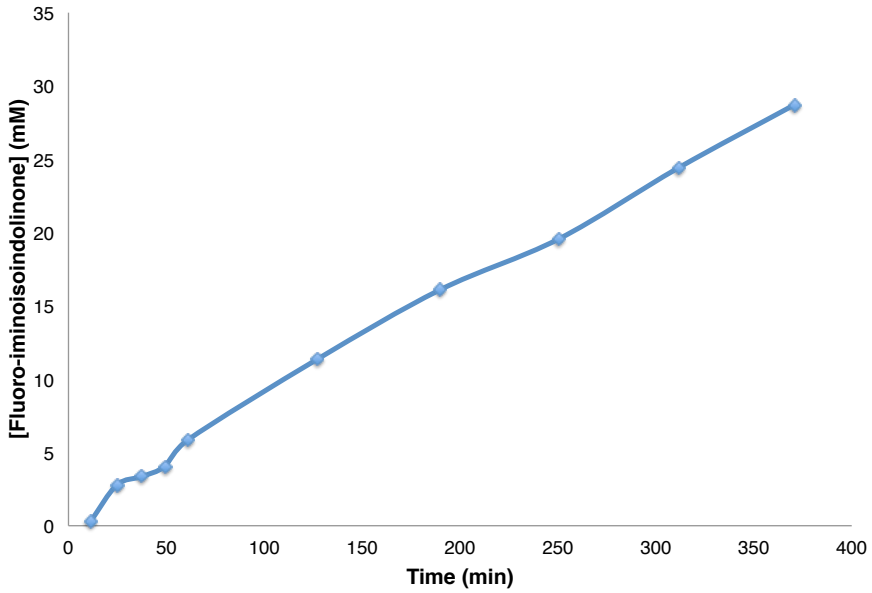


**Figure S22**. Time course of fluoroiminoisoindolinone product formation from the in situ J Young NMR experiment shown in eq S1. The concentration of each time point was determined from $^{19}$F NMR spectra.

**J. Procedure for Collection of ReactIR Data for Reaction of ($^t$BuNC)$_2$Pd(O$_2$) 1 with HSub$^{F2}$**

A two-neck flask containing a magnetic stir bar was placed in a dry ice-acetone bath contained in a dewar. **1** (32 mg, 0.11 mmol) was added to one of the two necks. To the other neck was added a solution of *N*-methoxy-2,6-difluorobenzamide in 2.0 mL dry $CH_2Cl_2$ (82 mg, 0.22 mmol, 0.11 M). To solid **1** was added 1.0 mL $CH_2Cl_2$ that had been precooled in a dry ice-acetone bath. The in situ IR spectrum of the Pd peroxo was then recorded. Then, the N-methoxy-2,6-difluorobenzamide solution was added to the Pd peroxo solution with stirring. Following this, the in situ IR spectrum of the reaction mixture was recorded, and the y axis in Figure 5B was scaled to account for the dilution. This data is shown in Figure 5 of the manuscript.

**K. Titration of ($^{tBu}$py)$_2$PdCl$_2$ with $^t$BuNC**

($^{tBu}$py)$_2$PdCl$_2$ (13.5 mg, 0.030 mmol) was added to an NMR tube. Then, the 3-fluorotoluene internal standard (4.0 µL, 0.036 mmol) and 0.60 mL $CDCl_3$ were added to the NMR tube, and the tube was capped and shaken. $^t$BuNC was titrated in (additions 1-2: 0.3 µL; additions 3-6: 0.6 µL; addition 7: 1.5 µL; additions 8-10: 2.7 µL). After each addition, the NMR tube was recapped and shaken prior to spectral acquisition. The spectra are shown in Figure S23. Figure 11 shows the analyzed results.

The mmol $^t$BuNC added was calculated based on the total integration of the $^t$BuNC-derived peaks, rather than the volume of $^t$BuNC added, as the NMR-derived values are likely more accurate due to the small $^t$BuNC volumes delivered in the experiment. Use of either method does not change the conclusions from the experiment.

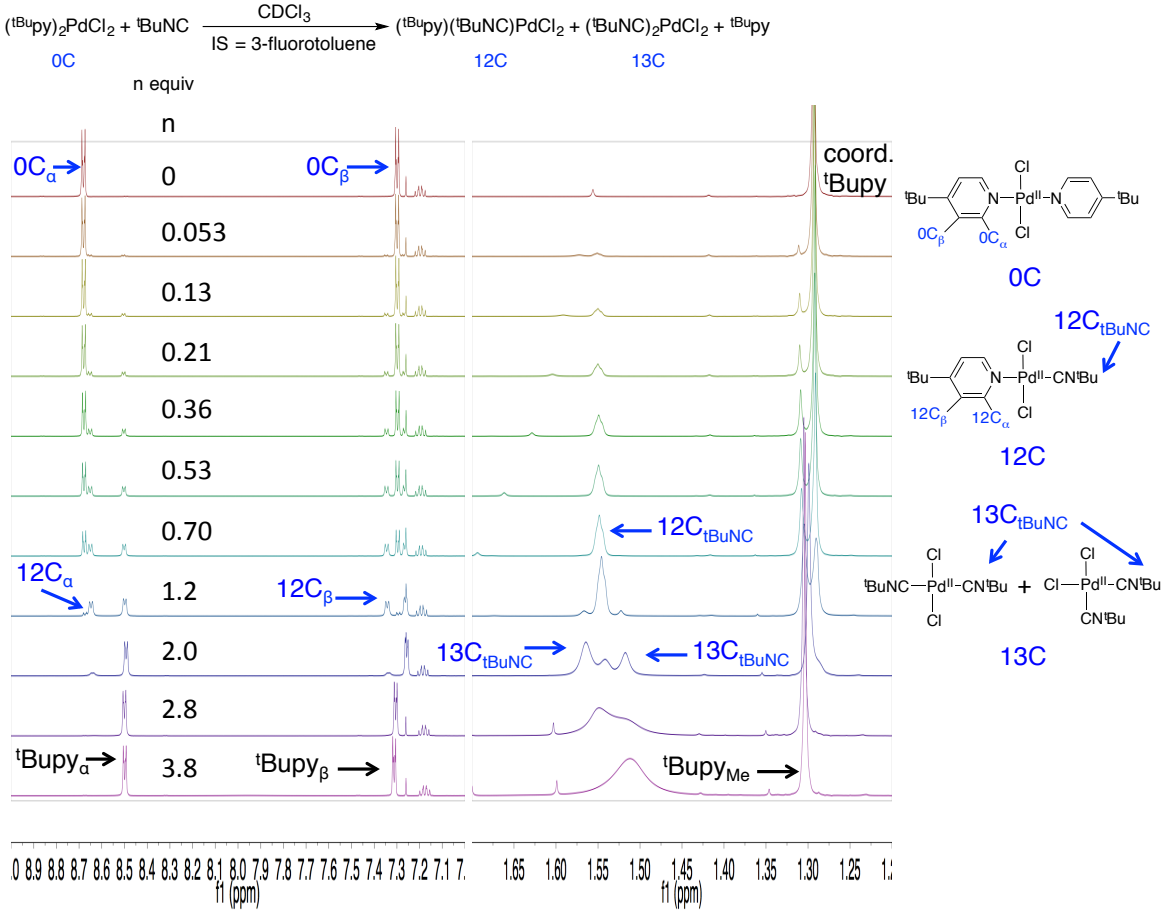


**Figure S23**. $^{1}$H NMR spectra of the titration of $(^{tBu}py)_2PdCl_2$ with $^{t}BuNC$.

**IV. X-Ray Absorption Spectroscopy Experimental Procedures, Spectral Processing, and Analysis**

*General Considerations for XAS Measurements*

Pd k-edge (E0 = 24352.6 eV) X-ray absorption measurements were conducted on the insertion device beamline (10-ID-B) of the Materials Research Collaborative Access Team (MRCAT) at the Advanced Photon Source (ring energy = 7.0 GeV) within Argonne National Laboratory, Argonne, IL, USA. Measurements were made in transmission quick scan mode. The experiments utilized a cryogenically cooled double-crystal Si(111) monochromator in conjunction with a glass coated mirror to minimize the presence of harmonics. The monochromator was scanned continuously ~200 eV lower in energy than the Pd k edge to ~900 eV higher in energy than the Pd k edge. Scans were taken with a Pd foil reference for energy correction during data analysis (see below).

*Homogeneous* Operando *Catalytic Measurement*

A solution of *N*-methoxybenzamide (60.6 mg, 0.20 M), $^{t}$BuNC (135 µL, 0.60 M), and anisole (44 µL, 0.20 M) in dioxane (2.0 mL total volume) was prepared, and 1.5 mL of this solution was transferred to a cylindrical PEEK reactor which contained a magnetic stirbar. The reactor was sealed with a septum and copper wire, and it was placed in an aluminum heating block with circulating ethylene glycol/water bath, sitting above a magnetic stir plate. A ~1.5 L air balloon was attached to the septum of the reactor, and the mixture was warmed to 60 °C with the bath. A solution of $Pd_2(dba)_3$•$CHCl_3$ (10.4 mg, 0.0050 M) in 2.0 mL dioxane was prepared. Then, 1.5 mL of this solution was injected into the reactor with the substrate solution.

At the beginning of the reaction, each data point came from a scan that lasted for ~0.063 seconds, and then later in the reaction, each data point came from a scan that lasted for ~0.56 seconds.

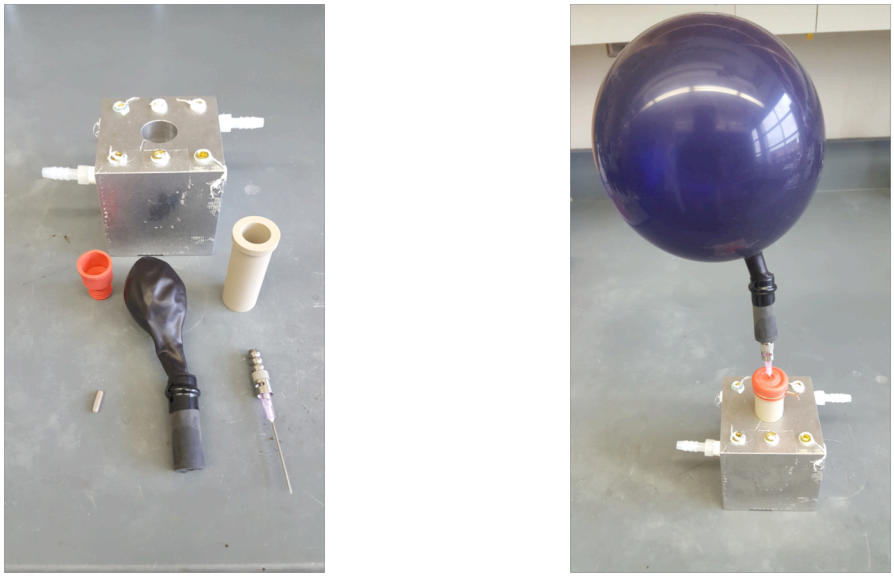

**Figure S24**. (Left) Individual components of the reactor and heating block used in the *operando* XAS experiments. Clockwise from the top: (a) the aluminum heating block with embedded water cooling line, (b) PEEK reactor cell, (c) needle with Luer lock adapter, (d) balloon secured to rubber tubing with electrical tape, (e) Teflon stir bar, (f) rubber septum. (Right) Components assembled together: the balloon is filled with air, and the septum is secured to the PEEK reactor with copper wire.

*Solid-State Reference Sample Preparation*

The reference compounds ($Pd_2(dba)_3$•$CHCl_3$, $Pd(TFA)_2$, or $[Pd^{I}(\mu\text{-}^{t}BuNC)(\mu\text{-}OBz)]_4$) and silica were crushed with a mortar and pestle to make an evenly dispersed sample that was 5 wt % in Pd. Each sample's powder was transferred to a different hole within a "six shooter" holder and pressed into a wafer. The sample holder was transferred to the 10-ID-B hutch and situated for sample measurement. Each data point came from a scan that lasted for ~0.56 seconds.

*XAS Spectral Processing and Analysis*

The program Athena[9] was used to process XANES spectra. The sample and Pd foil reference spectra were imported, and background removal and normalization was performed. Then, the Pd foil reference for every sample spectrum was energy corrected by selecting the maximum in the first derivative, finding the zero crossing in the second derivative, and setting the energy of the zero crossing to 24352.6 eV. The energy corrected Pd foil reference spectra were then "aligned." These actions put all the sample data on the same absolute energy grid for analysis purposes.

Several scans in the time course of the catalytic reaction (Figure S25) were further processed. The first three chronological spectra in the time course in Figure S25 are each two spectra collected at the beamline "merged" together, which was done to increase spectral quality. The first merged spectrum came from individual spectra taken 10 and 12 minutes after injection, the second merged spectrum came from individual spectra taken 15 and 17 minutes after injection, and the third merged spectrum came from individual spectra taken 22 and 30 minutes after injection.

As can be seen in Figure S25, the edge energy does not change until the very end of the experiment, which indicates that the catalyst resting state does not change during the reaction.

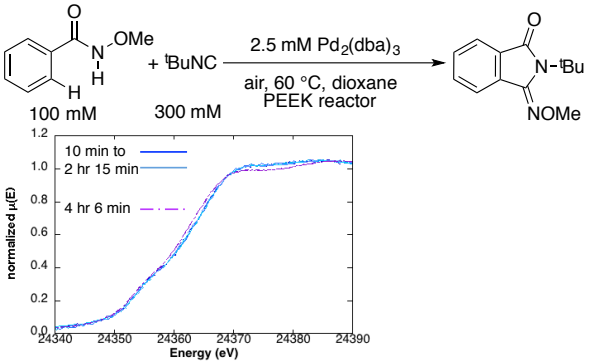


**Figure S25.** XANES spectra over the course of the catalytic imidoylation reaction. The figure includes the following time points: 11 minutes ("merge" of 10 and 12 minute spectra), 16 minutes (merge of 15 and 17 minute spectra), 26 minutes (merge of 22 and 30 minute spectra), 50 minutes, 1 hour 31 minutes, 2 hours 15 minutes, 3 hours 45 minutes, and 4 hours 6 minutes. All spectra have been referenced against Pd foil.

**V. Procedure, NMR Spectra, and Analyses of the Reactions of ($^{tBu}$py)$_2$PdX$_2$ (X = OAc, OBz, TFA, Cl) with *N*-methoxy-2,6-difluorobenzamide.**

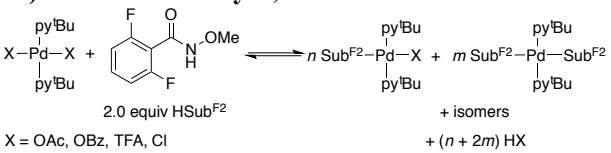


Solid ($^{tBu}$py)$_2$PdX$_2$ (0.0096 mmol) was weighed directly into a seven-inch NMR tube. Then, 0.60 mL of a stock solution of *N*-methoxy-2,6-difluorobenzamide (3.6 mg, 0.019 mmol) and 3-fluorotoluene (2.2 µL, 0.019 mmol) in $CDCl_3$ was added to the NMR tube, and the mixture was shaken until everything dissolved. NMR spectra were taken 90 minutes after mixing, 15 hours after mixing, and 38 hours after mixing. In the case of X = Cl, no reaction was observed by $^1$H and $^{19}$F NMR spectroscopy after 15 hours (Figures S62 and S63), and so the mixture was not monitored further. For the reactions with X = OAc, OBz, or TFA, the $^1$H and $^{19}$F NMR spectra 38 hours after mixing had barely changed from the 15 hour spectra, and so a variety of spectroscopies were collected to assess the solution speciation. These spectra are shown in Figures S26-S61.

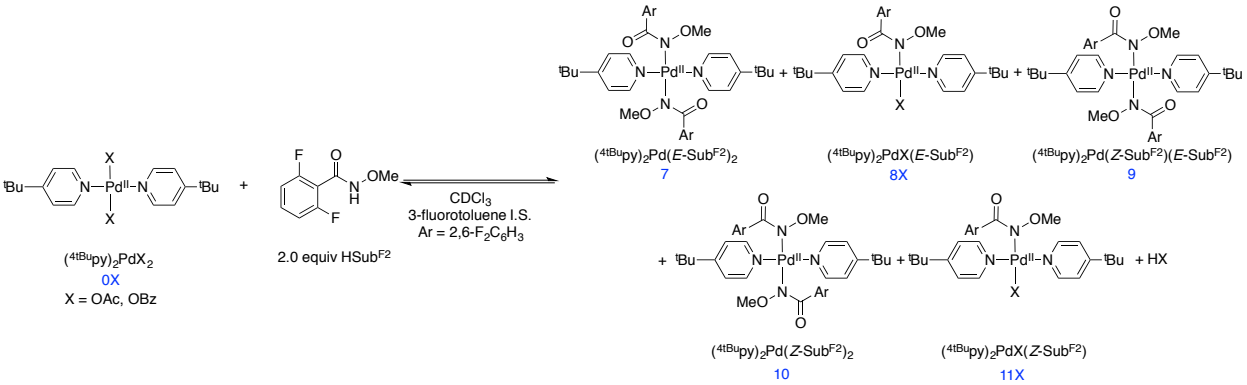


Based on the spectra of the reaction mixtures for X=OAc and X=OBz, we propose that (1) there are five Pd product species in these reactions, all of which have a *trans* geometry at Pd.[7] (2) In all five species, 4-t-butyl pyridine and amidate ligands are coordinated to Pd. (3) Two of the species contain bis-pyridine-mono-carboxylate-mono-amidate coordination spheres. (4) Three of the species contain bis-pyridine-bis-amidate coordination spheres. (5) Hindered rotation of the amide C–N bond leads to the existence of *cis* and *trans* isomerism in the amidate ligands.

For X=TFA, we propose that (1) there are two Pd product species. (2) Both of these Pd product species contain bis-pyridine-mono-trifluoroacetate-mono-amidate coordination spheres, one of which has a *trans* geometry at Pd and one of which has a *cis* geometry at Pd. For X=Cl, there is no reaction within the detection limits of the NMR measurements.

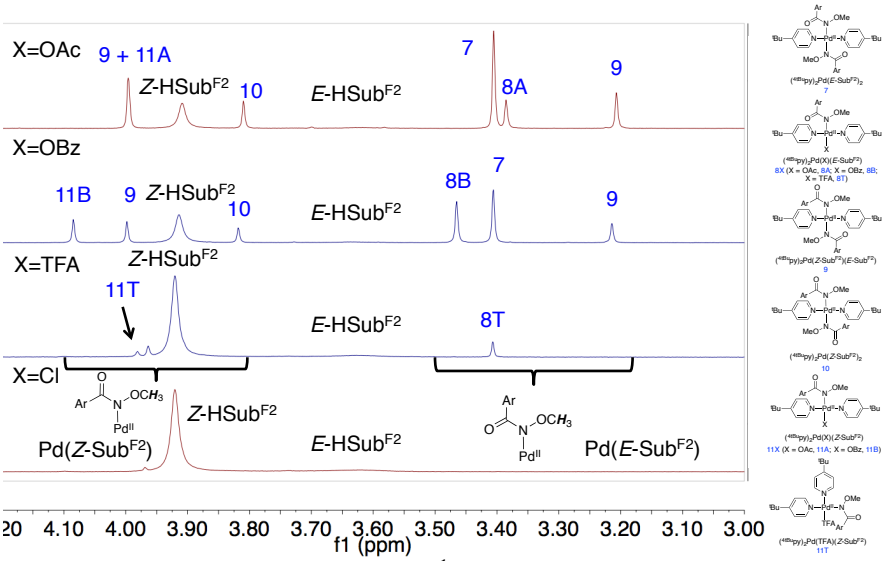


**Figure S26.** Methoxy region of the $^{1}$H NMR spectra of the reaction between 2.0 equiv *N*-methoxy-2,6-difluorobenzamide and (from the bottom to the top) (1) ($^{tBu}$py)$_2$PdCl$_2$ **0C**, 15 hours; (2) ($^{tBu}$py)$_2$Pd(TFA)$_2$ **0T**, 38 hours; (3) ($^{tBu}$py)$_2$Pd(OBz)$_2$ **0B**, 38 hours; (4) ($^{tBu}$py)$_2$Pd(OAc)$_2$ **0A**, 38 hours. The methoxy peaks that appear between ~3.20 and ~3.45 ppm are assigned to palladium-bound amidate ligands in which the methoxy group is *trans* to the carbonyl, as in the methoxy group of the minor *E* rotamer of HSub$^{F2}$ (3.62 ppm). The methoxy peaks that appear between ~3.80 and ~4.10 ppm are assigned to palladium-bound amidate ligands in which the methoxy group is *cis* to the carbonyl, as in the major *Z* rotamer of HSub$^{F2}$ (3.90 ppm).

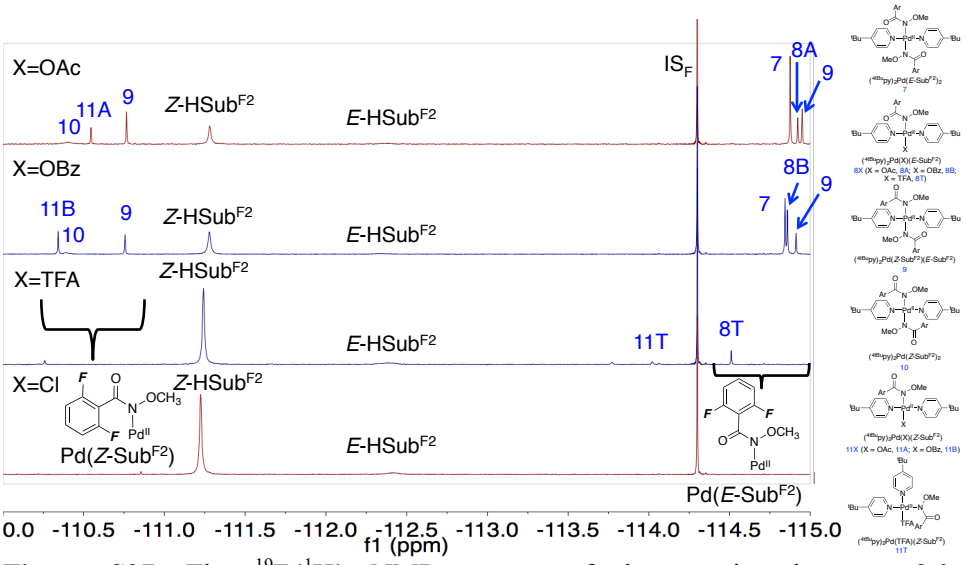


**Figure S27.** The $^{19}$F{$^{1}$H} NMR spectra of the reaction between 2.0 equiv *N*-methoxy-2,6-difluorobenzamide and (from the bottom to the top) (1) ($^{tBu}$py)$_2$PdCl$_2$ **0C**, 15 hours; (2) ($^{tBu}$py)$_2$Pd(TFA)$_2$ **0T**, 38 hours; (3) ($^{tBu}$py)$_2$Pd(OBz)$_2$ **0B**, 38 hours; (4) ($^{tBu}$py)$_2$Pd(OAc)$_2$ **0A**, 38 hours. (the TFA region in (2) is not included for clarity.) The fluorine peaks that appear between -114.5 and -115.0 ppm are assigned to palladium-bound amidate ligands in which the methoxy group is *trans* to the carbonyl, as in the minor *E* rotamer of HSub$^{F2}$ (~ -112.4 ppm). The fluorine peaks that appear between -110.3 and -110.8 ppm are assigned to palladium-bound amidate ligands in which the methoxy group is *cis* to the carbonyl, as in the major *Z* rotamer of HSub$^{F2}$ (~ -111.2 ppm). The fluorine peak of Species **11T** is an outlier since it is shifted noticeably upfield of the other *Z*-Sub$^{F2}$ fluorine peaks; this is attributed to a through-space shielding effect from a trifluoroacetate ligand's fluorines: unlike all the other species in this study, **11T** is proposed to be a *cis*, rather than a *trans*, species (see Figures S56-S60).

**Table S4**. Concentrations of the species in solution (in mM) from the reaction of *N*-methoxy-2,6-difluorobenzamide with ($^{tBu}$py)PdX$_2$ in $CDCl_3$ after 38 hours as measured by $^1$H NMR spectroscopy, unless otherwise noted.

| X | 0X | HSub$^{F2}$ | 7 | 8X | 9 | 10 | 11X | HX |
|---|---|---|---|---|---|---|---|---|
| OAc | 0.15 | 8.9 | 4.9 | 3.1 | 3.9 | 1.4 | 2.0 | 26.2 |
| OBz | 0.95 | 12.2 | 3.4 | 5.5 | 2.6 | 1.0 | 2.8 | 22.6 |
| TFA | 13 | 31 | 0 | 1.7 | 0 | 0 | 1.3 | 4.1[a] |
| Cl | 16 | 32 | 0 | 0 | 0 | 0 | 0 | 0 |

a. Measured by $^{19}$F{$^1$H} NMR spectroscopy.

*Spectra and information for the reaction of ($^{tBu}$py)$_2$Pd(OAc)$_2$* ***0A*** *with 2.0 equiv* N*-methoxy-2,6-difluorobenzamide*

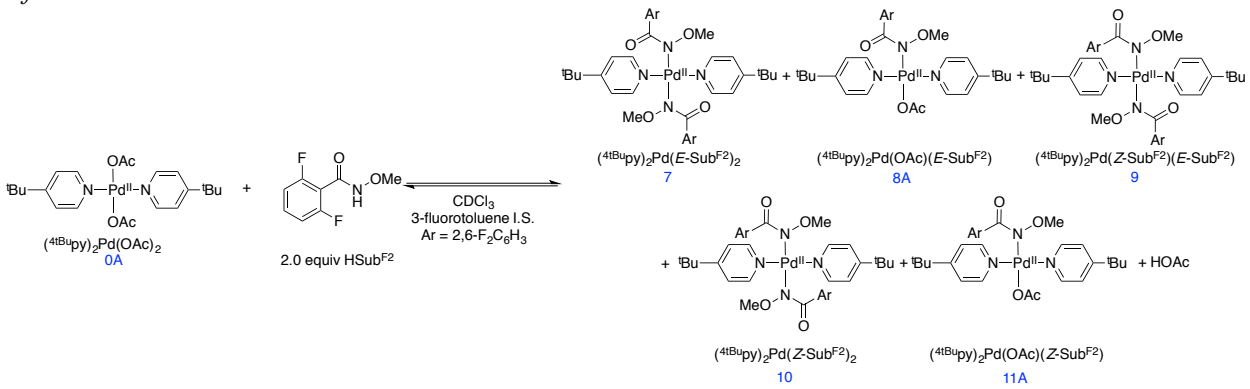


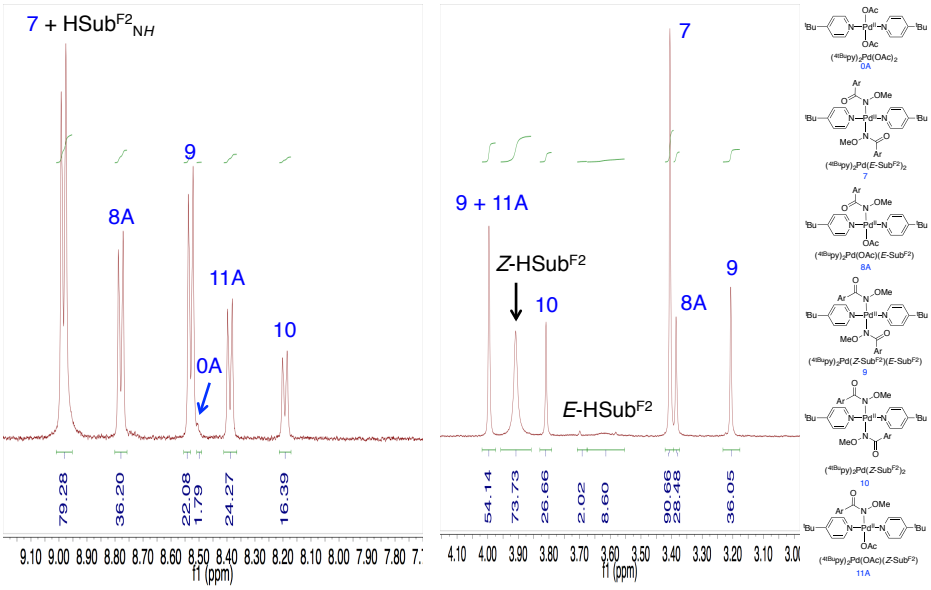


**Figure S28**. Magnified (left) aromatic and (right) methoxy regions of the integrated $^1$H NMR spectrum of the reaction of ($^{tBu}$py)$_2$Pd(OAc)$_2$ **0A** with 2.0 equiv *N*-methoxy-2,6-difluorobenzamide 38 hours after the reactants were mixed, with assigned species.

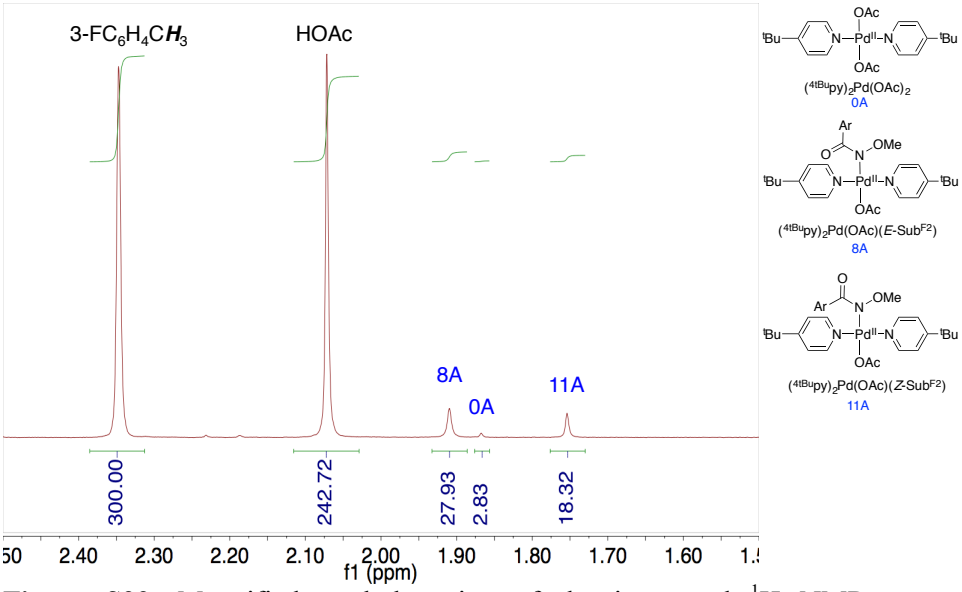


**Figure S29**. Magnified methyl region of the integrated $^{1}$H NMR spectrum of the reaction of ($^{tBu}$py)$_2$Pd(OAc)$_2$ **0A** with 2.0 equiv *N*-methoxy-2,6-difluorobenzamide 38 hours after the reactants were mixed, with assigned species.

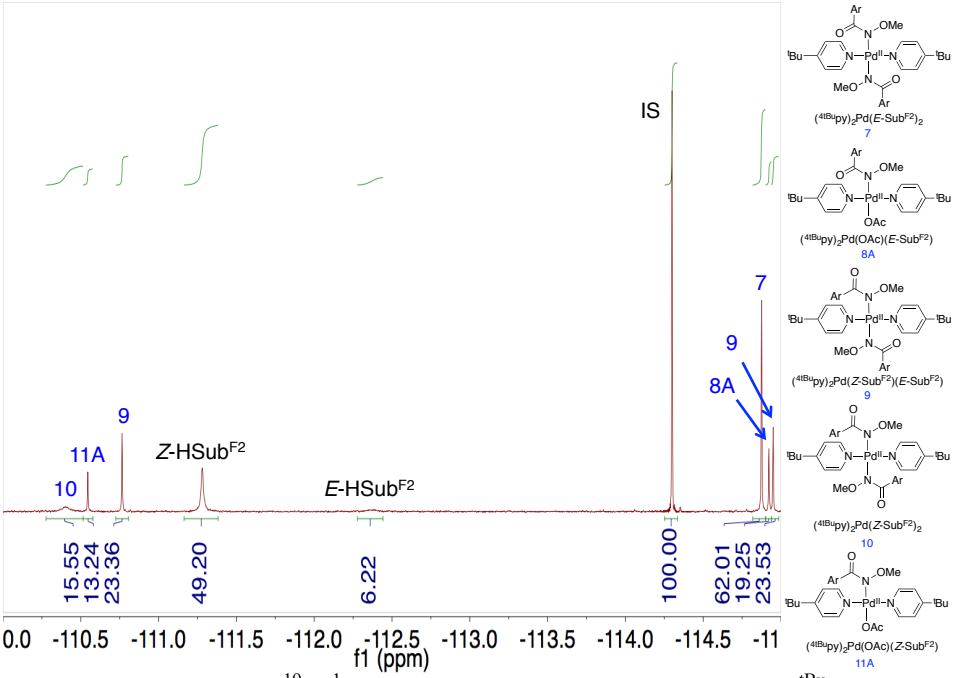


**Figure S30**. Integrated $^{19}$F{$^{1}$H} NMR spectrum of the reaction of ($^{tBu}$py)$_2$Pd(OAc)$_2$ **0A** with 2.0 equiv *N*-methoxy-2,6-difluorobenzamide 38 hours after the reactants were mixed, with assigned species.

**Table S5**. Integrations of the key $^{1}$H NMR peaks for each assigned species in the reaction of ($^{tBu}$py)$_2$Pd(OAc)$_2$ **0A** with 2.0 equiv *N*-methoxy-2,6-difluorobenzamide 38 hours after the reactants were mixed. The α-$^{4tBu}$py proton integrals were set to 4.0 for computing the adjusted integrals of the methoxy and the acetate protons for a given species.

| Species | α-$^{4tBu}$py (ppm) | α-$^{4tBu}$py integral | $H_3$CON- (ppm) | $H_3$CON- integral | -$O_2$CC$H_3$ (ppm) | -$O_2$CC$H_3$ integral |
|---|---|---|---|---|---|---|
| **0A** | 8.52[a] | 4.0 | - | - | 1.87 | 2.1 |
| **7** | 8.98[b] | 4.0 | 3.41 | 6.6 | - | - |
| **8A** | 8.78 | 4.0 | 3.39 | 3.1 | 1.91 | 3.1 |
| **9** | 8.53[a] | 4.0 | 4.00[c]<br>3.21 | 3.3<br>3.3 | - | - |
| **10** | 8.20 | 4.0 | 3.81 | 6.5 | - | - |
| **11A** | 8.39 | 4.0 | 4.00[c] | 3.0 | 1.75 | 3.0 |
| HOAc | - | - | - | - | 2.07 | 3.0 |
| HSub$^{F2}$ | - | - | 3.91<br>3.62 | 3.0<br>3.0 | - | - |

(a) The integrals of these overlapping peaks were calculated by integrating the half of each multiplet that does not overlap with the other peak and doubling that value. (b) This integral, which overlaps with the amide proton of the major rotamer of the substrate, was computed by subtracting one-third of the major rotamer's methoxy integral from the total integral of this peak. (c) The integrals of these overlapping peaks were computed by taking the integral of the 3.21 ppm methoxy singlet of species **9**, using that value as the integral of species **9**'s methoxy singlet at 4.00 ppm, and subtracting that value from the total integral of the peak at 4.00 ppm for the integral of the methoxy singlet due to species **11A**.

**Table S6**. Tabulated chemical shifts from the $^{1}$H-$^{15}$N HMBC and $^{19}$F{$^{1}$H} spectra of the reaction of ($^{tBu}$py)$_2$Pd(OAc)$_2$ **0A** with 2.0 equiv *N*-methoxy-2,6-difluorobenzamide several days after the reactants were mixed, with assigned species. For each species, the first row corresponds to chemical shifts for the $^{tBu}$py ligand, and the second (and third row, where applicable) corresponds to chemical shifts for the amidate ligand.

| Species | $^{1}$H chemical shift (ppm) | $^{15}$N chemical shift (ppm) | $^{19}$F chemical shift (ppm) |
|---|---|---|---|
| **7** | 8.98 | -163.26 | |
| | 3.41 | -169.28 | -114.88 |
| **8A** | 8.78 | -164.61 | |
| | 3.39 | -184.95 | -114.92 |
| **9** | 8.53 | -163.64 | |
| | 4.00 | -168.70 | -110.77 |
| | 3.21 | -172.34 | -114.95 |
| **10** | 8.20 | -163.06 | |
| | 3.81 | -167.73 | -110.40 |
| **11A** | 8.39 | -164.44 | |
| | 4.00 | -183.60 | -110.55 |

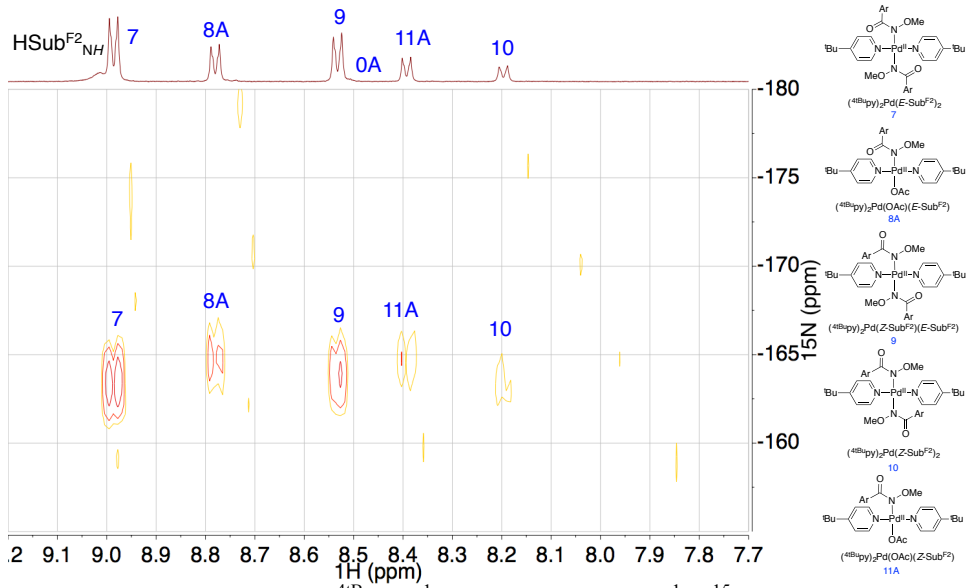


**Figure S31**. Aromatic α-$^{4tBu}$py $^1$H region of the $^1$H-$^{15}$N HMBC spectrum of the reaction of ($^{tBu}$py)$_2$Pd(OAc)$_2$ with 2.0 equiv *N*-methoxy-2,6-difluorobenzamide several days after the reactants were mixed. This spectrum supports that the $^{tBu}$py ligands in each species are bound to Pd because the peaks are shifted ~90 ppm upfield from unligated $^{tBu}$py.

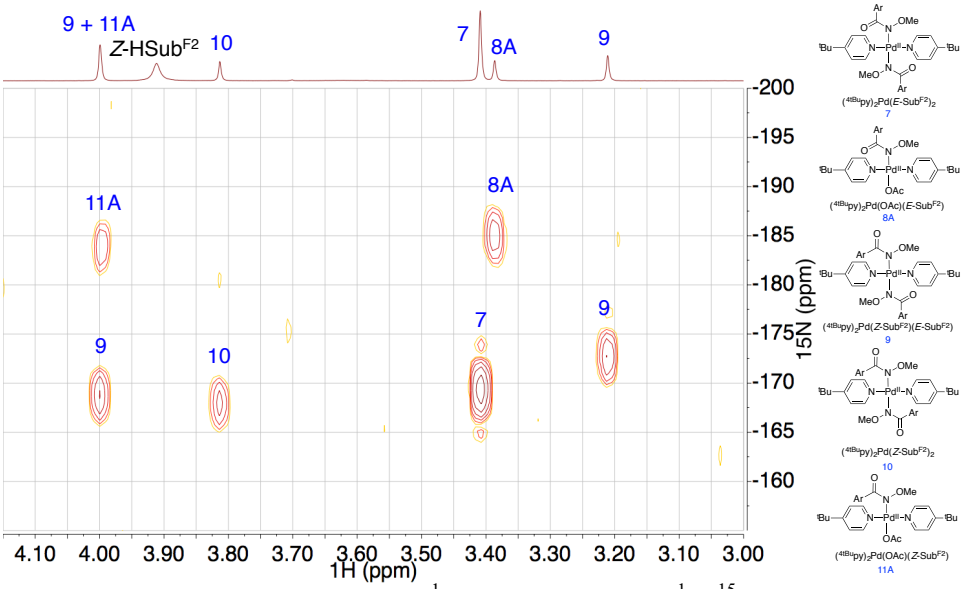


**Figure S32**. Aliphatic methoxy $^1$H region of the $^1$H-$^{15}$N HMBC spectrum of the reaction of ($^{tBu}$py)$_2$Pd(OAc)$_2$ with 2.0 equiv *N*-methoxy-2,6-difluorobenzamide several days after the reactants were mixed, with assigned species. The observation of a cluster of crosspeaks at δ($^{15}$N)~ -170 ppm (Species **7**, **9**, and **10**) supports that these are all bisamidate species. A similar argument supports the assignment of Species **11A** and **8A** (δ($^{15}$N)~ -185 ppm) as mono-acetate-mono-amidate species. These assignments are consistent with the integrations from Table S2.

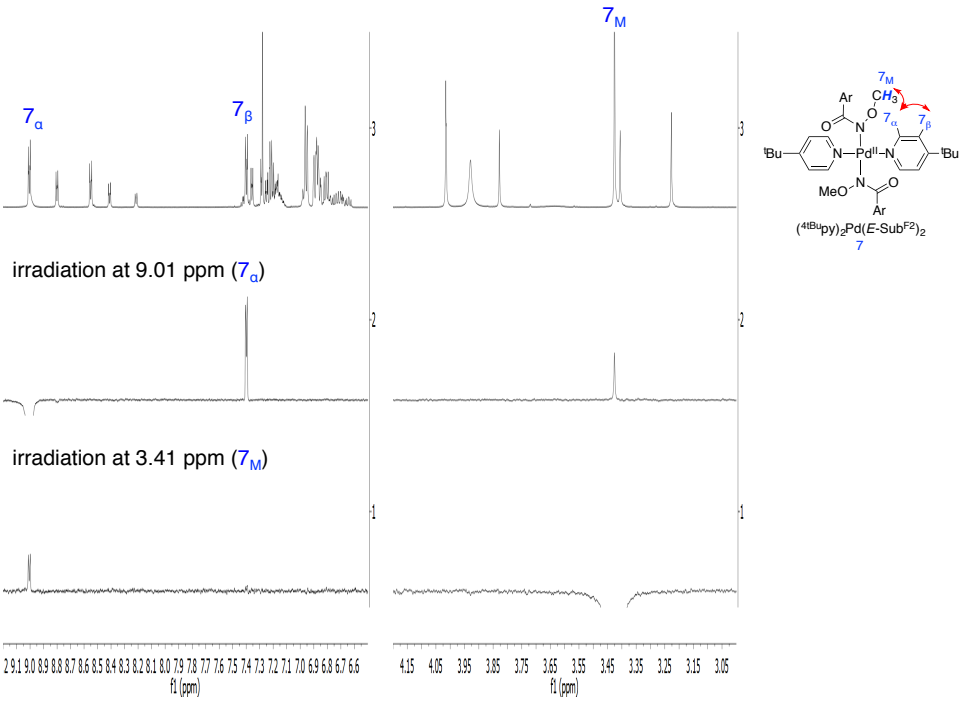


**Figure S33**. NOEs for Species **7** with 16 scans, mix time = 0.55 s, 10 s relaxation delay. The observation of NOEs confirms the coordination of both the amidate and the $^{4tBu}$py ligands in Species **7**.

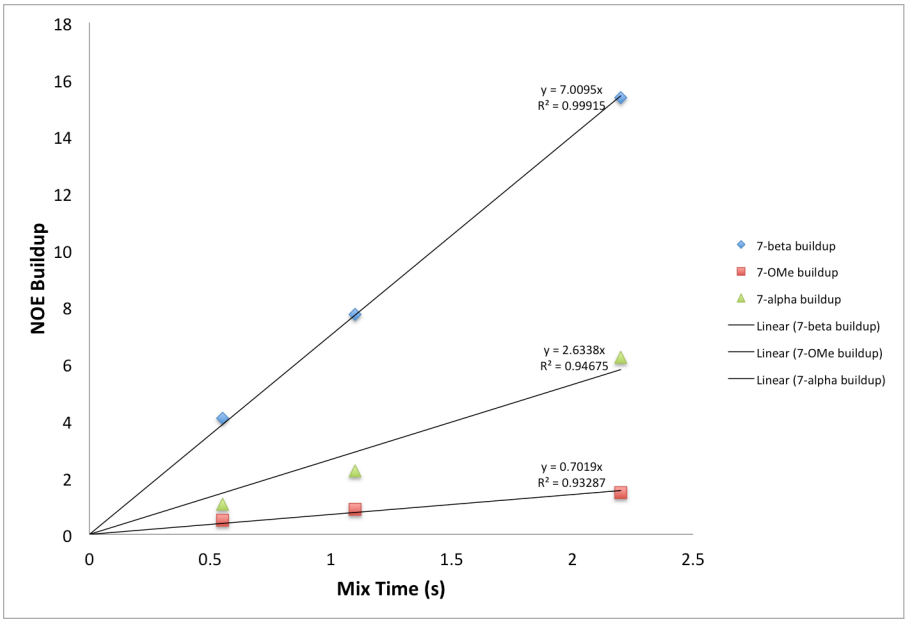


**Figure S34**. NOE buildup curves for Species **7** with 16 scans, 10 s relaxation delay, mix time = 0.55, 1.1, and 2.2 s. These suggest that the observed peaks are not artifacts but true NOEs.

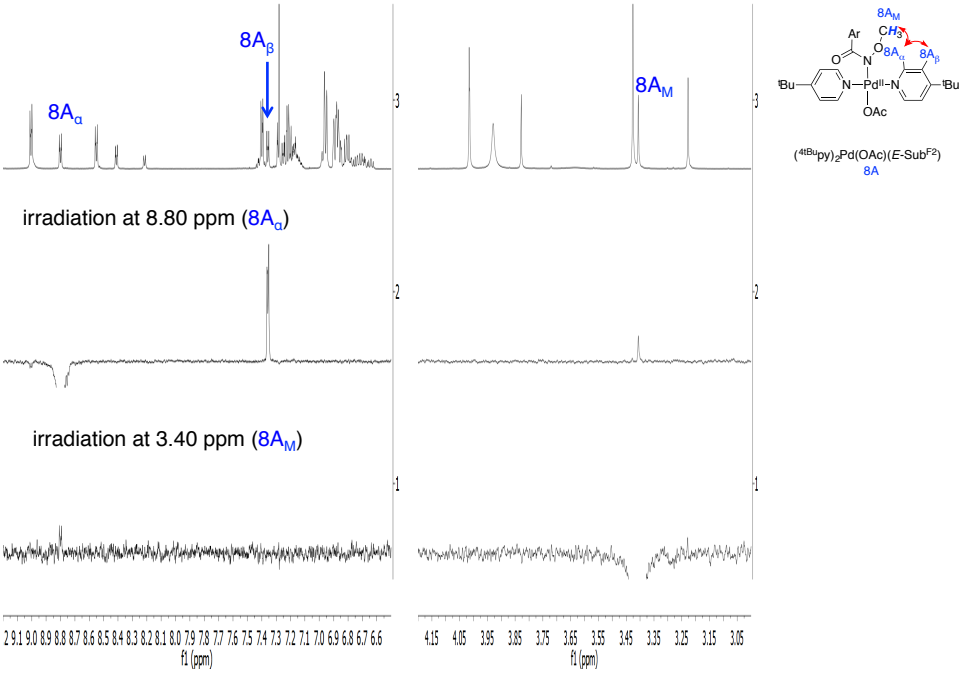


**Figure S35**. NOEs for Species **8A** with 16 scans, mix time = 0.55 s, 10 s relaxation delay. The observation of NOEs confirms the coordination of both the amidate and the $^{4tBu}$py ligands in Species **8A**.

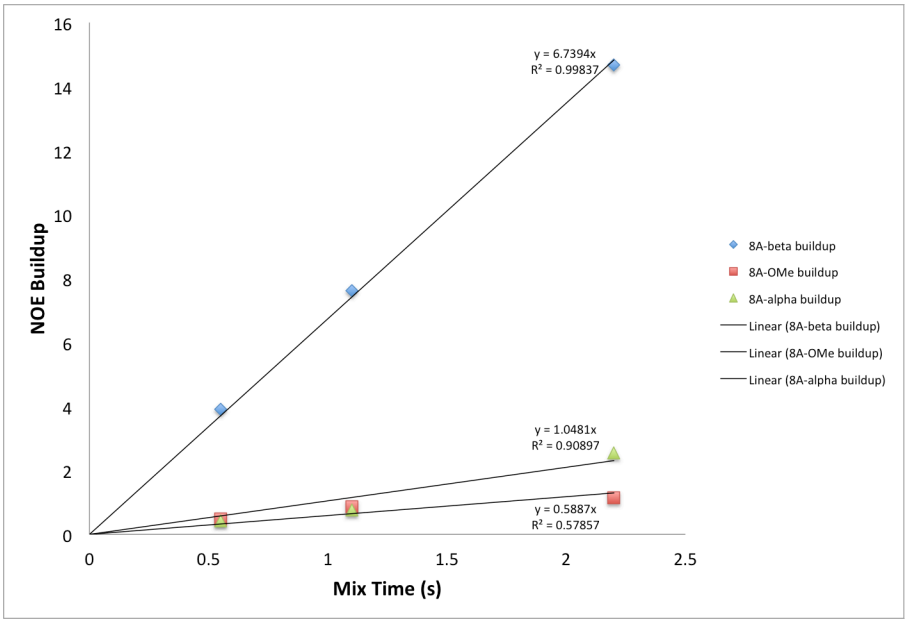


**Figure S36**. NOE buildup curves for Species **8A** with 16 scans, 10 s relaxation delay, and mix time = 0.55, 1.1, and 2.2 s. These suggest that the observed peaks are not artifacts but true NOEs.

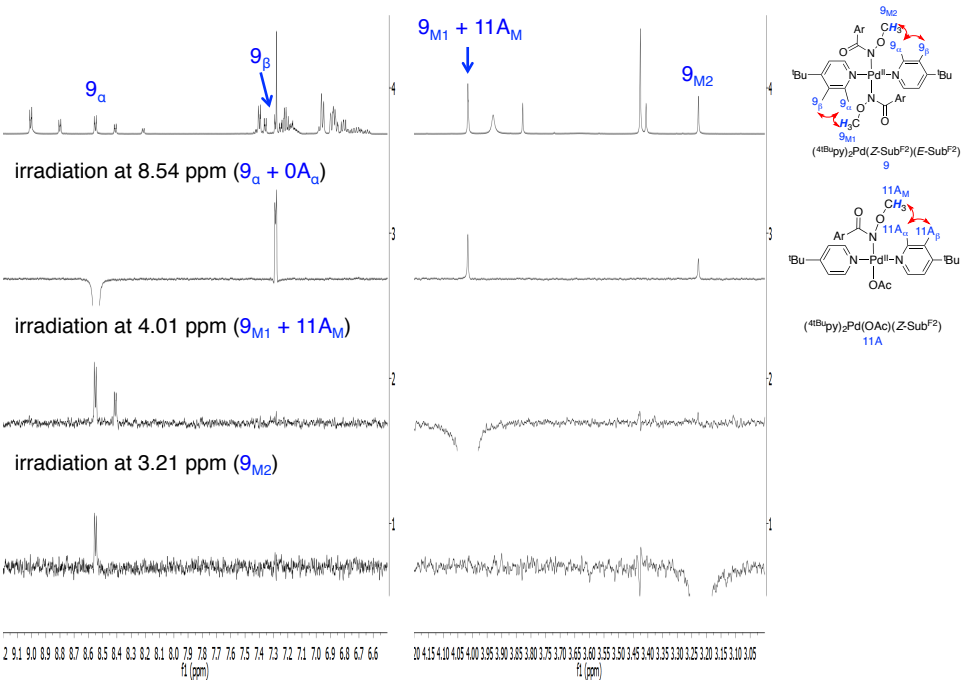


**Figure S37**. NOEs for Species **9** with 16 scans, mix time = 0.55 s, 10 s relaxation delay. The observation of NOEs confirms the coordination of both the amidate and the $^{4tBu}$py ligands in Species **9**.

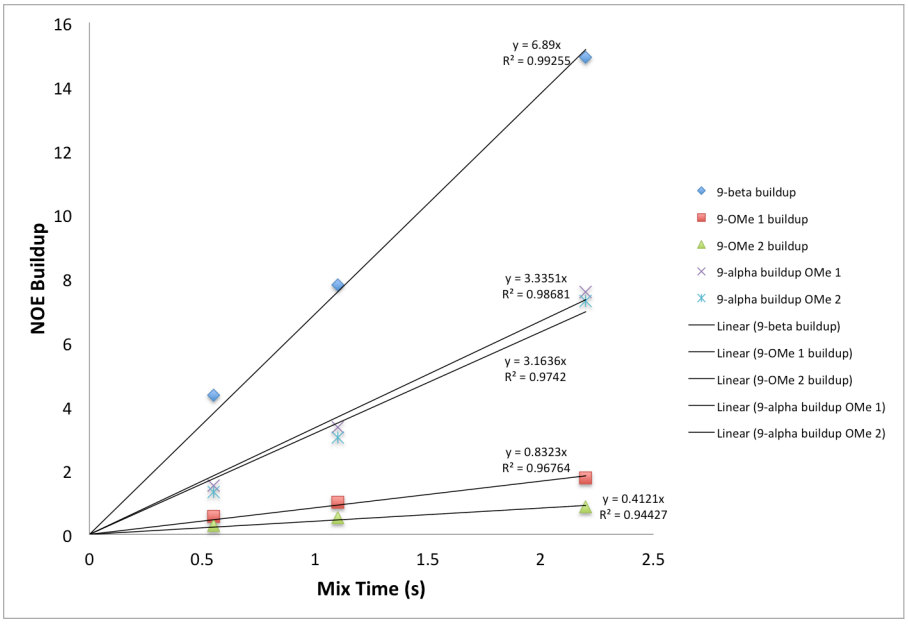


**Figure S38**. NOE buildup curves for Species **9** with 16 scans, 10 s relaxation delay, and mix time = 0.55, 1.1, and 2.2 s. These suggest that the observed peaks are not artifacts but true NOEs.

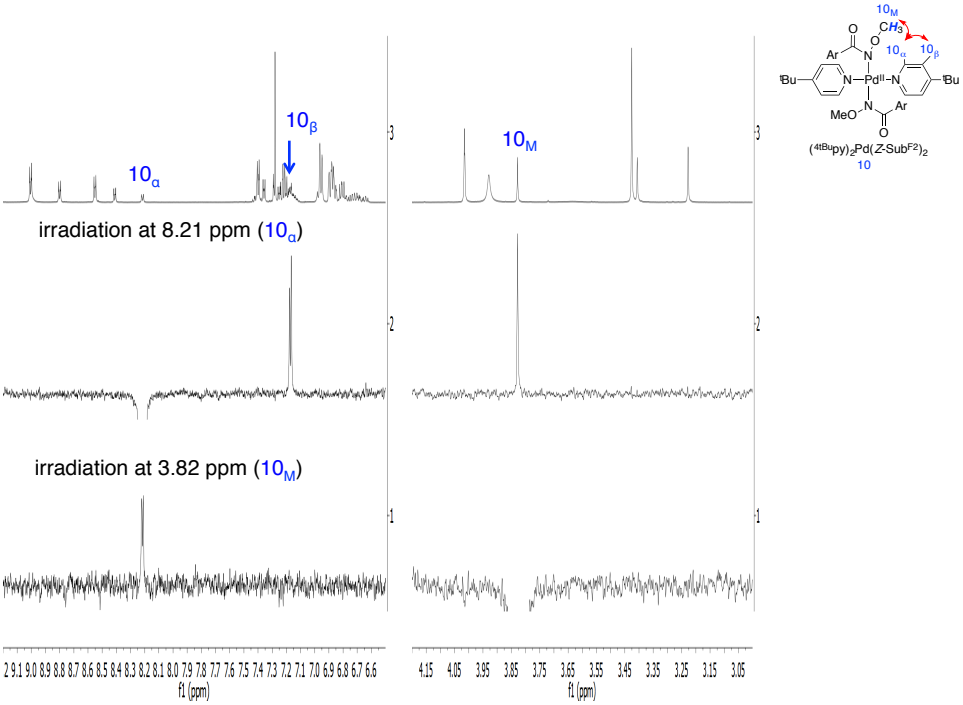


**Figure S39**. NOEs for Species **10** with 16 scans, mix time = 0.55 s, 10 s relaxation delay. The observation of NOEs confirms the coordination of both the amidate and the $^{4tBu}$py ligands in Species **10**.

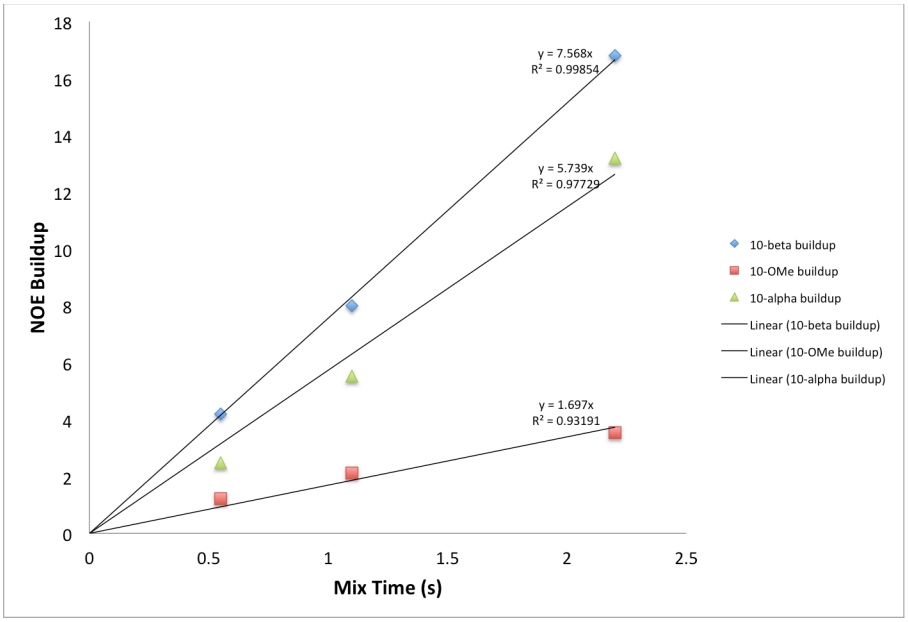


**Figure S40**. NOE buildup curves for Species **10** with 16 scans, 10 s relaxation delay, and mix time = 0.55, 1.1, and 2.2 s. These suggest that the observed peaks are not artifacts but true NOEs.

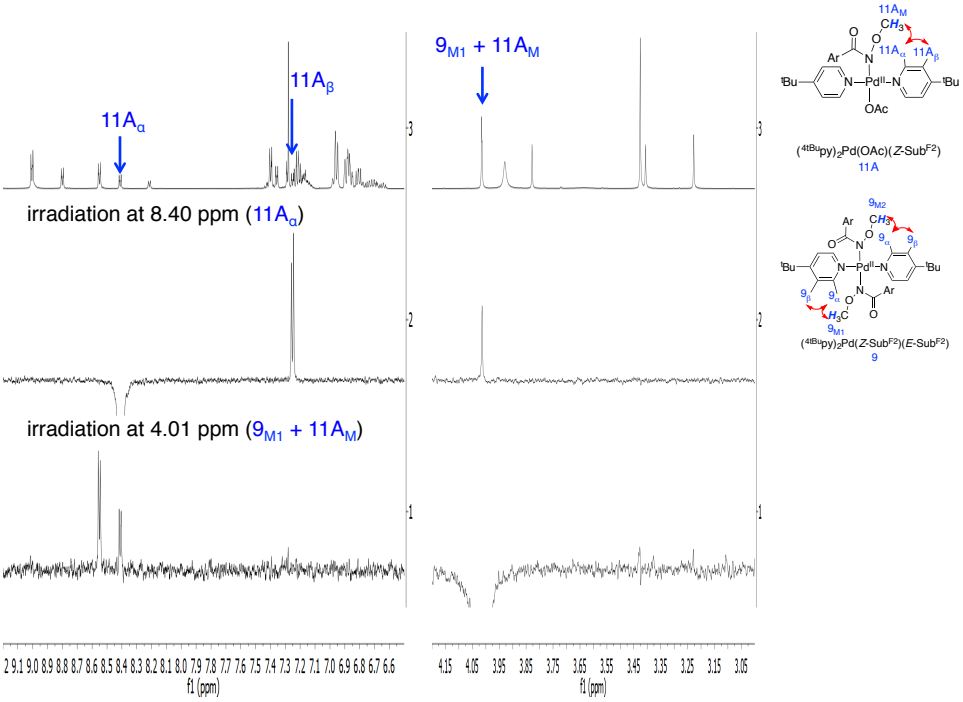


**Figure S41**. NOEs for Species **11A** with 16 scans, mix time = 0.55 s, 10 s relaxation delay. The observation of NOEs confirms the coordination of both the amidate and the $^{4tBu}$py ligands in Species **11A**.

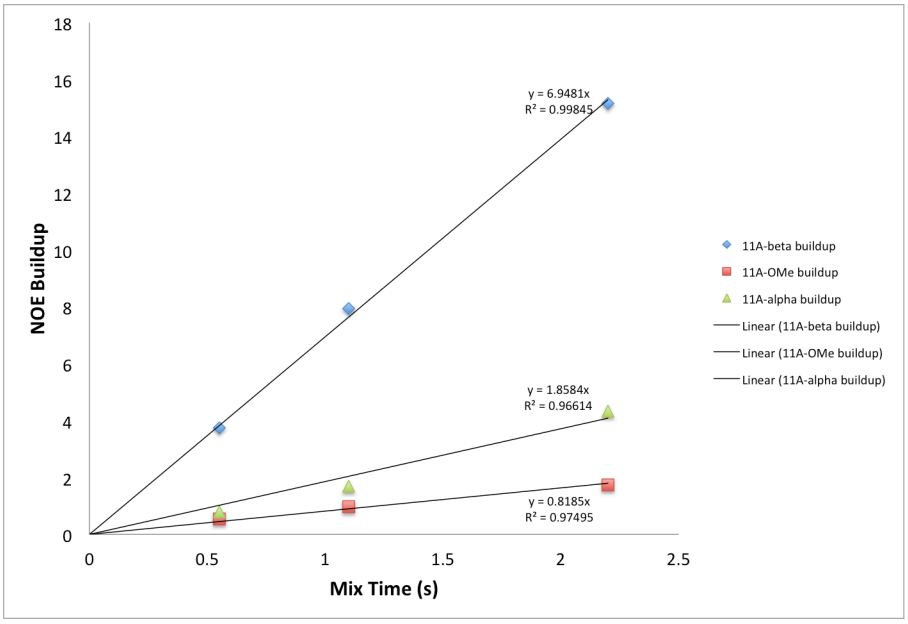


**Figure S42**. NOE buildup curves for Species **11A** with 16 scans, 10 s relaxation delay, and mix time = 0.55, 1.1, and 2.2 s. These suggest that the observed peaks are not artifacts but true NOEs.

*Spectra and information for the reaction of ($^{tBu}$py)$_2$Pd(OBz)$_2$* ***0B*** *with 2.0 equiv* N*-methoxy-2,6-difluorobenzamide*

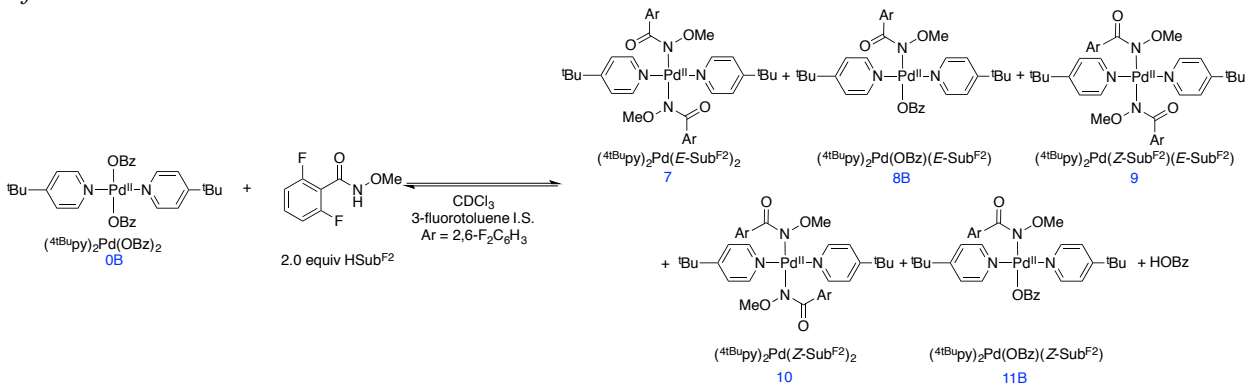


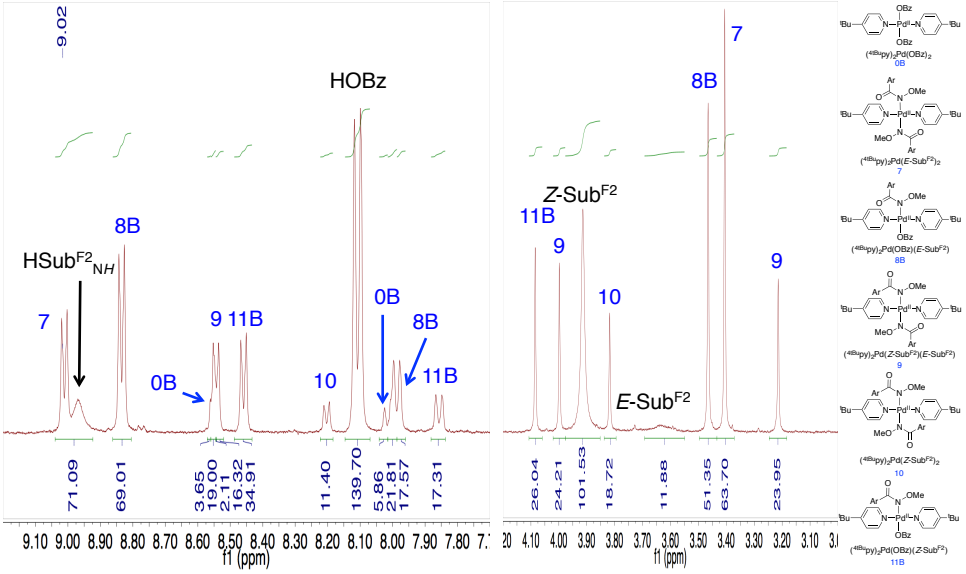


**Figure S43**. Magnified (left) aromatic and (right) aliphatic methoxy regions of the integrated $^1$H NMR spectrum of the reaction of ($^{tBu}$py)$_2$Pd(OBz)$_2$ **0B** with 2.0 equiv *N*-methoxy-2,6-difluorobenzamide 38 hours after the reactants were mixed, with assigned species.

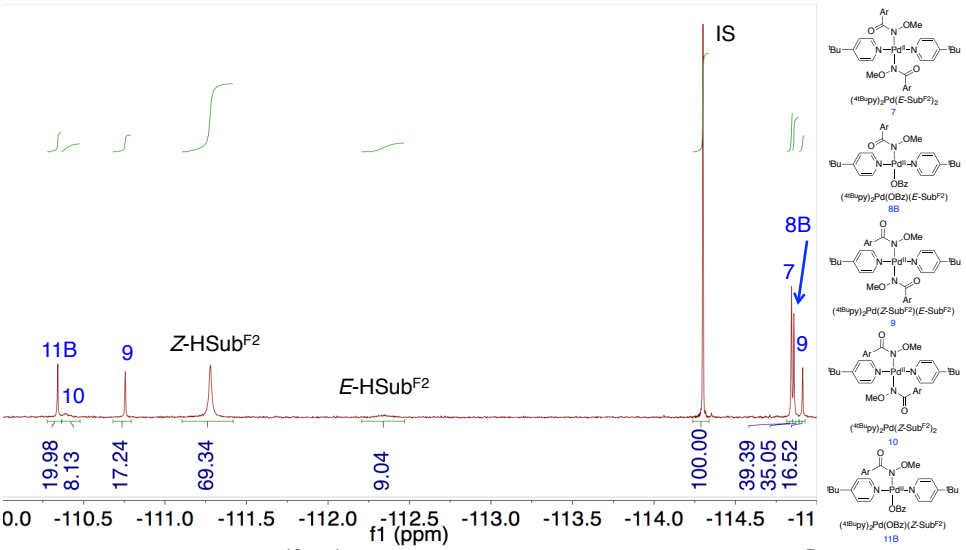


**Figure S44**. Integrated $^{19}F\{^{1}H\}$ NMR spectrum of the reaction of $(^{tBu}py)_2Pd(OBz)_2$ **0B** with 2.0 equiv *N*-methoxy-2,6-difluorobenzamide 38 hours after the reactants were mixed, with assigned species.

**Table S7**. Integrations of the key $^{1}H$ NMR peaks for each assigned species in the reaction of $(^{tBu}py)_2Pd(OBz)_2$ **0B** with 2.0 equiv *N*-methoxy-2,6-difluorobenzamide 38 hours after the reactants were mixed. The α-$^{4tBu}$py proton integrals were set to 4.0 for computing the adjusted integrals of the methoxy and the *ortho* benzoate protons for a given species.

| Species | α-$^{4tBu}$py (ppm) | α-$^{4tBu}$py integral | $H_3CO$- (ppm) | $H_3CO$- integral | *o*-$O_2CPh$ (ppm) | *o*-$O_2CPh$ integral |
|---|---|---|---|---|---|---|
| **0B** | 8.55[a] | 4.0 | - | - | 8.01[a] | 5.3 |
| **7** | 9.01[b] | 4.0 | 3.41 | 6.1 | - | - |
| **8B** | 8.83 | 4.0 | 3.47 | 3.0 | 7.99[a] | 2.0 |
| **9** | 8.54[a] | 4.0 | 4.00<br>3.21 | 3.0<br>2.9 | - | - |
| **10** | 8.20 | 4.0 | 3.82 | 6.6 | - | - |
| **11B** | 8.46 | 4.0 | 4.09 | 3.0 | 7.86 | 2.0 |
| HOBz | - | - | - | - | 8.11 | 2.0 |
| $HSub^{F2}$ | - | - | 3.92<br>3.64 | 3.0<br>3.0 | - | - |

(a) The integrals of these overlapping peaks were computed by integrating half the corresponding multiplet and doubling that value. (b) This multiplet overlaps with the amide proton of the major rotamer of the substrate; its integral was computed by lineshape analysis using MestReNova 10.0.2-15465.

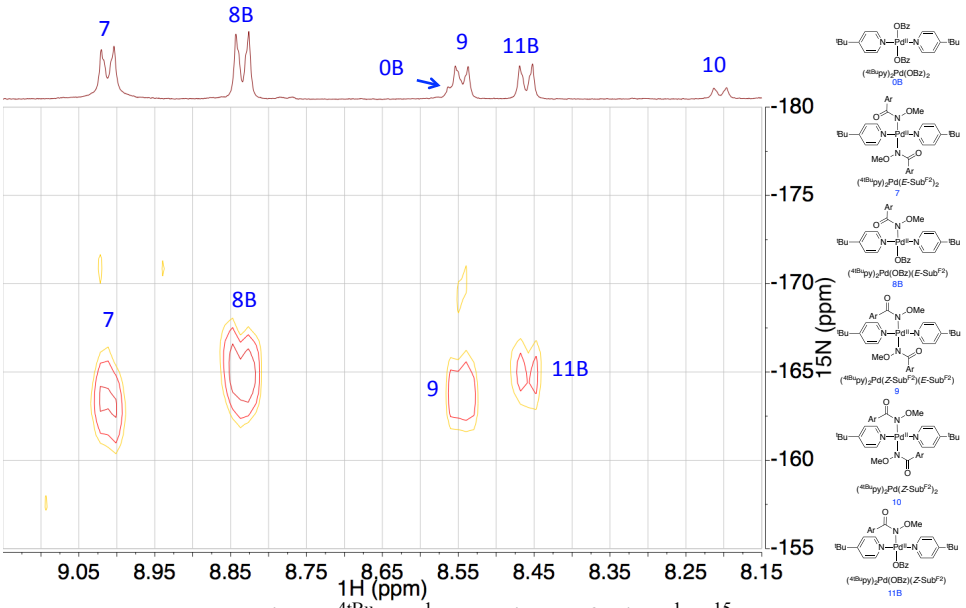


**Figure S45**. Aromatic α-$^{4tBu}$py $^{1}$H region of the $^{1}$H-$^{15}$N HMBC spectrum of the reaction of ($^{tBu}$py)$_2$Pd(OBz)$_2$ **0B** with 2.0 equiv *N*-methoxy-2,6-difluorobenzamide several days after the reactants were mixed. This spectrum supports that the $^{4tBu}$py ligands in each species are bound to Pd because the peaks are shifted ~90 ppm upfield from unligated $^{4tBu}$py. Although the $10_{\alpha}/10_{pyN}$ crosspeak was not observed, the existence of an NOE with the methoxy amidate proton resonance $10_M$ when $10_{\alpha}$ was irradiated (Figures S52 and S53), as well as the observation of this species' crosspeak in the acetate reaction, confirms that the $^{4tBu}$py ligand is coordinated to Pd.

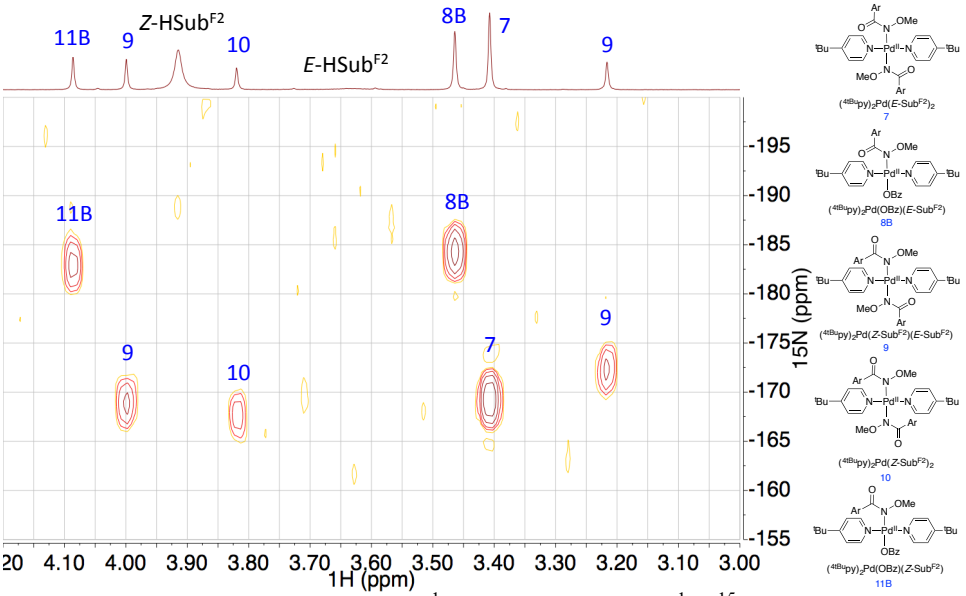


**Figure S46**. Aliphatic methoxy $^{1}$H region of the $^{1}$H-$^{15}$N HMBC spectrum of the reaction of ($^{tBu}$py)$_2$Pd(OBz)$_2$ **0B** with 2.0 equiv *N*-methoxy-2,6-difluorobenzamide several days after the reactants were mixed. The observation of a cluster of tightly distributed crosspeaks at δ($^{15}$N)~ -170 ppm (Species **7**, **9**, and **10**), as well as the lack of variation in the $^{1}$H and $^{15}$N chemical shifts compared to the acetate reaction, supports that these are all bisamidate species. The fact that the $^{1}$H methoxy resonances for $11B_M$ and $8B_M$ are shifted ~0.10 ppm downfield from the $^{1}$H resonances for $11A_M$ and $8A_M$, and that the $^{15}$N resonances (δ($^{15}$N)~ -185 ppm) are similar to those of $11A_M$ and $8A_M$, supports the assignment of Species **11B** and **8B** as mono-benzoate-mono-amidate species. These assignments are consistent with the integrations from Table S7.

**Table S8**. Tabulated chemical shifts from the $^{1}H$-$^{15}N$ HMBC and $^{19}F\{^{1}H\}$ spectra of the reaction of ($^{tBu}$py)$_2$Pd(OBz)$_2$ **0B** with 2.0 equiv *N*-methoxy-2,6-difluorobenzamide several days after the reactants were mixed, with assigned species. For each species, the first row corresponds to chemical shifts for the $^{4tBu}$py ligand, and the second (and third row, where applicable) corresponds to chemical shifts for the amidate ligand.

| Species | $^{1}H$ chemical shift (ppm) | $^{15}N$ chemical shift (ppm) | $^{19}F$ chemical shift (ppm) |
|---|---|---|---|
| **7** | 9.01 | -163.24 | |
| | 3.41 | -169.19 | -114.85 |
| **8B** | 8.84 | -164.84 | |
| | 3.46 | -184.17 | -114.86 |
| **9** | 8.54 | -163.83 | |
| | 4.00 | -168.76 | -110.76 |
| | 3.22 | -172.22 | -114.91 |
| **10** | 8.20 | Not observed | |
| | 3.82 | -167.62 | -110.39 |
| **11B** | 8.46 | -164.84 | |
| | 4.09 | -182.88 | -110.34 |

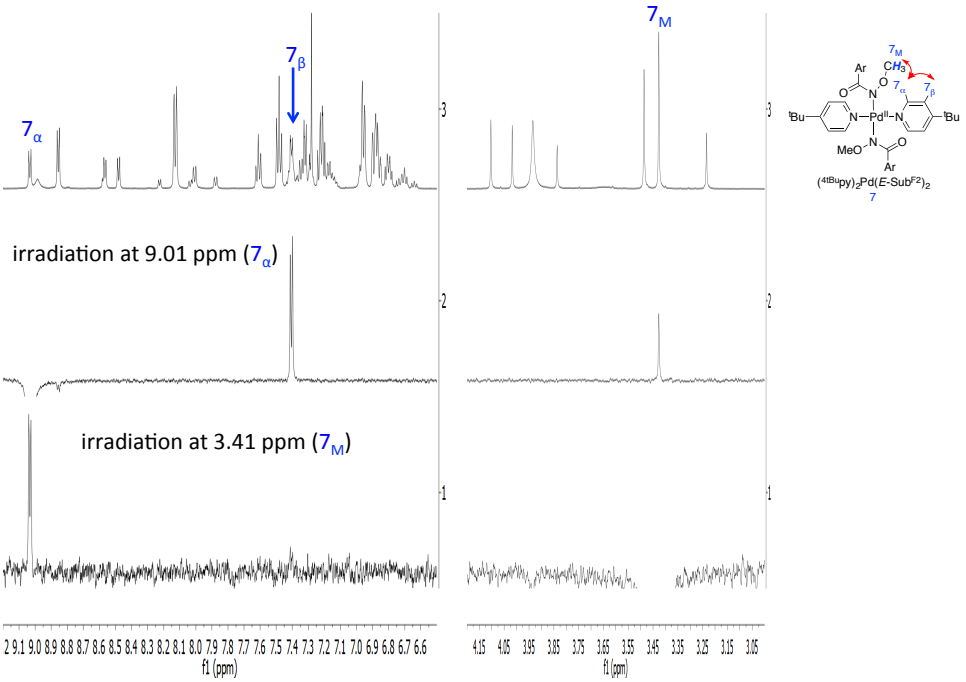


**Figure S47**. NOEs for Species **7** with 16 scans, mix time = 0.66 s, 12 s relaxation delay. The observation of NOEs confirms the coordination of both the amidate and the $^{4tBu}$py ligands in Species **7**.

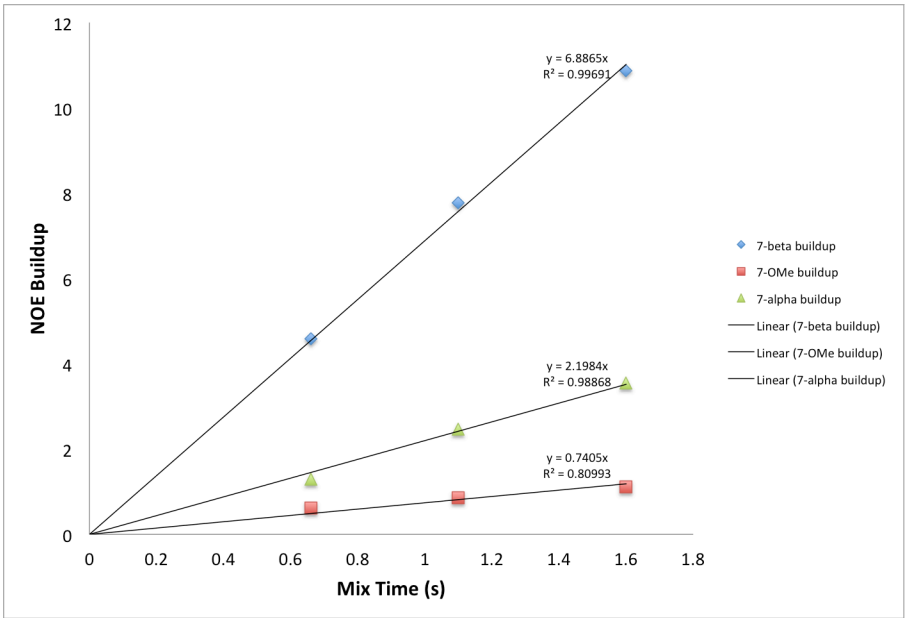


**Figure S48**. NOE buildup curves for Species **7** with 16 scans, 12 s relaxation delay, and mix time = 0.66, 1.1, and 1.6 s. These suggest that the observed peaks are not artifacts but true NOEs.

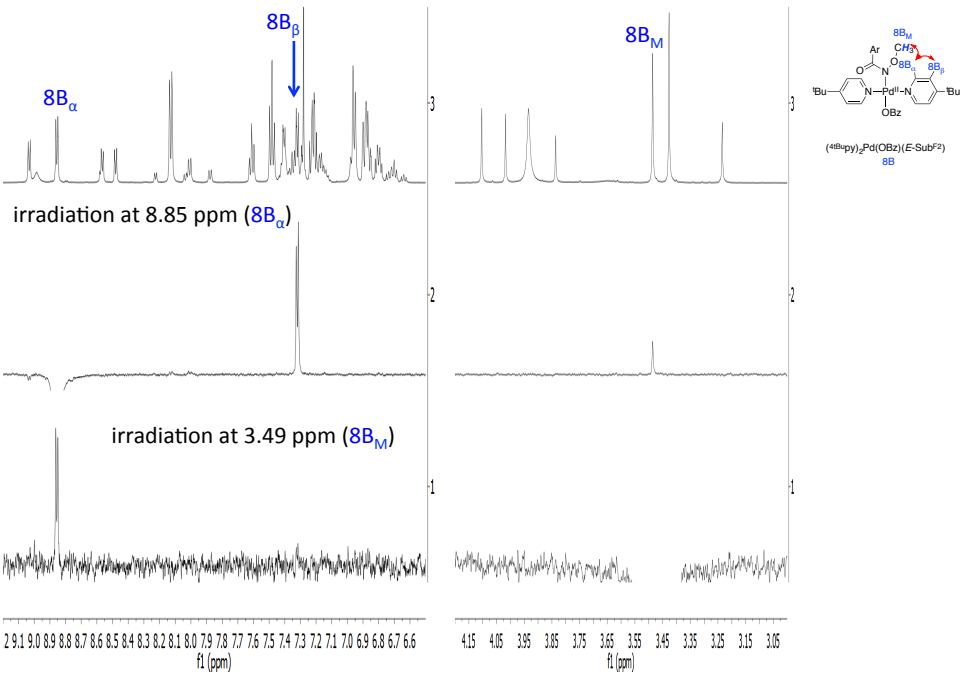


**Figure S49**. NOEs for Species **8B** with 16 scans, mix time = 0.66 s, 12 s relaxation delay. The observation of NOEs confirms the coordination of both the amidate and the $^{4tBu}$py ligands in Species **8B**.

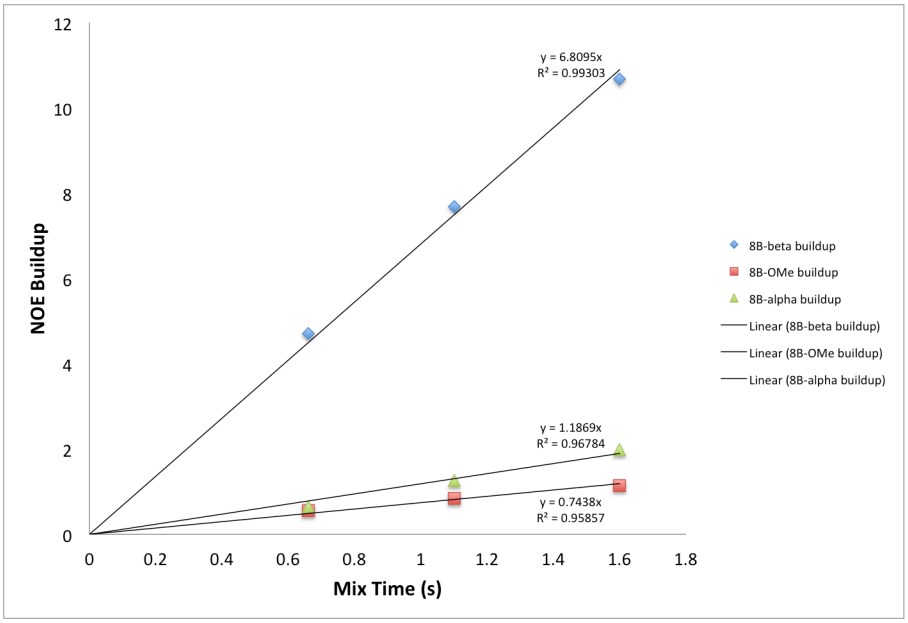


**Figure S50**. NOE buildup curves for Species **8B** with 16 scans, 12 s relaxation delay, and mix time = 0.66, 1.1, and 1.6 s. These suggest that the observed peaks are not artifacts but true NOEs.

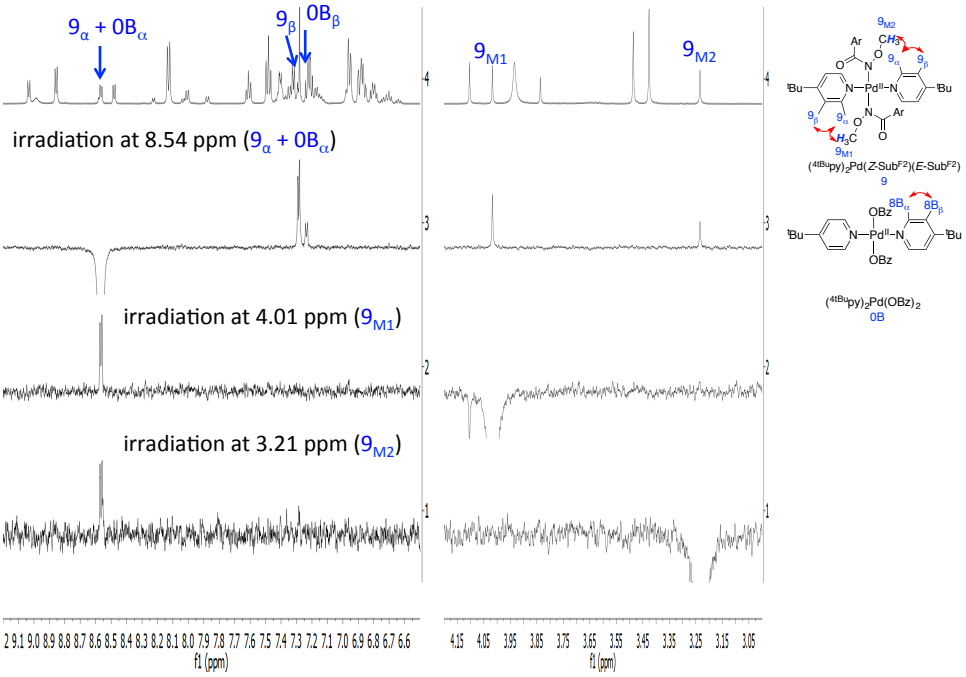


**Figure S51**. NOEs for Species **9** with 16 scans, mix time = 0.66 s, 12 s relaxation delay. The observation of NOEs confirms the coordination of both the amidate and the $^{4tBu}$py ligands in Species **9**.

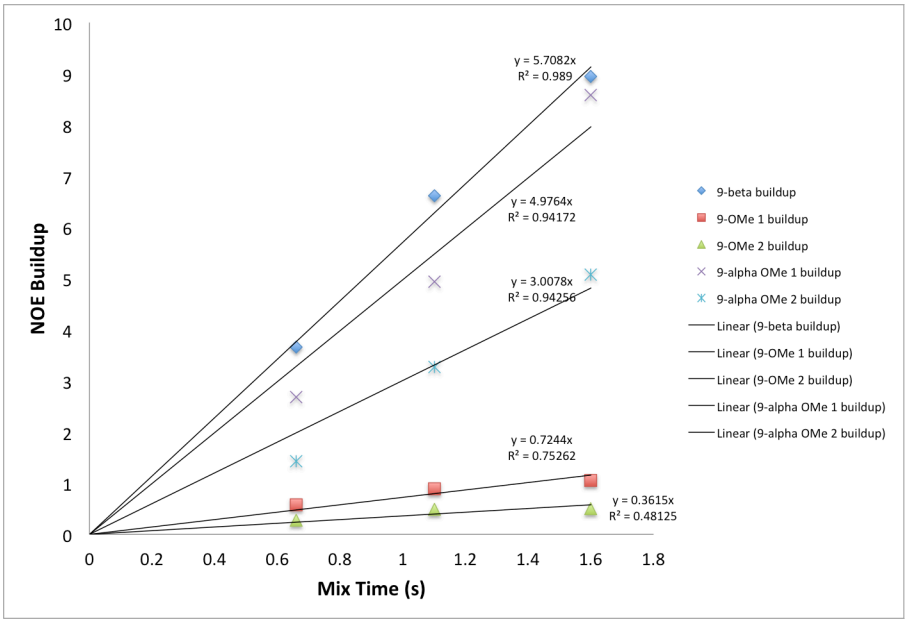


**Figure S52**. NOE buildup curves for Species **9** with 16 scans, 12 s relaxation delay, and mix time = 0.66, 1.1, and 1.6 s. These suggest that the observed peaks are not artifacts but true NOEs.

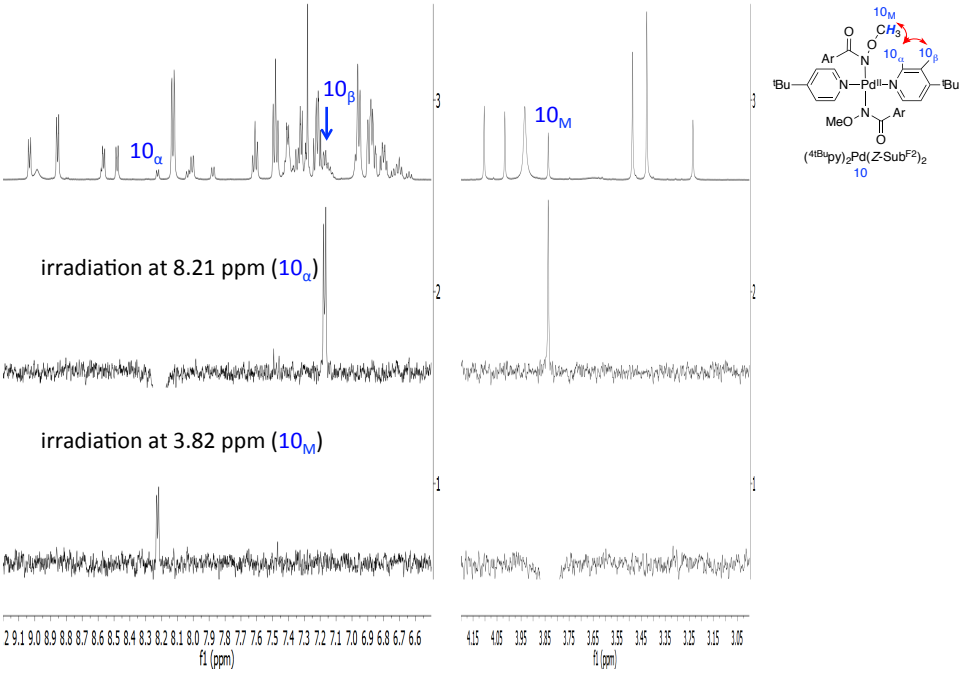


**Figure S53**. NOEs for Species **10** with 16 scans, mix time = 0.66 s, 12 s relaxation delay. The observation of NOEs confirms the coordination of both the amidate and the $^{4tBu}$py ligands in Species **10**.

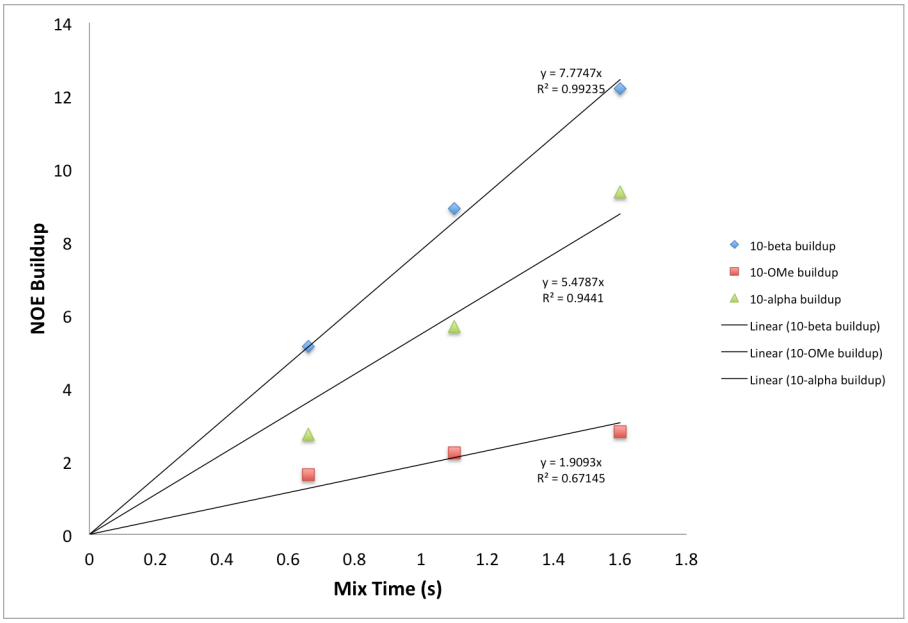


**Figure S54**. NOE buildup curves for Species **10** with 16 scans, 12 s relaxation delay, and mix time = 0.66, 1.1, and 1.6 s. These suggest that the observed peaks are not artifacts but true NOEs.

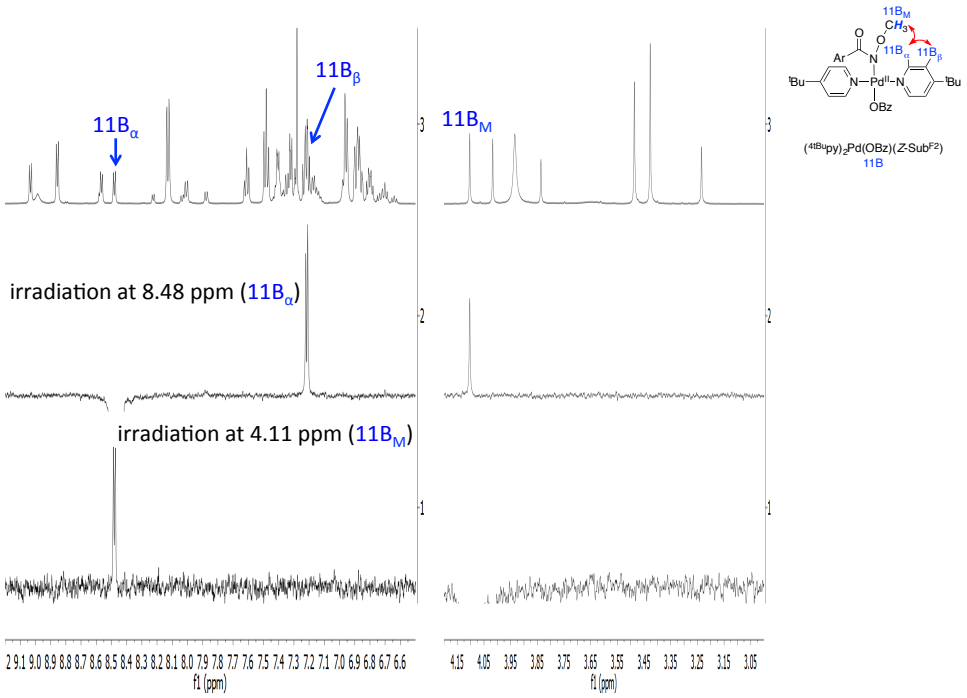


**Figure S55**. NOEs for Species **11B** with ns = 16, mix time = 0.66 s, d1 = 12 s. The observation of NOEs confirms the coordination of both the amidate and the $^{4tBu}$py ligands in Species **11B**.

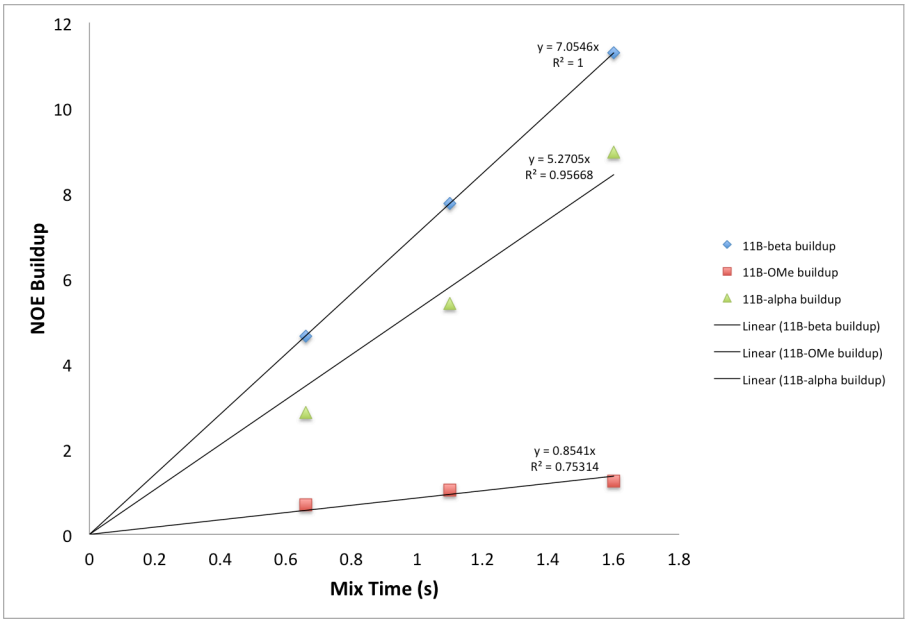


**Figure S56**. NOE buildup curves for Species **11B** with 16 scans, 12 s relaxation delay, and mix time = 0.66, 1.1, and 1.6 s. These suggest that the observed peaks are not artifacts but true NOEs.

*Spectra and information for the reaction of ($^{tBu}$py)$_2$Pd(TFA)$_2$ with 2.0 equiv* N*-methoxy-2,6-difluorobenzamide*

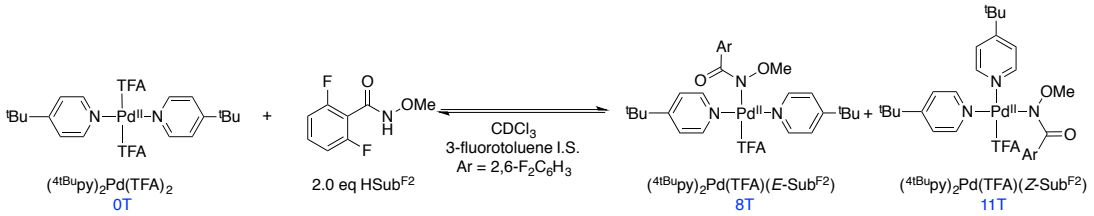


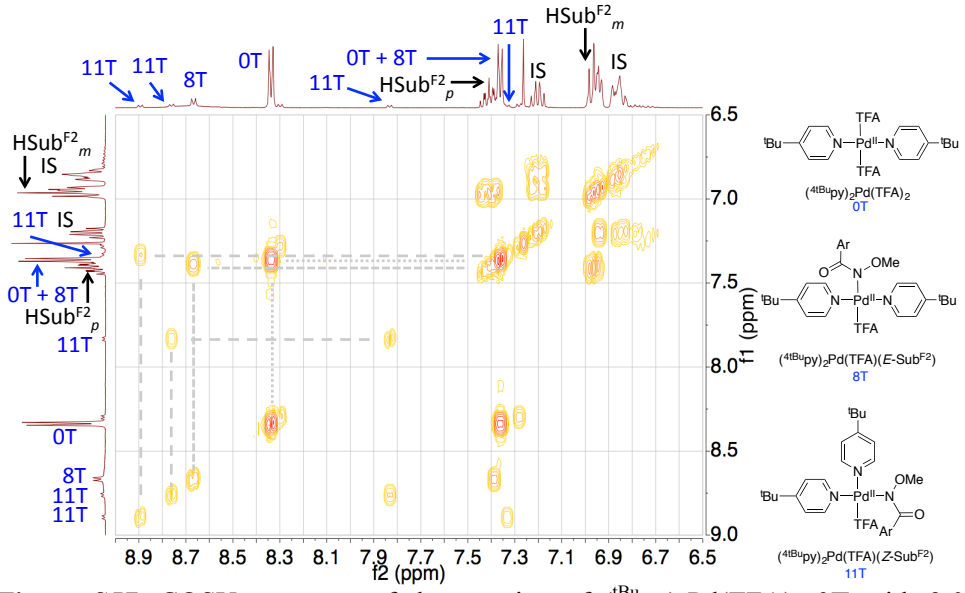


**Figure S57**. COSY spectrum of the reaction of ($^{tBu}$py)$_2$Pd(TFA)$_2$ **0T** with 2.0 equiv *N*-methoxy-2,6-difluorobenzamide several days after the reactants were mixed, with assigned species. The existence of two sets of pyridine resonances for Species **11T** suggests that this is *cis*-($^{tBu}$py)$_2$Pd(TFA)(Sub$^{F2}$).

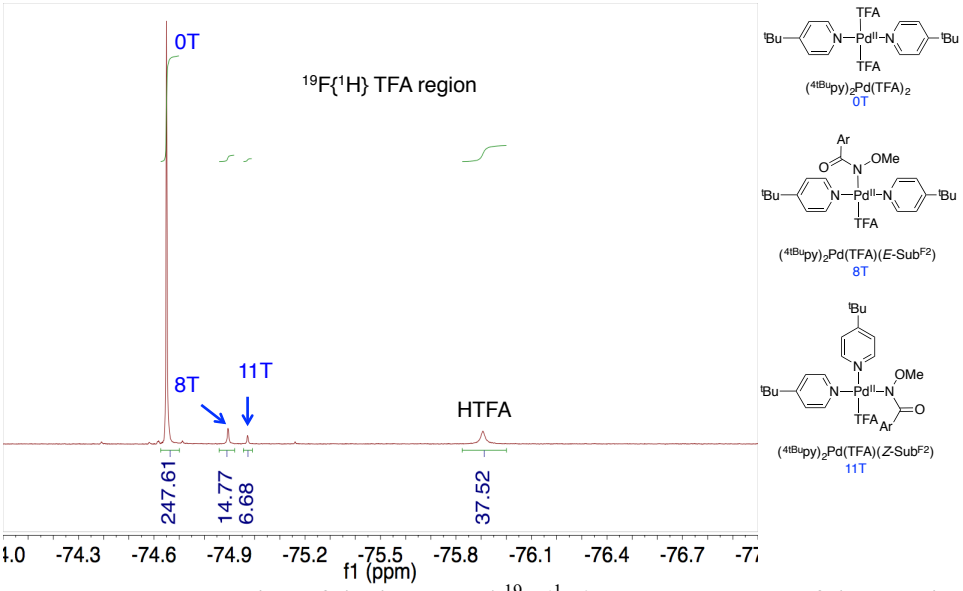


**Figure S58**. TFA region of the integrated $^{19}F\{^{1}H\}$ NMR spectrum of the reaction of ($^{tBu}$py)$_2$Pd(TFA)$_2$ **0T** with 2.0 equiv *N*-methoxy-2,6-difluorobenzamide 38 hours after the reactants were mixed.

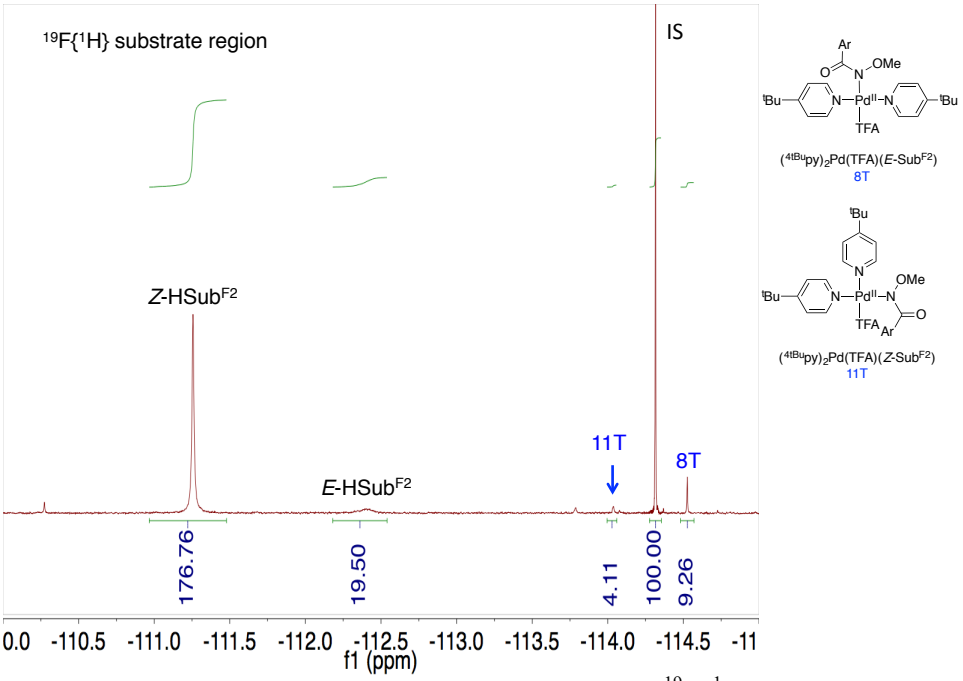


**Figure S59**. Substrate region of the integrated $^{19}F\{^{1}H\}$ NMR spectrum of the reaction of ($^{tBu}$py)$_2$Pd(TFA)$_2$ **0T** with 2.0 equiv *N*-methoxy-2,6-difluorobenzamide 38 hours after the reactants were mixed.

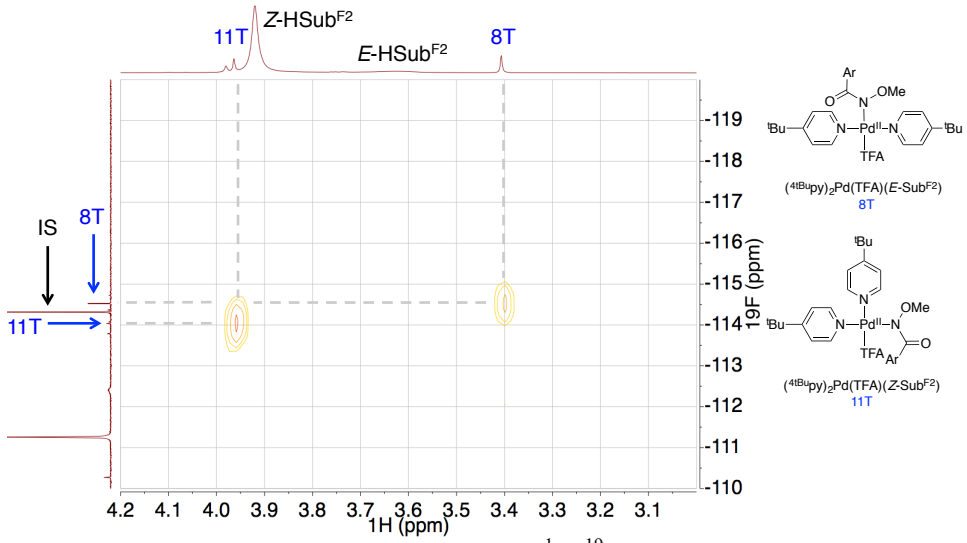


**Figure S60**. Magnified methoxy region of the $^{1}$H-$^{19}$F HMBC spectrum of the reaction of ($^{tBu}$py)$_2$Pd(TFA)$_2$ **0T** with 2.0 equiv *N*-methoxy-2,6-difluorobenzamide, several days after the reactants were mixed, with assigned cross peaks.

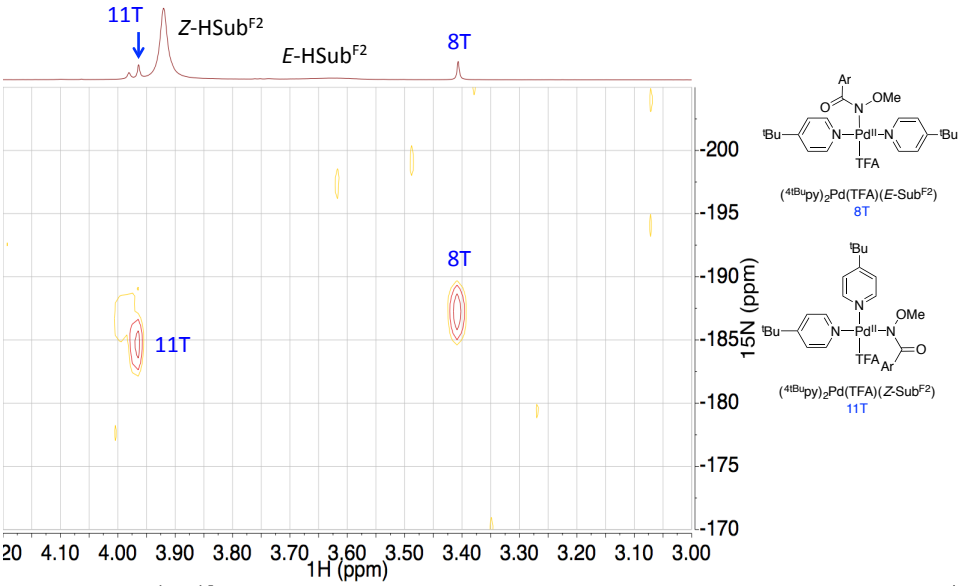


**Figure S61**. $^{1}$H-$^{15}$N HMBC spectrum of the methoxy region of the reaction of ($^{4tBu}$py)$_2$Pd(TFA)$_2$ **0T** with 2.0 equiv *N*-methoxy-2,6-difluorobenzamide, several days after the reactants were mixed, with assigned cross peaks. Because the $^{15}$N chemical shifts of these species are similar to those of **8A**, **8B**, **11A**, and **11B**, these are assigned as mono-trifluoroacetate-mono-amidate species.

**Table S9**. Key $^{1}$H, $^{19}$F{$^{1}$H}, and $^{15}$N NMR peaks for each assigned species in the reaction of ($^{tBu}$py)$_2$Pd(TFA)$_2$ **0T** with 2.0 equiv *N*-methoxy-2,6-difluorobenzamide 38 hours after the reactants were mixed.

| Species | α-$^{4tBu}$py (ppm) | $H_3$CON- (ppm) | $^{19}$F{$^{1}$H} (ppm) | $^{15}$N ($H_3$CO*N*-) (ppm) |
|---|---|---|---|---|
| **0T** | 8.33 | - | -74.64 | |
| **8T** | | 3.41 | -74.88 | -187.17 |
| | 8.67 | | -114.51 | |
| **11T** | 8.89 | 3.97 | -74.96 | -184.57 |
| | 8.76 | | -114.02 | |
| HTFA | - | - | -75.89 | |
| HSub$^{F2}$ | - | 3.91 | -111.24 | Not observed |
| | | 3.62 | -112.39 | Not observed |

*Spectra for the attempted reaction of ($^{tBu}$py)$_2$PdCl$_2$ **0C** with 2.0 equiv* N*-methoxy-2,6-difluorobenzamide*

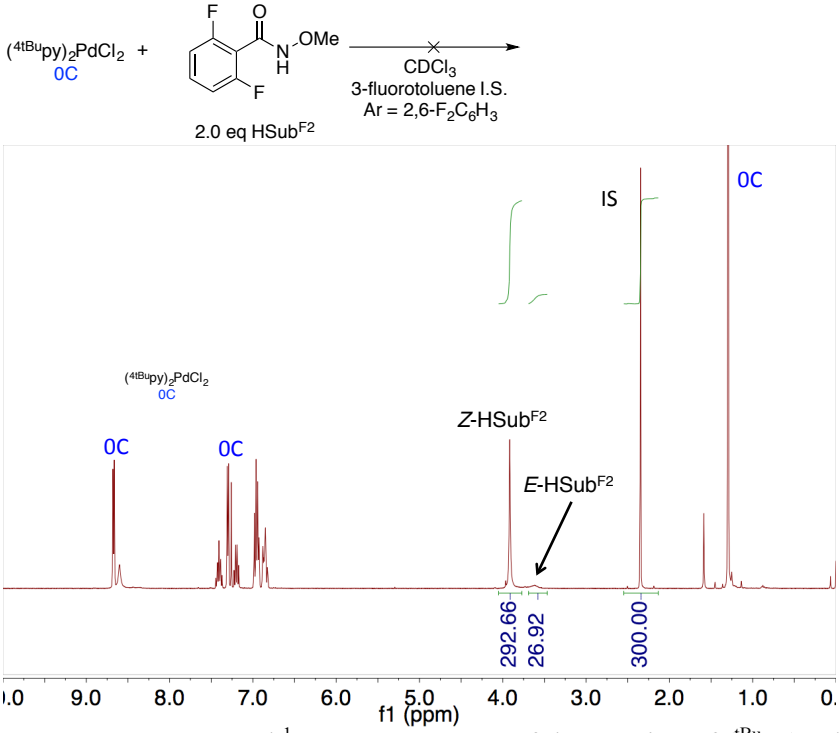


**Figure S62**. Integrated $^{1}$H NMR spectrum of the reaction of ($^{tBu}$py)$_2$PdCl$_2$ **0C** with 2.0 equiv *N*-methoxy-2,6-difluorobenzamide 15 hours after the reactants were mixed.

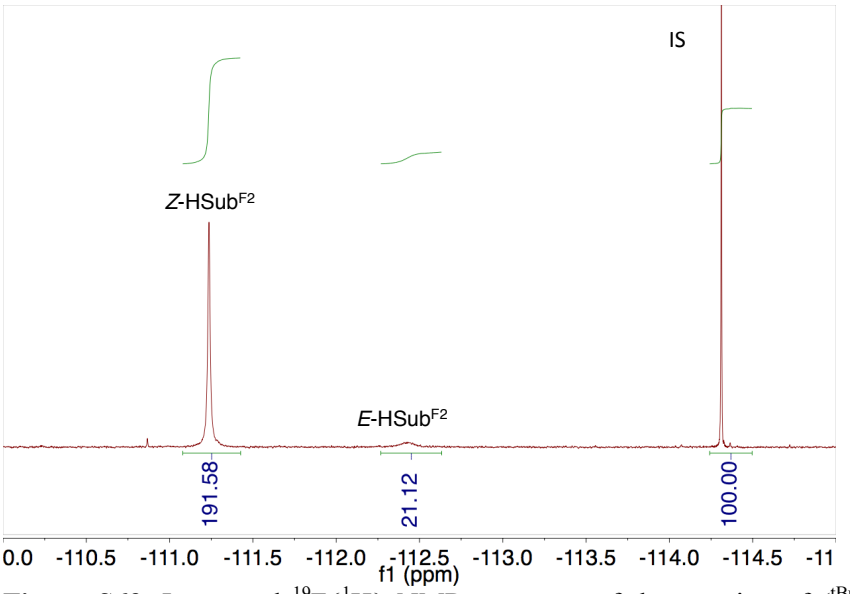


**Figure S63**. Integrated $^{19}F\{^{1}H\}$ NMR spectrum of the reaction of $(^{tBu}py)_2PdCl_2$ **0C** with 2.0 equiv *N*-methoxy-2,6-difluorobenzamide 15 hours after the reactants were mixed.

## VI. Compound Spectral Characterization

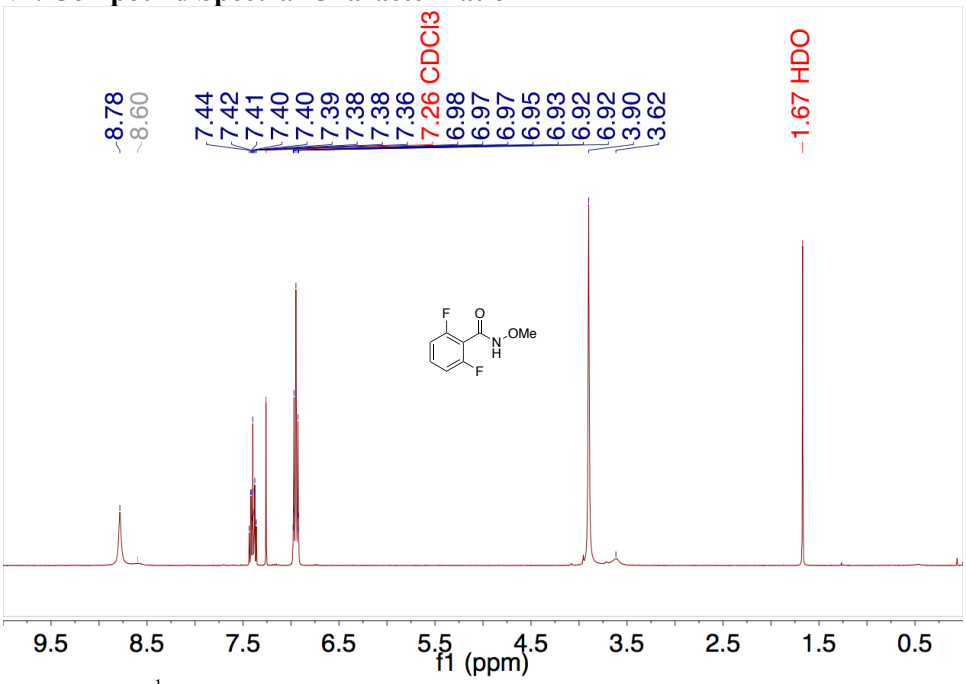


**Figure S64**. $^{1}$H NMR spectrum of *N*-methoxy-2,6-difluorobenzamide in $CDCl_3$.

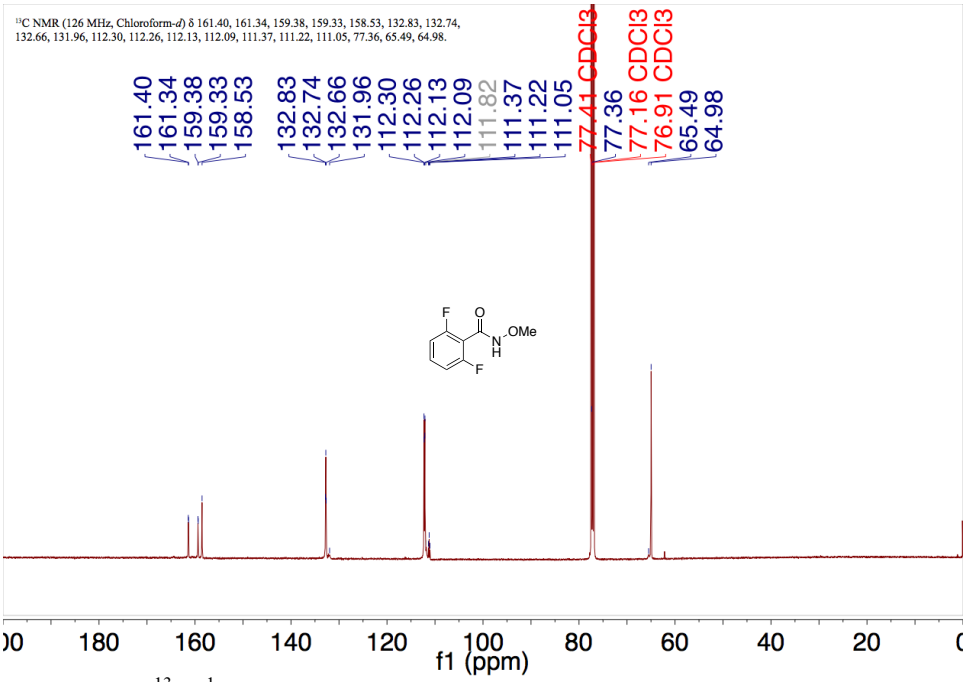


**Figure S65**. $^{13}C\{^{1}H\}$ NMR spectrum of *N*-methoxy-2,6-difluorobenzamide in $CDCl_3$.

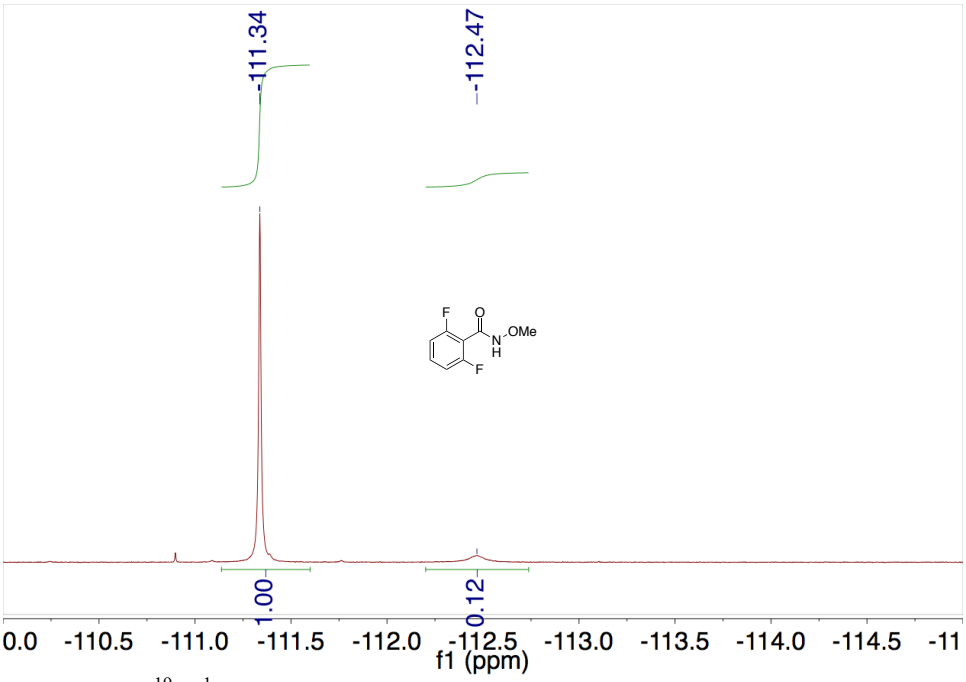


**Figure S66**. $^{19}F\{^{1}H\}$ NMR spectrum of *N*-methoxy-2,6-difluorobenzamide in $CDCl_3$.

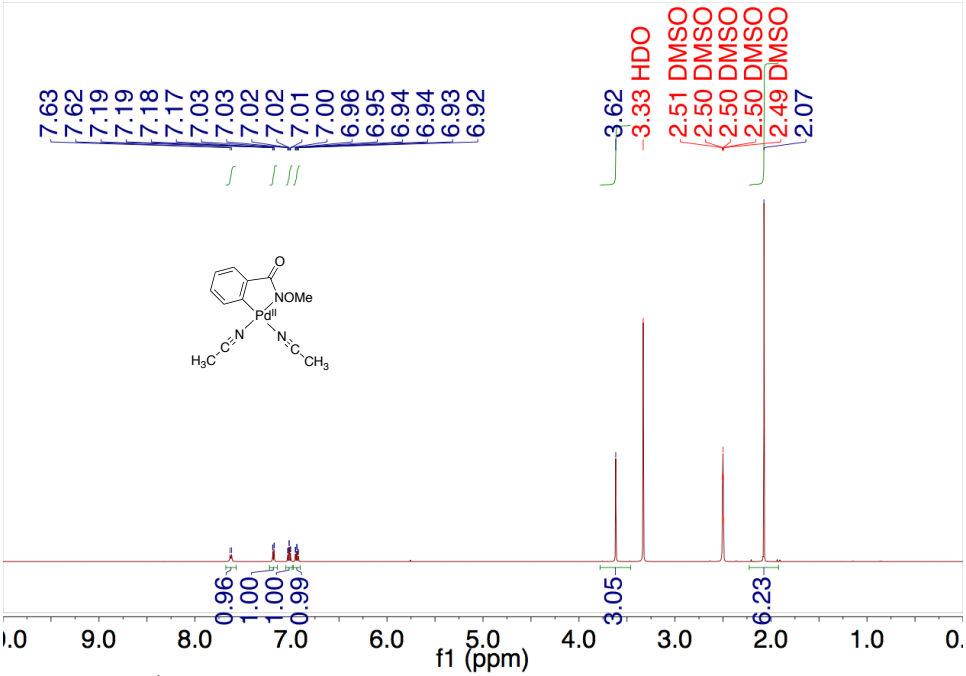


**Figure S67**. $^{1}$H NMR spectrum of $(CH_3CN)_2Pd(C\sim N)$ **2A** in DMSO-$d_6$.

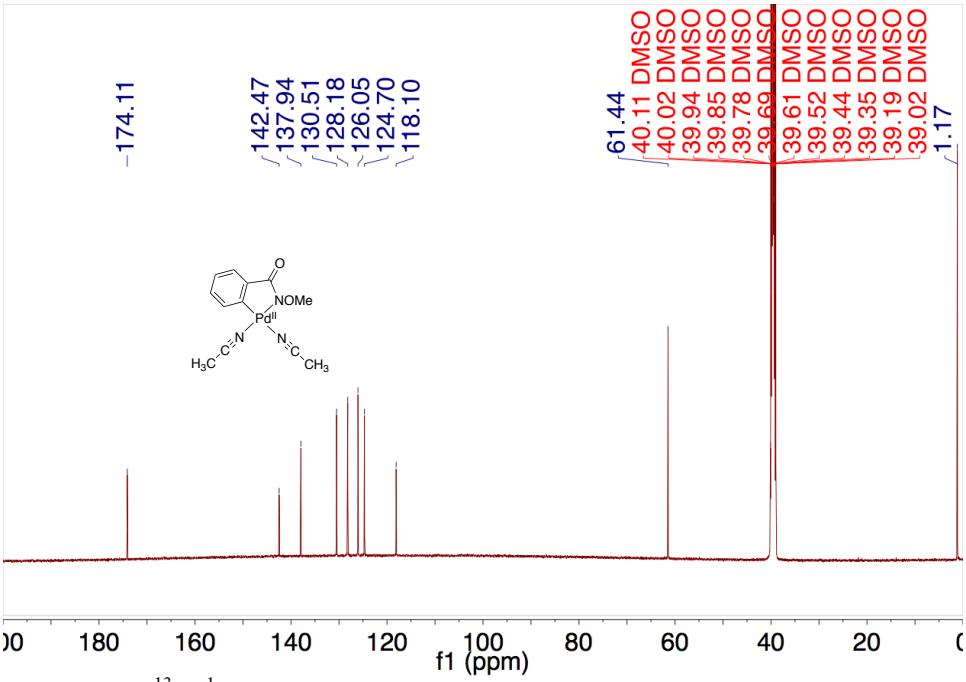


**Figure S68**. $^{13}C\{^{1}H\}$ NMR spectrum of $(CH_3CN)_2Pd(C\sim N)$ **2A** in DMSO-$d_6$.

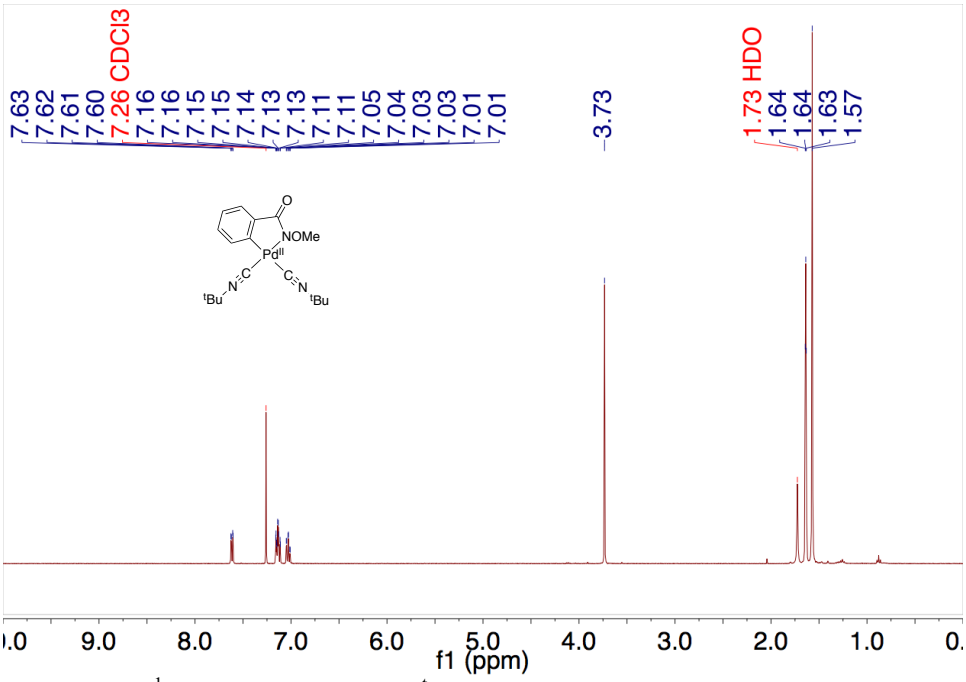


**Figure S69**. $^{1}$H NMR spectrum of ($^{t}$BuNC)$_2$Pd(C~N) **2** in $CDCl_3$.

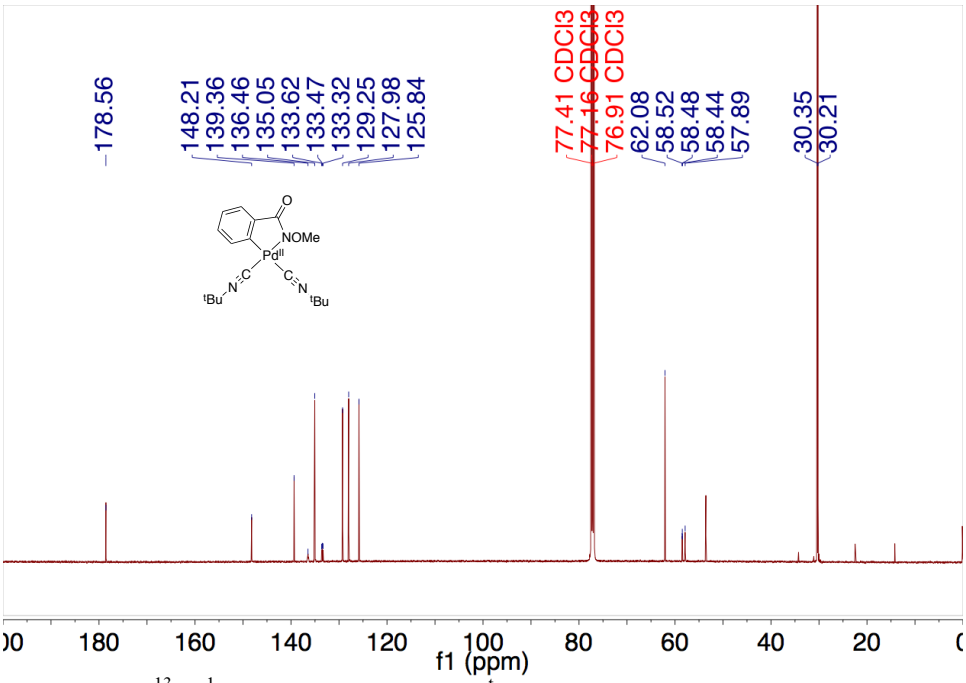


**Figure S70**. $^{13}C\{^{1}H\}$ NMR spectrum of ($^{t}$BuNC)$_2$Pd(C~N) **2** in $CDCl_3$.

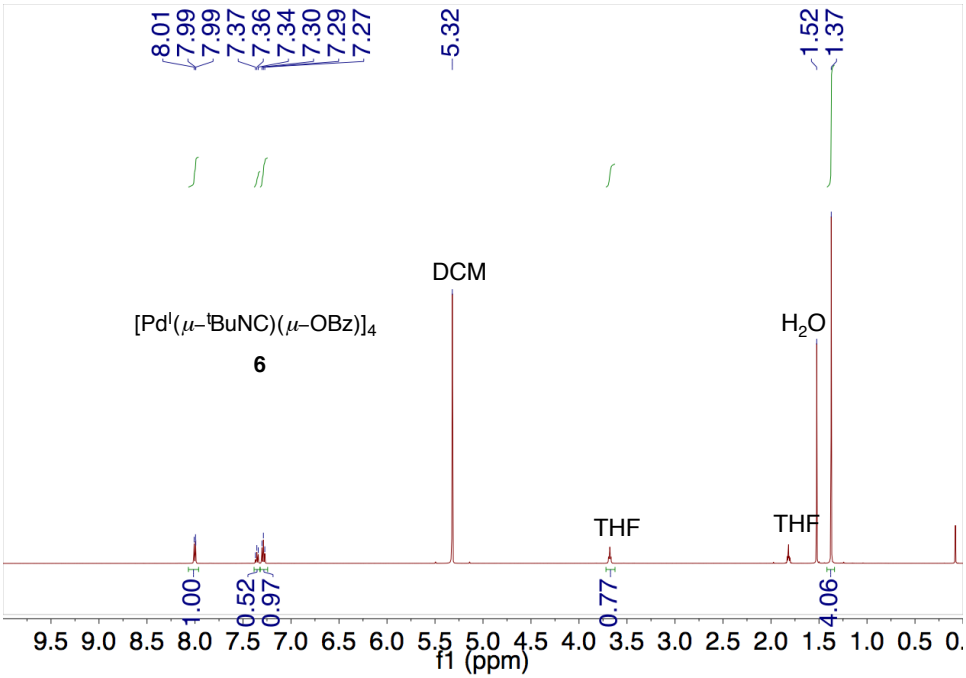


**Figure S71**. $^{1}$H NMR spectrum of [Pd$^{I}$(μ-$^{t}$BuNC)(μ-OBz)]$_4$ **6** in $CD_2Cl_2$.

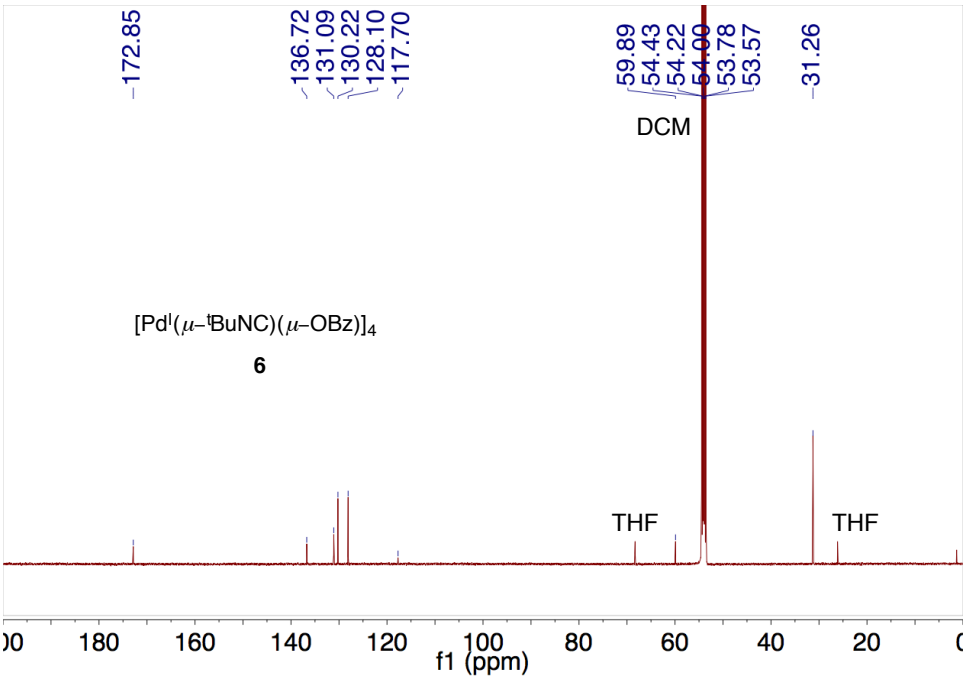


**Figure S72**. $^{13}$C{$^{1}$H} NMR spectrum of [Pd$^{I}$(μ-$^{t}$BuNC)(μ-OBz)]$_4$ **6** in $CD_2Cl_2$.

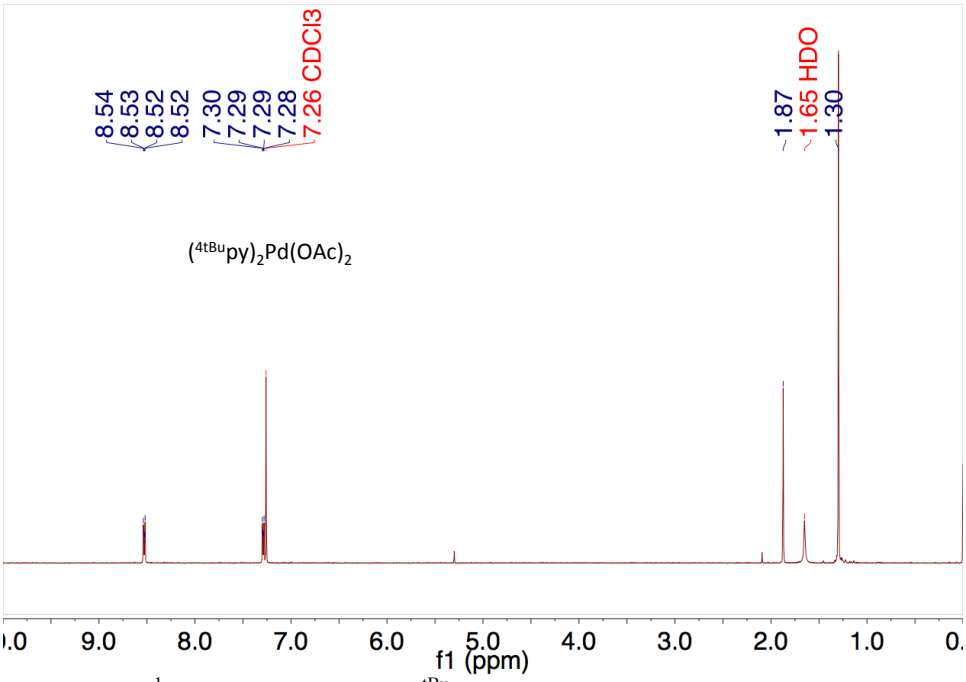


**Figure S73**. $^{1}H$ NMR spectrum of $(^{tBu}py)_2Pd(OAc)_2$ **0A** in $CDCl_3$.

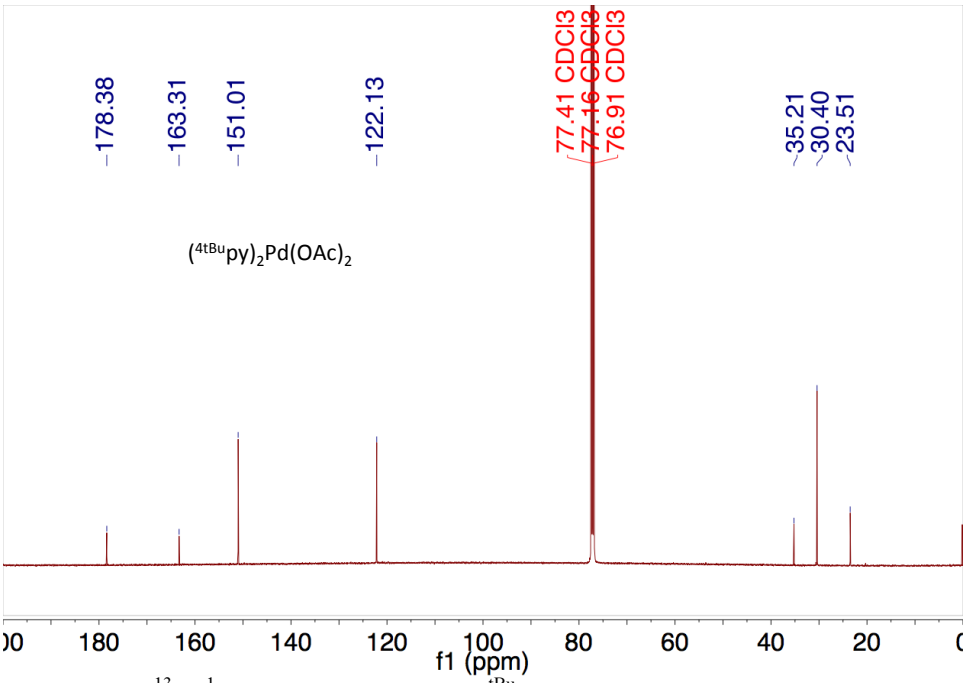


**Figure S74**. $^{13}C\{^{1}H\}$ NMR spectrum of $(^{tBu}py)_2Pd(OAc)_2$ **0A** in $CDCl_3$.

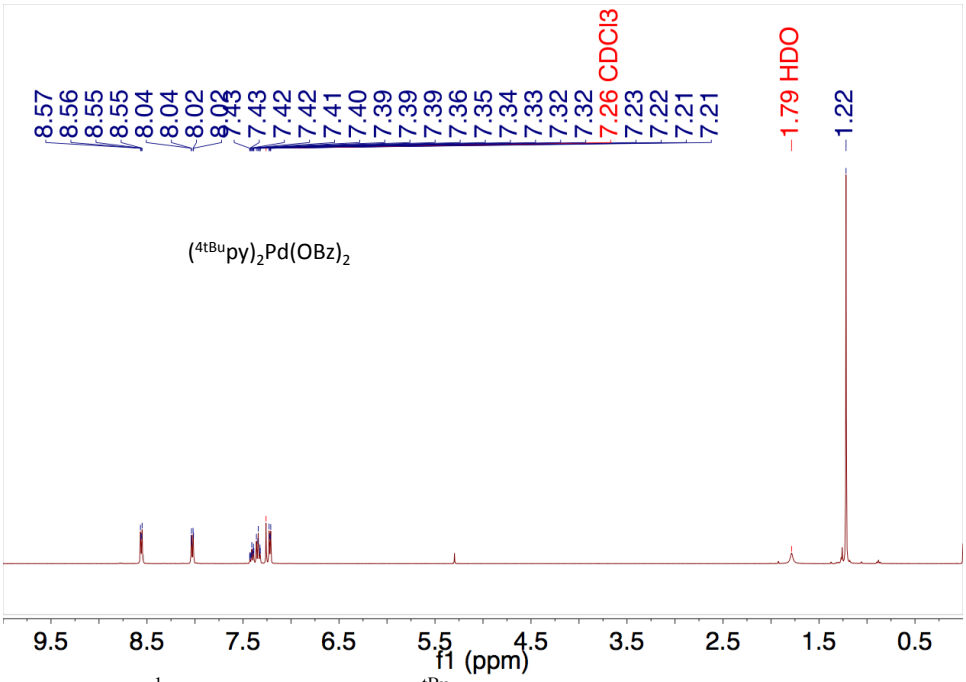


**Figure S75**. $^{1}$H NMR spectrum of ($^{tBu}$py)$_2$Pd(OBz)$_2$ **0B** in $CDCl_3$.

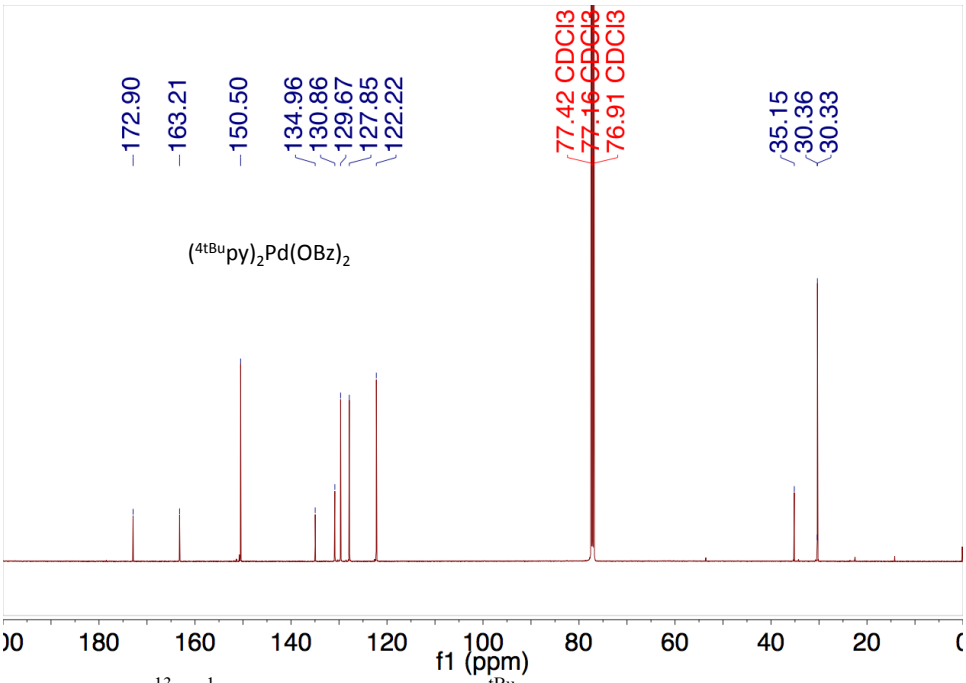


**Figure S76**. $^{13}C\{^{1}H\}$ NMR spectrum of ($^{tBu}$py)$_2$Pd(OBz)$_2$ **0B** in $CDCl_3$.

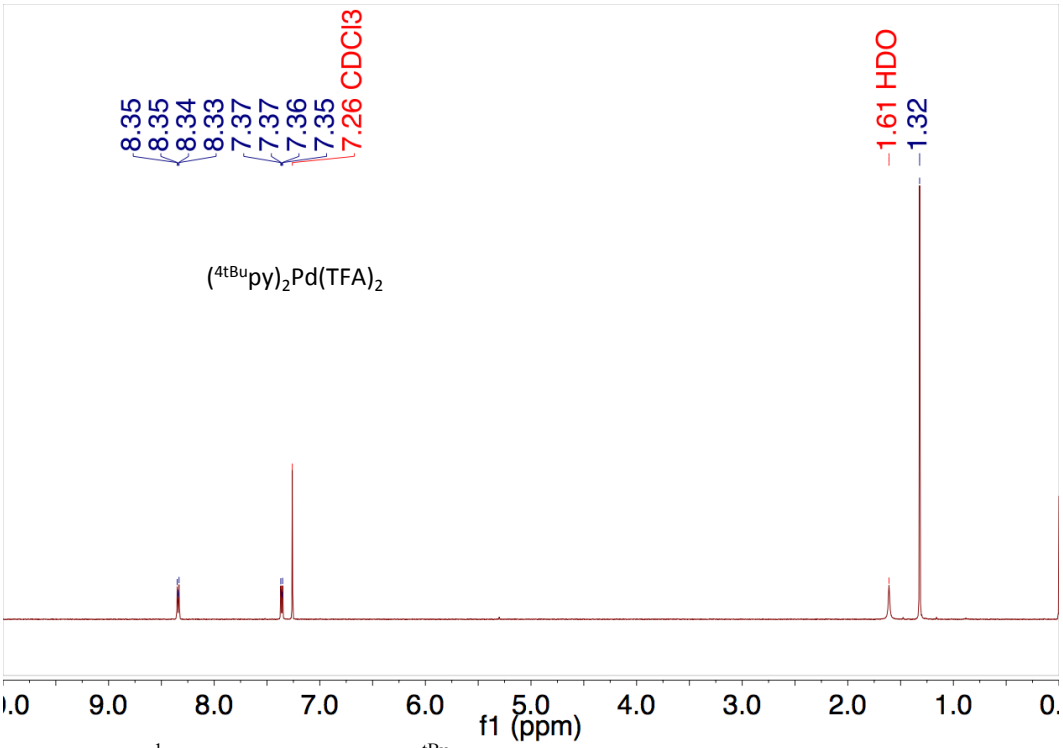


**Figure S77**. $^{1}$H NMR spectrum of ($^{tBu}$py)$_2$Pd(TFA)$_2$ **0T** in $CDCl_3$.

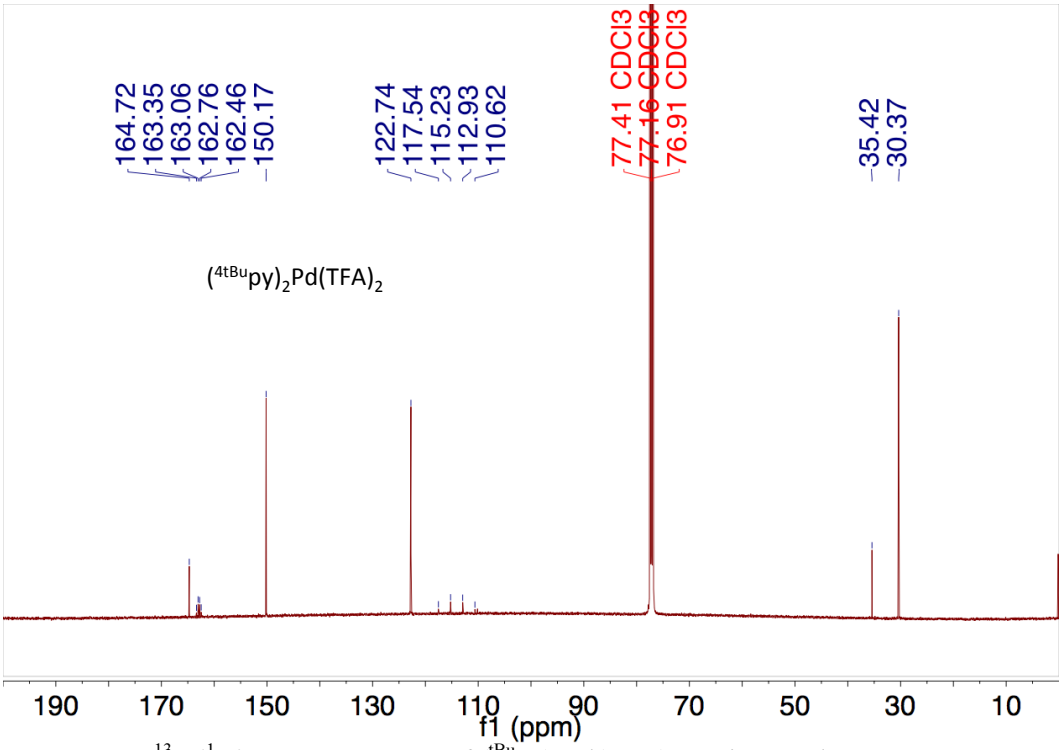


**Figure S78**. $^{13}C\{^{1}H\}$ NMR spectrum of ($^{tBu}$py)$_2$Pd(TFA)$_2$ **0T** in $CDCl_3$.

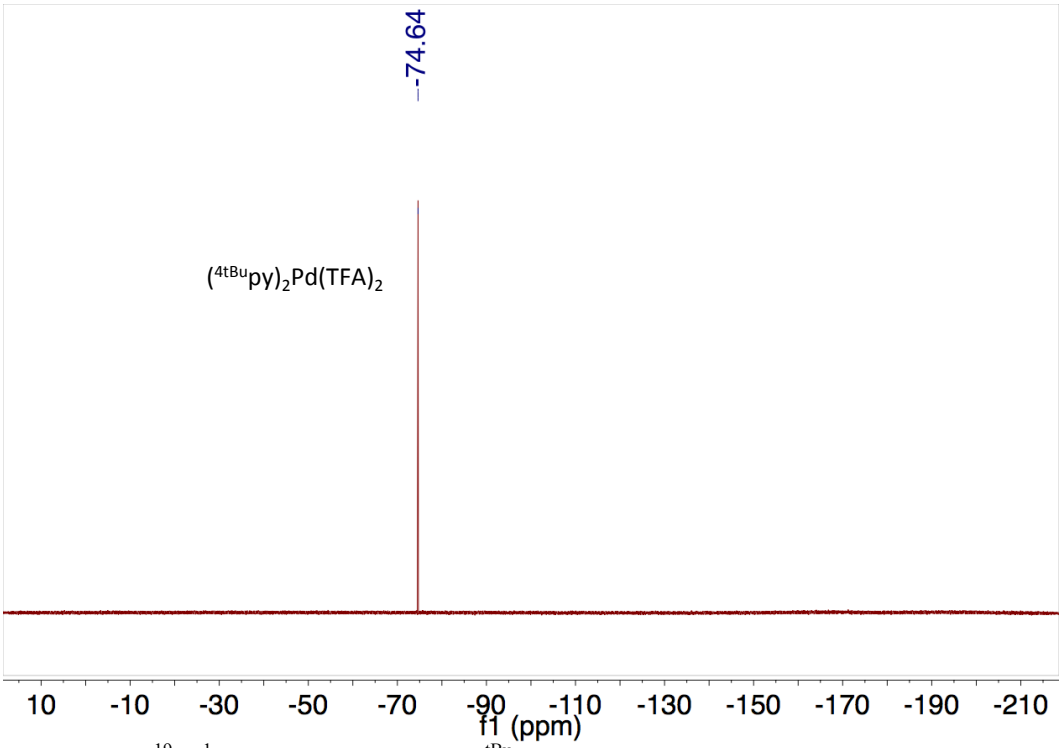


**Figure S79**. $^{19}F\{^{1}H\}$ NMR spectrum of ($^{tBu}$py)$_2$Pd(TFA)$_2$ **0T** in $CDCl_3$.

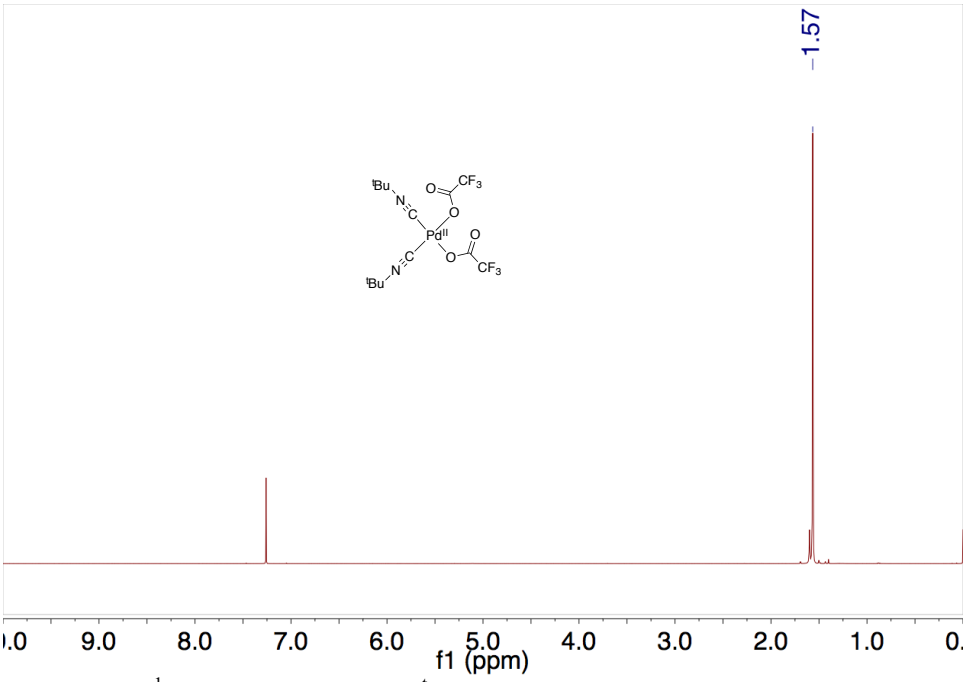


**Figure S80**. $^{1}H$ NMR spectrum of $(^{t}BuNC)_2Pd(TFA)_2$ in $CDCl_3$.

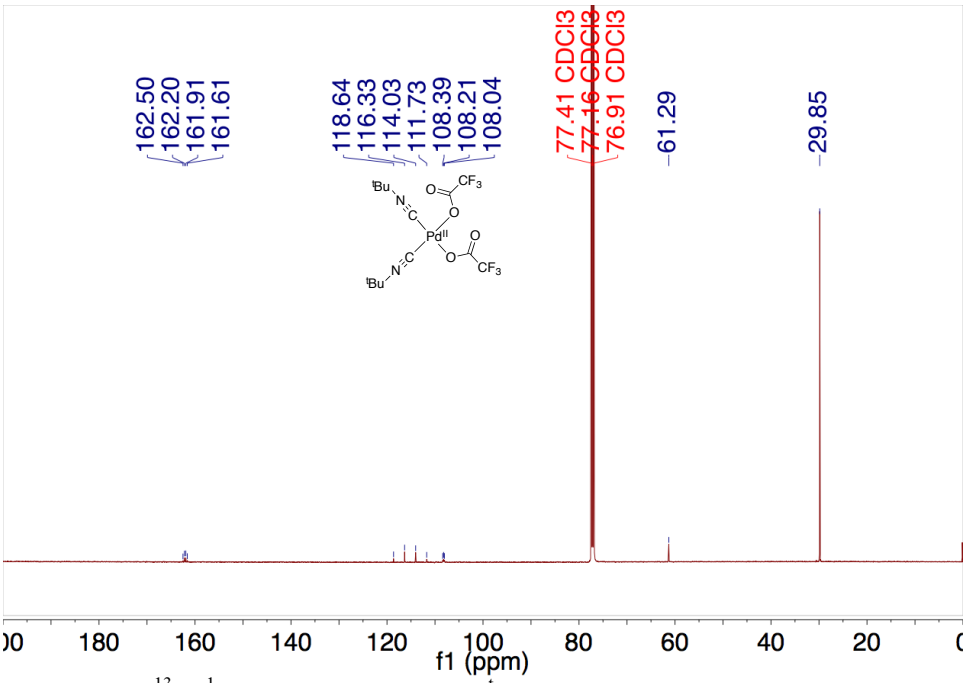


**Figure S81**. $^{13}C\{^{1}H\}$ NMR spectrum of $(^{t}BuNC)_2Pd(TFA)_2$ in $CDCl_3$.

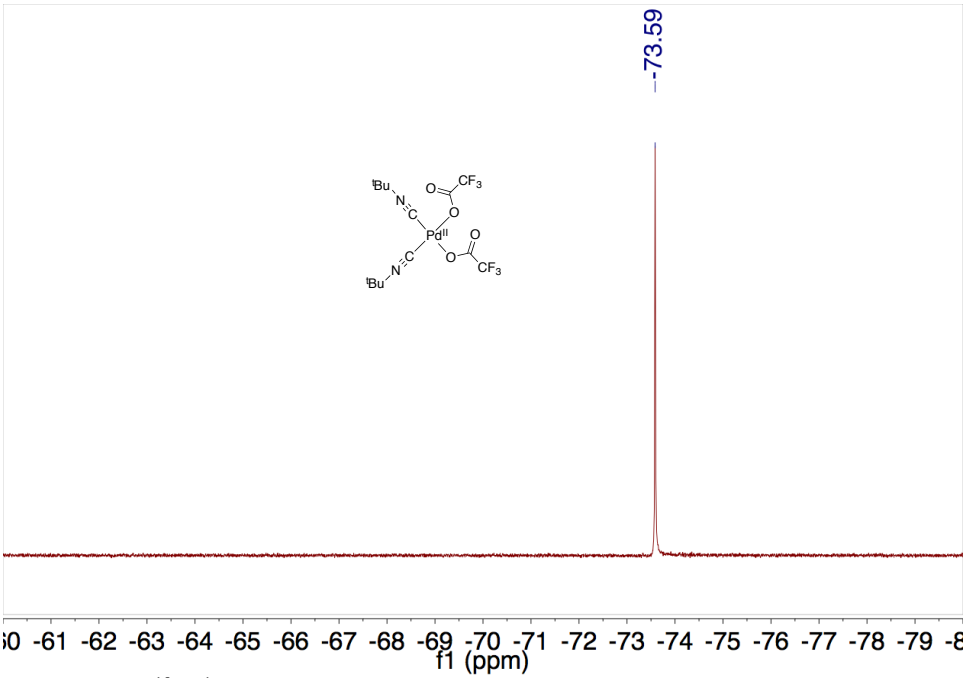


**Figure S82**. $^{19}F\{^{1}H\}$ NMR spectrum of $(^{t}BuNC)_2Pd(TFA)_2$ in $CDCl_3$.

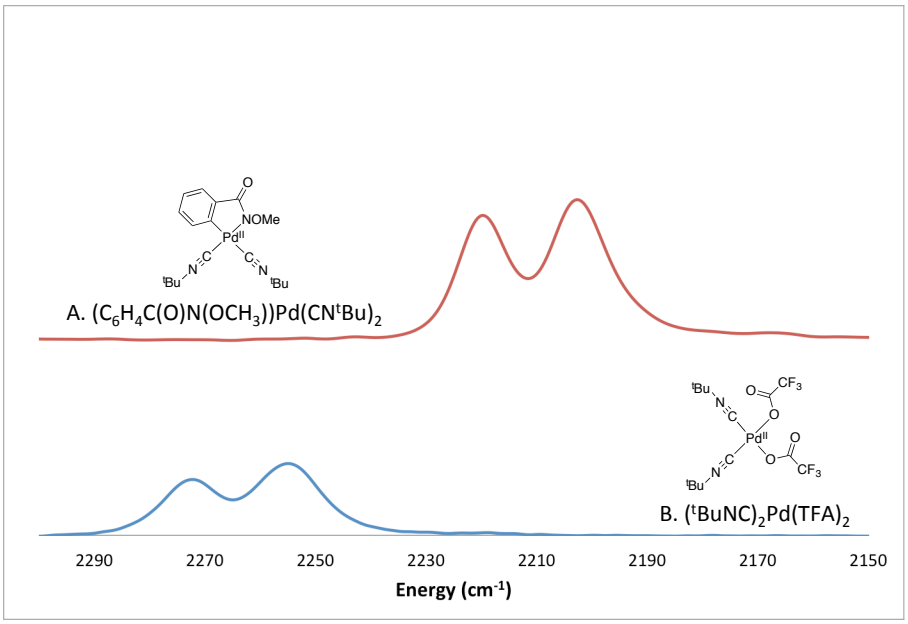


**Figure S83**. The symmetric and asymmetric CN stretches in the solid-state FT-IR spectra of (A) $(^{t}BuNC)_2Pd(C\sim N)$ **2**, and (B) $(^{t}BuNC)_2Pd(TFA)_2$.

## VII. X-Ray Crystallography

### Data collection for $[Pd^{I}(\mu\text{-}^{t}BuNC)(\mu\text{-}OBz)]_4$ 6.

A yellow crystal with approximate dimensions 0.074 x 0.14 x 0.19 $mm^3$ was selected under oil under ambient conditions and attached to the tip of a MiTeGen MicroMount©. The crystal was mounted in a stream of cold nitrogen at 100(1) K and centered in the X-ray beam by using a video camera.

The crystal evaluation and data collection were performed on a Bruker SMART APEXII diffractometer with Cu $K_\alpha$ ($\lambda$ = 1.54178 Å) radiation and the diffractometer to crystal distance of 4.03 cm.[10]

The initial cell constants were obtained from three series of ω scans at different starting angles. Each series consisted of 41 frames collected at intervals of 0.5º in a 25º range about ω with the exposure time of 10 seconds per frame. The reflections were successfully indexed by an automated indexing routine built in the APEXII program. The final cell constants were calculated from a set of 9883 strong reflections from the actual data collection.

The data were collected by using the full sphere data collection routine to survey the reciprocal space to the extent of a full sphere to a resolution of 0.82 Å. A total of 25176 data were harvested by collecting 27 sets of frames with 0.5º scans in ω and φ with an exposure time 10-30 sec per frame. These highly redundant datasets were corrected for Lorentz and polarization effects. The absorption correction was based on fitting a function to the empirical transmission surface as sampled by multiple equivalent measurements. [11]

### Structure Solution and Refinement for $[Pd^{I}(\mu\text{-}^{t}BuNC)(\mu\text{-}OBz)]_4$ 6.

The systematic absences in the diffraction data were consistent for the space groups $P\bar{1}$ and $P1$. The *E*-statistics strongly suggested the centrosymmetric space group $P\bar{1}$ that yielded chemically reasonable and computationally stable results of refinement.[12-17]

A successful solution by the direct methods provided most non-hydrogen atoms from the *E*-map. The remaining non-hydrogen atoms were located in an alternating series of least-squares cycles and difference Fourier maps. All non-hydrogen atoms except for the minor component of the disordered tert-butyl group were refined with anisotropic displacement coefficients. All hydrogen atoms were included in the structure factor calculation at idealized positions and were allowed to ride on the neighboring atoms with relative isotropic displacement coefficients.

The tert-butyl group of one of the tert-butyl isonitrile ligands was disordered over two positions with a major component occupancy of 83.7(5)%. The carbon atoms of the disordered tert-butyl group were refined isotropically and bond distance constraints were applied to ensure a chemically reasonable and computationally stable refinement.

The final least-squares refinement of 605 parameters against 9030 data resulted in residuals *R* (based on $F^2$ for $I \geq 2\sigma$) and *wR* (based on $F^2$ for all data) of 0.0199 and 0.0542, respectively. The final difference Fourier map was featureless.

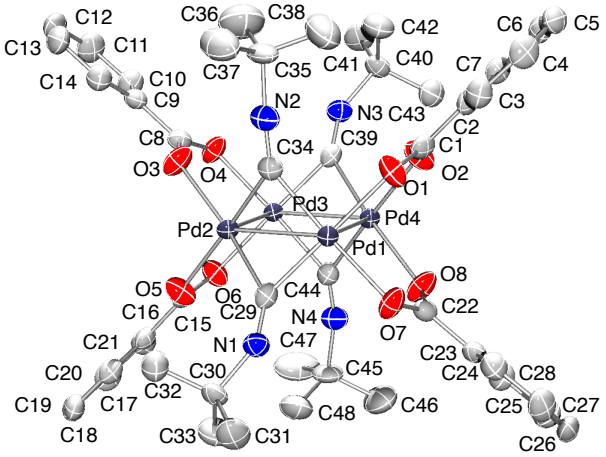


**Figure S84**. Molecular drawing of $[Pd^{I}(\mu\text{-}^{t}BuNC)(\mu\text{-}OBz)]_4$ **6**. All atoms are shown as 50% thermal probability ellipsoids. Only one of the two positions of the disordered tBu group are shown. All H atoms are omitted.

**Table S10. Crystal data and structure refinement for $[Pd^{I}(\mu\text{-}^{t}BuNC)(\mu\text{-}OBz)]_4$ 6.**

| | |
|---|---|
| Identification code | Stahl219 |
| Empirical formula | $(C_7H_5O_2)_4(C_5H_9N)_4Pd_4$ |
| Formula weight | 1242.56 |
| Temperature/K | 99.91 |
| Crystal system | triclinic |
| Space group | P-1 |
| a/Å | 10.628(3) |
| b/Å | 11.7410(17) |
| c/Å | 19.964(3) |
| α/° | 103.971(5) |
| β/° | 99.063(7) |
| γ/° | 92.649(11) |
| Volume/Å$^3$ | 2378.0(7) |
| Z | 2 |
| $\rho_{calc}$g/cm$^3$ | 1.735 |
| μ/mm$^{-1}$ | 12.471 |
| F(000) | 1240.0 |
| Crystal size/mm$^3$ | 0.19 × 0.14 × 0.074 |
| Radiation | CuKα (λ = 1.54178) |
| 2Θ range for data collection/° | 4.632 to 140.508 |
| Index ranges | $-12 \le h \le 12$, $-14 \le k \le 14$, $-24 \le l \le 24$ |
| Reflections collected | 66589 |
| Independent reflections | 9030 [$R_{int}$ = 0.0283, $R_{sigma}$ = 0.0154] |
| Data/restraints/parameters | 9030/54/605 |
| Goodness-of-fit on $F^2$ | 1.090 |
| Final R indexes [I>=2σ (I)] | $R_1$ = 0.0199, $wR_2$ = 0.0536 |
| Final R indexes [all data] | $R_1$ = 0.0210, $wR_2$ = 0.0542 |
| Largest diff. peak/hole / e Å$^{-3}$ | 0.42/-0.45 |

**Data collection for $(H_3CCN)_2Pd(C\sim N)$ 2A.**

A colorless crystal with approximate dimensions 0.28 x 0.19 x 0.09 mm$^3$ was selected under oil under ambient conditions and attached to the tip of a MiTeGen MicroMount©. The crystal was mounted in a stream of cold nitrogen at 100(1) K and centered in the X-ray beam by using a video camera.

The crystal evaluation and data collection were performed on a Bruker SMART APEXII diffractometer with Cu $K_\alpha$ (λ = 1.54178 Å) radiation and the diffractometer to crystal distance of 4.03 cm.[10]

The initial cell constants were obtained from three series of ω scans at different starting angles. Each series consisted of 41 frames collected at intervals of 0.6º in a 25º range about ω with the exposure time of 6 seconds per frame. The reflections were successfully indexed by an automated indexing routine built in the APEXII program. The final cell constants were calculated from a set of 9887 strong reflections from the actual data collection.

The data were collected by using the full sphere data collection routine to survey the reciprocal space to the extent of a full sphere to a resolution of 0.82 Å. A total of 18978 data were harvested by collecting 13 sets of frames with 0.7º scans in ω and φ with an exposure time 6-16 sec per frame. These highly redundant datasets were corrected for Lorentz and polarization effects. The absorption correction was based on fitting a function to the empirical transmission surface as sampled by multiple equivalent measurements.[11]

**Structure Solution and Refinement for $(H_3CCN)_2Pd(C\sim N)$ 2A.**

The systematic absences in the diffraction data were uniquely consistent for the space group $P2_1/c$ that yielded chemically reasonable and computationally stable results of refinement.[12-17]

A successful solution by the direct methods provided most non-hydrogen atoms from the *E*-map. The remaining non-hydrogen atoms were located in an alternating series of least-squares cycles and difference Fourier maps. All non-hydrogen atoms were refined with anisotropic displacement coefficients. All hydrogen atoms were found in the difference Fourier map and refined independently.

The final least-squares refinement of 215 parameters against 2623 data resulted in residuals *R* (based on $F^2$ for $I \geq 2\sigma$) and *wR* (based on $F^2$ for all data) of 0.0156 and 0.0387, respectively. The final difference Fourier map was featureless.

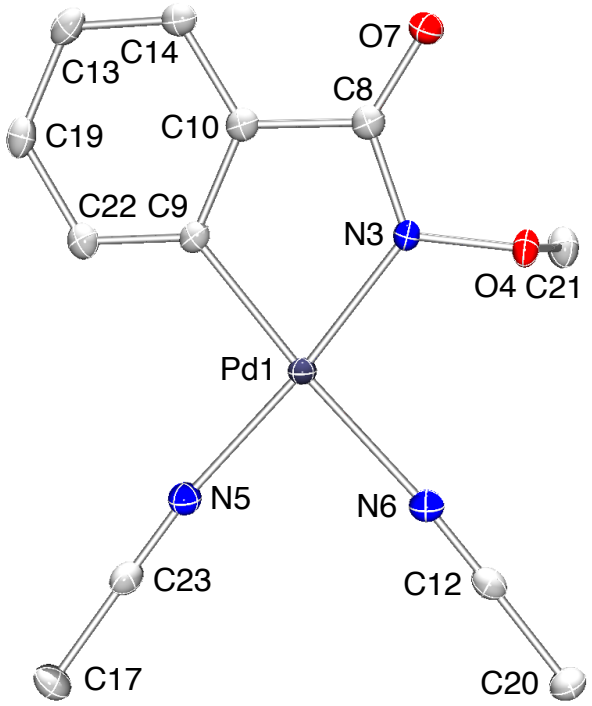


**Figure S85**. Molecular drawing of $(H_3CCN)_2Pd(C\sim N)$ **2A**. All atoms are shown as 50% thermal probability ellipsoids. All H atoms are omitted.

**Table S11. Crystal data and structure refinement for $(H_3CCN)_2Pd(C\sim N)$ 2A.**

| | |
|---|---|
| Identification code | stahl226 |
| Empirical formula | $C_{12}H_{13}N_3O_2Pd$ |
| Formula weight | 337.65 |
| Temperature/K | 100.0 |
| Crystal system | monoclinic |
| Space group | $P2_1/c$ |
| a/Å | 10.0503(8) |
| b/Å | 8.7166(5) |
| c/Å | 15.0873(9) |
| α/° | 90 |
| β/° | 91.120(3) |
| γ/° | 90 |
| Volume/Å$^3$ | 1321.46(15) |
| Z | 4 |
| $\rho_{calc}$g/cm$^3$ | 1.697 |
| μ/mm$^{-1}$ | 11.325 |
| F(000) | 672.0 |
| Crystal size/mm$^3$ | 0.279 × 0.19 × 0.092 |
| Radiation | CuKα (λ = 1.54178) |
| 2Θ range for data collection/° | 11.726 to 146.42 |
| Index ranges | $-10 \le h \le 12$, $-10 \le k \le 10$, $-18 \le l \le 18$ |
| Reflections collected | 18978 |
| Independent reflections | 2623 [$R_{int}$ = 0.0233, $R_{sigma}$ = 0.0124] |
| Data/restraints/parameters | 2623/0/215 |
| Goodness-of-fit on $F^2$ | 1.131 |
| Final R indexes [I>=2σ (I)] | $R_1$ = 0.0156, $wR_2$ = 0.0387 |
| Final R indexes [all data] | $R_1$ = 0.0158, $wR_2$ = 0.0387 |
| Largest diff. peak/hole / e Å$^{-3}$ | 0.29/-0.33 |

**Data collection for $(^tBuNC)_2Pd(C\sim N)$ 2.**

A colorless crystal with approximate dimensions 0.01 x 0.08 x 0.12 mm$^3$ was selected under oil under ambient conditions and attached to the tip of a MiTeGen MicroMount©. The crystal was mounted in a stream of cold nitrogen at 100(1) K and centered in the X-ray beam by using a video camera.

The crystal evaluation and data collection were performed on a Bruker Quazar SMART APEXII diffractometer with Mo $K_\alpha$ (λ = 0.71073 Å) radiation and the diffractometer to crystal distance of 5.0 cm.[10]

The initial cell constants were obtained from three series of ω scans at different starting angles. Each series consisted of 12 frames collected at intervals of 0.5º in a 6º range about ω with the exposure time of 10 seconds per frame. The reflections were successfully indexed by an automated indexing routine built in the APEXII program suite. The final cell constants were calculated from a set of 9898 strong reflections from the actual data collection.

The data were collected by using the full sphere data collection routine to survey the reciprocal space to the extent of a full sphere to a resolution of 0.69 Å. A total of 21360 data were harvested by collecting 5 sets of frames with 0.5º scans in ω and φ with exposure times of 25 sec per frame. These highly redundant datasets were corrected for Lorentz and polarization effects. The absorption correction

was based on fitting a function to the empirical transmission surface as sampled by multiple equivalent measurements. [11]

**Structure Solution and Refinement for ($^t$BuNC)$_2$Pd(C~N) 2.**

The systematic absences in the diffraction data were consistent for the space groups $P\bar{1}$ and $P1$. The *E*-statistics strongly suggested the centrosymmetric space group $P\bar{1}$ that yielded chemically reasonable and computationally stable results of refinement.[12-17]

A successful solution by the direct methods provided most non-hydrogen atoms from the *E*-map. The remaining non-hydrogen atoms were located in an alternating series of least-squares cycles and difference Fourier maps. All non-hydrogen atoms were refined with anisotropic displacement coefficients. All hydrogen atoms were included in the structure factor calculation at idealized positions and were allowed to ride on the neighboring atoms with relative isotropic displacement coefficients.

The crystal was composed of two domains with a minor domain contribution of about 10%. The minor component was rotated by 14.7° from the major component relative to the [ ¾ 1 $\bar{1}$/3 ] axis. The best results were obtained when this second component was ignored.

The final least-squares refinement of 224 parameters against 6186 data resulted in residuals *R* (based on $F^2$ for $I \geq 2\sigma$) and *wR* (based on $F^2$ for all data) of 0.0244 and 0.0537, respectively. The final difference Fourier map was featureless.

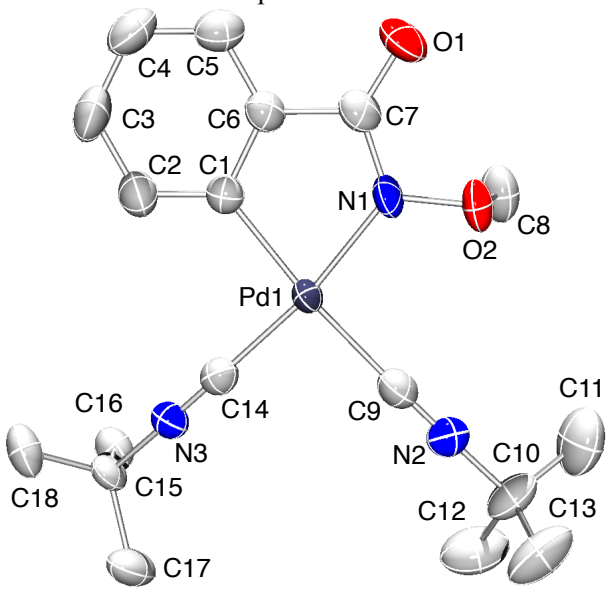


**Figure S86**. Molecular drawing of ($^t$BuNC)$_2$Pd(C~N) **2**. All atoms are shown as 90% thermal probability ellipsoids. All H atoms are omitted.

**Table S12. Crystal data and structure refinement for ($^t$BuNC)$_2$Pd(C~N) 2.**

| | |
|---|---|
| Identification code | Stahl217b |
| Empirical formula | $C_{18}H_{25}N_3O_2Pd$ |
| Formula weight | 421.81 |
| Temperature/K | 100.05 |
| Crystal system | triclinic |
| Space group | $P\bar{1}$ |
| a/Å | 9.600(3) |
| b/Å | 10.020(3) |
| c/Å | 11.759(4) |
| α/° | 109.470(18) |
| β/° | 104.215(11) |
| γ/° | 99.016(16) |
| Volume/Å$^3$ | 998.0(5) |
| Z | 2 |
| $\rho_{calc}$g/cm$^3$ | 1.404 |
| μ/mm$^{-1}$ | 0.943 |
| F(000) | 432.0 |
| Crystal size/mm$^3$ | 0.12 × 0.08 × 0.01 |
| Radiation | MoKα (λ = 0.71073) |
| 2Θ range for data collection/° | 3.878 to 61.484 |
| Index ranges | $-13 \leq h \leq 13$, $-14 \leq k \leq 14$, $-16 \leq l \leq 16$ |
| Reflections collected | 24590 |
| Independent reflections | 6186 [$R_{int}$ = 0.0398, $R_{sigma}$ = 0.0367] |
| Data/restraints/parameters | 6186/0/224 |
| Goodness-of-fit on $F^2$ | 1.028 |
| Final R indexes [I>=2σ (I)] | $R_1$ = 0.0244, $wR_2$ = 0.0519 |
| Final R indexes [all data] | $R_1$ = 0.0289, $wR_2$ = 0.0537 |
| Largest diff. peak/hole / e Å$^{-3}$ | 0.62/-0.52 |

**VIII. References.**


1. Kapdi, A. R.; Whitwood, A. C.; Williamson, D. C.; Lynam, J. M.; Burns, M. J.; Williams, T. J.; Reay, A. J.; Holmes, J.; Fairlamb, I. J. S. *J. Am. Chem. Soc.* **2013**, *135*, 8388.
2. Otsuka, S.; Nakamura, A.; Tatsuno, Y. *J. Am. Chem. Soc.* **1969**, *91*, 6994.
3. Le Stang, S.; Paul, F.; Lapinte, C. *Inorg. Chim. Acta* **1999**, *291*, 403.
4. Hornung, M.; Wesemann, L. *Eur. J. Inorg. Chem.* **2010**, *2010*, 2949.
5. Fukui, Y.; Liu, P.; Liu, Q.; He, Z.-T.; Wu, N.-Y.; Tian, P.; Lin, G.-Q. *J. Am. Chem. Soc.* **2014**, *136*, 15607.
6. Liu, Y.-J.; Xu, H.; Kong, W.-J.; Shang, M.; Dai, H.-X.; Yu, J.-Q. *Nature* **2014**, *515*, 389.
7. Based on the crystallographic structures of other $L_2PdX_2$ compounds with substituted pyridine ligands, we propose that these are *trans*-disposed molecules. For example, see: Izawa, Y.; Stahl, S. S. *Adv. Synth. Catal.* **2010**, *352*, 3223.
8. Lee, Y.; Park, G. Y.; Lucas, H. R.; Vajda, P. L.; Kamaraj, K.; Vance, M. A.; Milligan, A. E.; Woertink, J. S.; Siegler, M. A.; Narducci Sarjeant, A. A.; Zakharov, L. N.; Rheingold, A. L.; Solomon, E. I.; Karlin, K. D. *Inorg. Chem.* **2009**, *48*, 11297.
9. Athena is part of the Demeter 0.9.22 software package, (c) 2006-2015, Bruce Ravel, National Institute of Standards and Technology/Brookhaven National Laboratory; Athena uses Ifeffit 1.2.11d, (c) 2008 Matt Newville, U. Chicago (Ravel, B.; Newville, M. *J. Syncrotron Radiat.* **2005,** *12*, 537.)
10. Bruker-AXS (2014). *APEX2.* Version 2014.11-0. Madison, Wisconsin, USA.
11. Krause, L., Herbst-Irmer, R., Sheldrick, G. M. & Stalke, D. (2015). *J. Appl. Cryst.* 48. 3-10.
12. Sheldrick, G. M. (2013b). *XPREP*. Version 2013/1. Georg-August-Universität Göttingen, Göttingen, Germany.
13. Sheldrick, G. M. (2013a). The *SHELX* homepage, http://shelx.uni-ac.gwdg.de/SHELX/.
14. Sheldrick, G. M. (2015a). *Acta Cryst. A*, 71, 3-8.
15. Sheldrick, G. M. (2015b). *Acta Cryst. C*, 71, 3-8.
16. Dolomanov, O. V., Bourhis, L. J., Gildea, R. J., Howard, J. A. K. & Puschmann, H. (2009). *J. Appl. Crystallogr.* 42, 339-341.

17. Guzei, I. A. (2007-2013). Programs *Gn*. University of Wisconsin-Madison, Madison, Wisconsin, USA.